

Indoor Object Localization for Tracking and Progress Reporting in Construction

Hassan Bardareh

A Thesis

In the Department

of

Building, Civil and Environmental Engineering

Presented in Partial Fulfillment of the Requirements

For the Degree of

Doctor of Philosophy (Building Engineering) at

Concordia University

Montréal, Québec, Canada

February 2025

© Hassan Bardareh, 2025

CONCORDIA UNIVERSITY
SCHOOL OF GRADUATE STUDIES

This is to certify that the thesis prepared

By: Hassan Bardareh

Entitled: Indoor Object Localization for Tracking and Progress Reporting in Construction

and submitted in partial fulfillment of the requirements for the degree of

Doctor of Philosophy (Building Engineering)

complies with the regulations of the University and meets the accepted standards with respect to originality and quality.

Signed by the final examining committee:

| | |
|----------------------|----------------------|
| _____ | Chair |
| Dr. Christian Moreau | |
| _____ | External Examiner |
| Dr. Ahmad Jrade | |
| _____ | Arms-Length Examiner |
| Dr. Amin Hammad | |
| _____ | Examiner |
| Dr. Fuzhan Nasiri | |
| _____ | Examiner |
| Dr. Sang Hyeok Han | |
| _____ | Thesis Supervisor |
| Dr. Osama Moselhi | |

Approved by

Dr. Mohamed Ouf, Graduate Program Director

3/27/2025

Dr. Mourad Debbabi, Dean, Gina Cody School of Engineering and Computer Science

Abstract

Indoor Object Localization for Tracking and Progress Reporting in Construction

Hassan Bardareh, Ph.D.

Concordia University, 2025

This research investigates the application of indoor object localization to enhance tracking and progress reporting in construction projects by automating the generation of onsite inspection reports and location identification of project components. In this study, “inspection reports” refers to the documents used to monitor and record the progress of installed project components and track their target locations. Indoor object tracking is challenging due to the complex nature of construction environments, which typically are congested and contain many obstacles. Moreover, translating object-tracking information into meaningful progress reports is inherently challenging. To address these challenges, this study explores the integrated use of advanced technologies, such as RTLS and LiDAR, for location identification of the target objects. The study includes four main streams: (1) developing an object localization method based on integrated RTLS technologies and using trilateration techniques for 2D and 3D localization in indoor spaces, (2) integrating the object tracking with the progress tracking introducing MSI and QSI indices, and employing a cloud-based BIM platform for data collection and visualization, (3) integrating RTLS with point cloud data to refine the 3D object detection and localization functions, and (4) developing a digital-twin platform for automated generation of onsite inspection reports and visualization of the location and status of the objects associated with indoor construction operations. These reports are visualized through a bi-directional construction twin dashboard, facilitating ready access to progress-related information for site managers. The methods developed are validated through laboratory experiments and a case study conducted at a job site. In the laboratory experiments, the RTLS demonstrates an accuracy of approximately 0.52 m and 1.15 m, respectively, for 2D and 3D object localization. The 3D localization accuracy for the integrated RTLS and point cloud data, meanwhile, is found to be 27 cm. The case study also validates the effectiveness of the introduced indices in reporting the progress of the installation of components in mechanical rooms as part of a swimming pool construction project.

Acknowledgements

I would like to express my deepest gratitude to my mentor and supervisor, Prof. Osama Moselhi, for his unwavering guidance and motivation. His support has been instrumental in the completion of this dissertation. I am grateful to my examining committee members, Dr. Amin Hammad, Dr. Fuzhan Nasiri, Dr. Sang Hyeok Han, and Dr. Ahmed Jrade for their comments and feedback, which have elevated my work.

I also want to acknowledge the financial support of the Natural Sciences and Engineering Research Council of Canada, Mitacs, and Pomerleau Inc. My heartfelt thanks go to my colleagues at Concordia University, especially Angat Bhatia, Farzaneh Golkhoo, Moe Roghabadi, Araham Martinez, Dena Shamsollahi, shrouk Gharib and Ehab Elhosary for their help and support.

Finally, I express my deepest appreciation to my beloved parents, brothers, and friends, especially Kiarash Jalali, Reza Rajaie, Mehdi Taheri and Behnood Ghanbari for their continuous support throughout my studies.

Table of Contents

| | |
|---|-------------|
| List of Figures..... | viii |
| List of Tables..... | x |
| List of Acronyms..... | xi |
| CHAPTER 1: INTRODUCTION..... | 1 |
| 1.1 Background and Motivation..... | 3 |
| 1.2 Problem Statement..... | 4 |
| 1.3 Research Objectives and Methodology..... | 5 |
| 1.4 Thesis Organization..... | 7 |
| CHAPTER 2: LITERATURE REVIEW..... | 8 |
| 2.1 Overview..... | 8 |
| 2.2 RS and Integrated RTLS Technologies in Construction..... | 8 |
| 2.3 Integrated Sensory Data and Cloud-based BIM Platform for Progress Monitoring..... | 20 |
| 2.4 3D Object Detection Using Computer Vision..... | 23 |
| 2.4.1 Volumetric CNN Algorithms..... | 29 |
| 2.4.2 Multiview CNN Algorithms..... | 30 |
| 2.4.3 Point-Based CNN Algorithms..... | 31 |
| 2.4.4 Dataset Benchmarks for Point Cloud Data..... | 33 |
| 2.5 Digital Twin in Construction for Automated Progress Reporting..... | 33 |
| 2.6 Summary..... | 37 |
| CHAPTER 3: Research Methodology..... | 39 |
| 3.1 Overview..... | 39 |
| 3.2 Integrated RFID–UWB for Indoor Object Localization..... | 40 |
| 3.3 Integrated RTLS and Cloud-based BIM for Tracking and Progress Reporting..... | 49 |

| | |
|--|-----------|
| 3.3.1 Indoor Material Tracking..... | 53 |
| 3.3.2 Site Inspection and Progress Reporting..... | 54 |
| 3.4 Integrated RTLS and Point Cloud Data for Refined Indoor Object Localization | 58 |
| 3.4.1 Evaluation Metrics..... | 62 |
| 3.4.2 Integrated PCD and RTLS Data..... | 63 |
| 3.5 Digital-twin Platform for Automated Generation of Onsite Inspection Reports | 64 |
| 3.5.1 RTLS in a Digital Twin..... | 67 |
| 3.5.2 PCD and Computer Vision in a Digital Twin..... | 68 |
| 3.5.3 Integrated RTLS and PCD for Automated Generation of Onsite Inspection Reports..... | 68 |
| 3.6 Summary..... | 71 |
| CHAPTER 4: Method Implementation and Results | 73 |
| 4.1 Overview..... | 73 |
| 4.2 Experimental Study for Testing RFID and UWB Devices | 74 |
| 4.2.1 Laboratory Layout..... | 74 |
| 4.2.2 Experimental Study on UWB..... | 76 |
| 4.2.3 Experimental Study on RFID..... | 79 |
| 4.2.4 Experimental Study on Integrated RFID and UWB..... | 81 |
| 4.3 Onsite Case Study for Progress Reporting using MSI and QSI | 84 |
| 4.4 Experimental Study on Integrated RTLS and PCD Data..... | 90 |
| 4.5 Summary..... | 94 |
| CHAPTER 5: Conclusion..... | 95 |
| 5.1 Summary and Concluding Remarks | 95 |
| 5.2 Research Contributions | 95 |
| 5.3 Research Limitations..... | 96 |

| | |
|---|------------|
| 5.4 Opportunities for Future Work | 97 |
| REFERENCES..... | 99 |
| Appendix I..... | 104 |
| Appendix II..... | 108 |
| Appendix III..... | 112 |

List of Figures

| | |
|--|----|
| Figure 1.1: A progress tracking system in the construction phase (Sacks et al. 2020)..... | 3 |
| Figure 1.2: Overview of the reserach method. | 7 |
| Figure 2.1: S3DIS and 3DFacilities point cloud-based benchmark..... | 33 |
| Figure 3.1: Overview of the developed method. | 40 |
| Figure 3.2: Schematic diagram of the developed method for indoor object localization | 42 |
| Figure 3.3: Various steps to achieve path–loss models..... | 44 |
| Figure 3.4: System localization diagram. | 47 |
| Figure 3.5: Improved Trilateration technique for 2D localization. (a) Radius variation in extent of the RFID system range measurement error (b) Combination with the highest SoD value (yellow dash-line). | 49 |
| Figure 3.6: Overview of the developed method for digitalized site inspection and progress reporting. | 50 |
| Figure 3.7: Overview of the developed method for tracking and site reporting. | 51 |
| Figure 3.8: 3D visualization of the RTLS data..... | 54 |
| Figure 3.9: The developed method to generate onsite inspection reports: (a) progress reports: MSI (quantity-based report) and status-based reports, and (b) QSI to highlight the quality of the components used, and their targetted location..... | 56 |
| Figure 3.10: Schematic diagram of the developed method for indoor object recognition and localization..... | 59 |
| Figure 3.11: PointNet algorithm. | 60 |
| Figure 3.12: Joint RFID-based and point cloud data..... | 63 |
| Figure 3.13: Developed framework for data collection and integration using RTLS and LiDAR data. | 65 |
| Figure 3.14: A construction twin dashboard to visualize progress reporting..... | 67 |
| Figure 3.15: Flowchart of the developed method for integrating RTLS and point cloud data..... | 69 |
| Figure 3.16: Various scenarios in integrating RTLS and point cloud data. | 71 |
| Figure 4.1: Technologies used for data collection: RTLS and LiDAR. | 74 |
| Figure 4.2: Layout of the tie-points in the lab. | 75 |
| Figure 4.3: Experiment environment in the lab. | 75 |

| | |
|--|----|
| Figure 4.4: Experiment environment: (a) UWB sensors (b) UWB receiver (c) Layout of the UWB sensors placement, RFID reference tags and tie-points. | 76 |
| Figure 4.5: Real versus measured ranges. | 78 |
| Figure 4.6: Error histogram in NLoS scenario. | 78 |
| Figure 4.7: Mean and SD error values with outliers (left), and without outliers (right)..... | 79 |
| Figure 4.8: RFID system path-loss models..... | 80 |
| Figure 4.9: Integrated RFID-UWB device. | 82 |
| Figure 4.10: Site layout for digitalized progress reporting: (a) Filtration room, (b) Boiler room. | 85 |
| Figure 4.11: Sample tagged component on site for progress reporting. | 86 |
| Figure 4.12: Overview of the site reporting hierarchy: (a) reporting hierarchy, and (b) data collected for each typr of reporting information..... | 89 |
| Figure 4.13: Layout of the tie-points in the laboratory. | 91 |
| Figure 4.14: Registered point cloud data of the laboratory. | 91 |

List of Tables

| | |
|--|----|
| Table 2.1: Capabilities and limitations of standalone RS technologies..... | 8 |
| Table 2.2: Capabilities and limitations of the integrated RS technologies. | 15 |
| Table 2.3: RS technologies for indoor material localization. | 20 |
| Table 2.4: Capabilities of individual and integrated vision-based technologies. | 24 |
| Table 2.5: Deep-learning techniques for object recognition..... | 28 |
| Table 4.1: Results for path-loss models..... | 81 |
| Table 4.2: Results of the various techniques for onsite material localization. | 82 |
| Table 4.3: Near-critical activities and tagged components for site progress reporting..... | 86 |
| Table 4.4: Material-based and activity-based reporting..... | 90 |
| Table 4.5: Targeted coordinates in the tie-points (as-planned status)..... | 92 |
| Table 4.6: Preliminary results of the integrated RTLS and point cloud data using PointNet algorithm for object detection..... | 92 |
| Table 4.7: Tagged chairs' estimated coordinates and their deviations from as-planned status using Vercator Cloud for object detection. | 93 |

List of Acronyms

| Acronym | Full Name |
|---------|--|
| ANN | Artificial Neural Network |
| BIM | Building Information Modeling |
| BLE | Bluetooth Low Energy |
| CNN | Convolutional Neural Network |
| DGCNN | Dynamic Graph Convolutional Neural Network |
| DNN | Deep Neural Network |
| DRV | Distance Reference Value |
| EVM | Earned Value Management |
| GIS | Geographic Information System |
| IoT | Internet of Things |
| IoU | Intersection-over-Union |
| IPS | Indoor Positioning System |
| KNN | k-Nearest Neighbours |
| LiDAR | Light Detection and Ranging |
| LoD | Level of Development |
| MSI | Material Status Index |

NLP Natural Language Processing

PCB Printed Circuit Board

PCD Point Cloud Data

PSO Particle Swarm Optimization

QSI Quality Status Index

RANSAC Random Sampling and Consensus

RFI Request for Information

RFID Radio Frequency Identification Device

ReLU Rectified Linear Unit

RMSE Root-Mean-Square-Error

RS Remote Sensing

RTLS Real-Time Location System

RTS Robotic Total Station

S3DIS Stanford 3D Indoor Scene

ToA Time-of-Arrival

UWB Ultra-WideBand

WSN Wireless Sensor Network

CHAPTER 1: INTRODUCTION

Real-time visualization of material availability allows construction managers to improve their decision-making, reduce wait times, and improve labour productivity. Li et al. (2017) reported poor data interoperability and lack of capacity to visualize and trace information in real time as key issues in prefabricated house construction. To overcome these challenges, job sites must be well planned, and resources (e.g., workforce, equipment, consumables) must be monitored continuously (Ziahou et al. 2018). This real-time visualization can be achieved through digitalization of material tracking and management. Moreover, comprehensive inventory tracking can be implemented to identify the material delivery deficiencies and verify material locations and quantities (Azarm 2013). Geo-contextual refers to the use of technology to automate material status and location throughout the project lifecycle. The problem of finding materials on site requires near-real-time tracking to identify the most recent location and status of materials. Depending on the type of activity, information about the location and status of onsite materials can be updated regularly. This allows for the work status on site to be tracked and reports related to material planning, physical progress, and safety on site issued accordingly.

Automated material locating and tracking methods have been widely applied in the construction industry, including but not limited to progress reporting, inventory planning and management, and onsite safety. Automated methods help to overcome the limitations of traditional approaches, which rely primarily on manual data acquisition for material localization and tracking. Automated approaches can efficiently localize and track a large number of objects related to various activities. They also enable activity tracking within a desired timespan, thereby enhancing project control on site (Montaser and Moselhi 2014, Moselhi et al. 2020). Moreover, indoor object localization can be useful in the operation and maintenance phase since it provides highly accurate as-built information for 3D modelling of the indoor environment (Li et al. 2013, Moselhi et al. 2020). Object localization has also been applied for tracking workers and equipment as a way of improving safety on construction sites (Huang et al. 2021).

The dynamic nature of construction sites makes monitoring the building's operations challenging. Nevertheless, tracking a project's progress and the quality of activity execution are critical tasks in project control, as these tracking activities provide a large amount of as-built information related to various activities on site. Such reporting, however, is highly

complex, given the challenges associated with real-time data acquisition and processing large amounts of information for various functions, such as scheduling and cost management. Onsite object tracking is an integral part of a progress reporting system that entails identifying and localizing the installed objects. Sacks et al. (2020) identified two main drawbacks in conventional project progress monitoring: (1) reactive correction, where actual performance is found to deviate from planned performance after it is too late to correct the project's direction; and (2) a focus on monitoring construction activities while overlooking the flow of materials, labour, equipment information, and locations. As an alternative to the conventional approach, they proposed a progress tracking system (see Figure 1.1) in which activities are monitored to capture the as-built state of the building under construction. Such a model can be used to compare the as-designed and as-planned information in order to determine discrepancies, which would, in turn, inform the next round of control.

Digital Twin is another innovation that has found applications across the project life cycle. Its application in the operation and maintenance phase has been widely investigated in many studies. Moreover, it has been used in the early project stages for planning and scheduling. “Construction twin” is a new term for applying digital twin in the construction phase and tracking the project's progress and execution capitalizing on the digital twin's capabilities. Technologies such as the Internet of Things (IoT), Real-Time Location system (RTLS) technologies, 3D imaging and computer vision, optimization, and simulation techniques have been integrated with digital twin to bring to bear significant innovations within the domain of construction project control (Sacks et al. 2020).

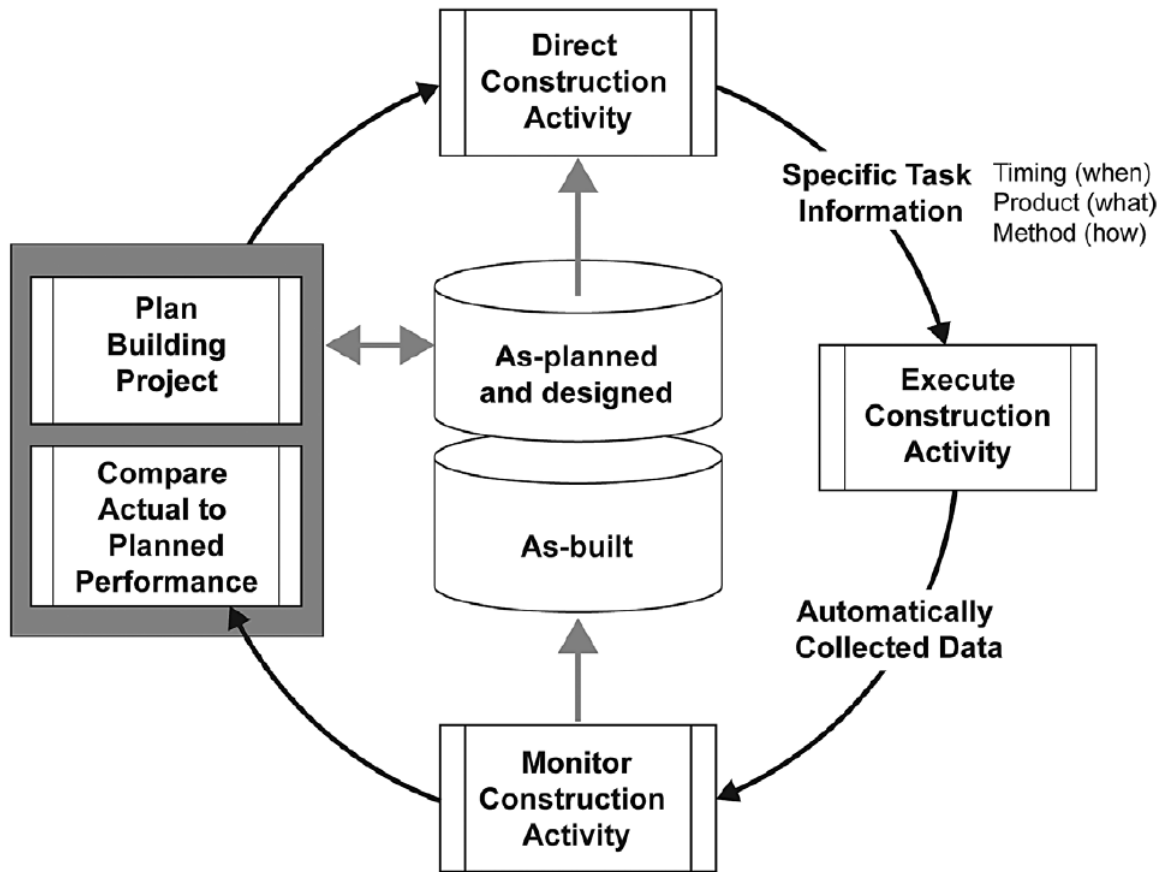


Figure 1.1: A progress tracking system in the construction phase (Sacks et al. 2020).

1.1 Background and Motivation

Having timely access to accurate and reliable onsite information is vital for efficient management of construction operations. Late detection of onsite operations' issues, on the other hand, can be problematic, leaving insufficient time for the project team to react, and thereby adversely affecting the project cost and schedule. Near-real-time information facilitates tracking of project operations and enhances project safety and productivity (Moselhi et al. 2020). Based on the project type and the associated activities, various technologies and data collection tools can be used to ensure sufficient information is captured to represent the performance and progress of the activities on site. Automated data acquisition aids in this regard, providing accurate and timely information. The captured data can be compared to the equivalent as-planned data to automatically generate progress reports and create as-built models (Moselhi et al. 2020).

In this regard, object localization has been widely applied in the operation and maintenance phase to obtain accurate as-built information for 3D modelling of the built environment

(Montaser and Moselhi 2014, Li et al. 2017). Indoor localization in particular warrants further study to overcome the limitations of using GPS-based solutions in indoor spaces. For indoor settings, various Remote Sensing (RS) technologies, such as Radio Frequency Identification Device (RFID), Ultra-WideBand (UWB), Bluetooth Low Energy (BLE), and Wi-Fi, have been investigated as cost-effective and practical solutions. These efforts have been mainly focused on using these technologies for indoor inventory management to avoid loss and damage of materials and tools (Bardareh and Moselhi 2022). Localization and accessing of onsite information can be challenging due to the dynamic nature of onsite operations, including material delivery and utilization. Furthermore, there are challenges associated with timely data acquisition and handling of large amounts of information for various operations onsite (Sacks et al.2020). An object localization system's feasibility and cost are other notable concerns. Overall, indoor material management and localization on project sites have been identified as areas with great potential for improvement (Li et al. 2013, Moselhi et al. 2020, Montaser and Moselhi 2014).

1.2 Problem Statement

Indoor object identification and localization using RS technologies have had various applications in project control. These includes near-real-time tracking of objects in indoor spaces and automated construction progress reporting. However, the following gaps are identified with respect to existing solutions:

- I. Many tasks associated with sensory data collection are still manual, inefficient, and expensive, especially in environments with high complexity and interconnectivity. Moreover, existing solutions require extensive infrastructure to be installed on site, while the presence of obstacles hinders their performance (Bardareh and Moselhi 2022, Moselhi et al. 2020). There is thus a need for a less costly and more practical indoor positioning system.
- II. Tracking onsite operations with RS technologies is inherently challenging. Researchers have introduced the integration of material tracking with progress tracking as a solution to track a project's progress by monitoring the consumed materials on site (Moselhi and Azarm 2013). However, a solution that supports various activities on the job site that are not necessarily connected to a moving object, and that enables tracking of the status and location of the consumed materials, needs further investigation.

- III. Tracking of onsite operations with objects in elevation, such as MEP activities, necessitates accurate 3D coordinates (i.e., within a range of a few centimetres) of the tracked objects. Some researchers have provided solutions for the 3D localization of objects in indoor spaces using technologies such as RFID and UWB. Moreover, the use of Light Detection and Ranging (LiDAR) devices to generate Point Cloud Data (PCD), and in integration with Building Information Modeling (BIM), Scan-To-BIM, has been investigated in many studies. However, these technologies have limitations associated with their range, accuracy and application for various construction activities and environment, besides their implementation's cost and effort (Bardareh and Moselhi 2023). A solution is needed to integrate these technologies and more fully leverage their capabilities to provide accurate as-built 3D coordinates. Furthermore, the use of computer-vision algorithms for 3D object detection and segmentation using PCD needs further study.
- IV. Applications of digital twin have been carried out in various phases of project life cycle. However, few studies have explored its application in the construction phase and for project control in particular (Sacks et al. 2020). Besides the application of IoT solutions through a digital twin to monitor the site environment, a digital twin that brings together AI and computer-vision capabilities to generate onsite inspection reports, and that provides information required for decision support during project execution, warrants further investigation.

1.3 Research Objectives and Methodology

In light of the challenges identified in the problem statement, the primary objective of this research is to develop a progress monitoring framework—comprising indoor object identification and localization—for automated inspection reporting in the construction phase. This objective is pursued through the following sub-objectives:

- I. Develop an Indoor Positioning System (IPS) for location identification of objects in indoor spaces: The integrated use of the two RS technologies—RFID and UWB—capitalizes on the benefits of each technology, providing a cost-effective and practical solution for acquiring accurate 2D and 3D coordinates of objects labelled with RFID tags.
- II. Achieve semi-automated progress reporting through the joint use of RTLS technologies and a cloud-based BIM platform: Under this sub-objective, leveraging Material Status

Index (MSI) and Quality Status Index (QSI), onsite information on object quantity, status, and location is used to generate progress reports.

- III. Integrate Real-Time Location System (RTLS) data and PCD, capitalizing on computer-vision algorithms to refine 3D localization in the scene. This integration is achieved by acquiring ID, status and 3D coordinates of the objects scanned on site with RTLS and LiDAR technologies. RTLS coordinates are refined through using accurate 3D coordinates of the detected objects using segmentation capability of a computer vision algorithm.
- IV. Developing a construction twin platform and a related dashboard to update 3D models and generate progress reports: The dashboard provides a direct line between the physical objects and the digital environment by creating a bi-directional connection between the BIM model and the objects on site.

Corresponding to the above-mentioned sub-objectives, the research method consists of four main streams, as depicted in Figure 1.2. The first stream involves the use of RTLS technologies, RFID, and UWB to develop an IPS for object identification and localization in 2D and 3D format. In the second stream, information about the location and status of the tagged objects is then visualized in a cloud-based BIM platform in Geographic Information System (GIS) cloud packages. Moreover, two indices, MSI and QSI, are introduced to track the overall and detailed progress of project activities by monitoring material consumption and quality. The third stream involves the use of a computer-vision method to refine the 3D localization information obtained using the RTLS technologies. For this purpose, the accurate PCD (i.e., coordinates) obtained using computer-vision algorithms is exchanged with the 3D coordinates of the objects identified by the RTLS. In the fourth stream, the RTLS and PCD is mapped to a cloud-based BIM platform in order to visualize the tagged objects and generate the onsite inspection reports via a digital-twin platform. The onsite inspection reports contain the progress information and the object locations (obtained using the quantity and status of the identified and localized objects).

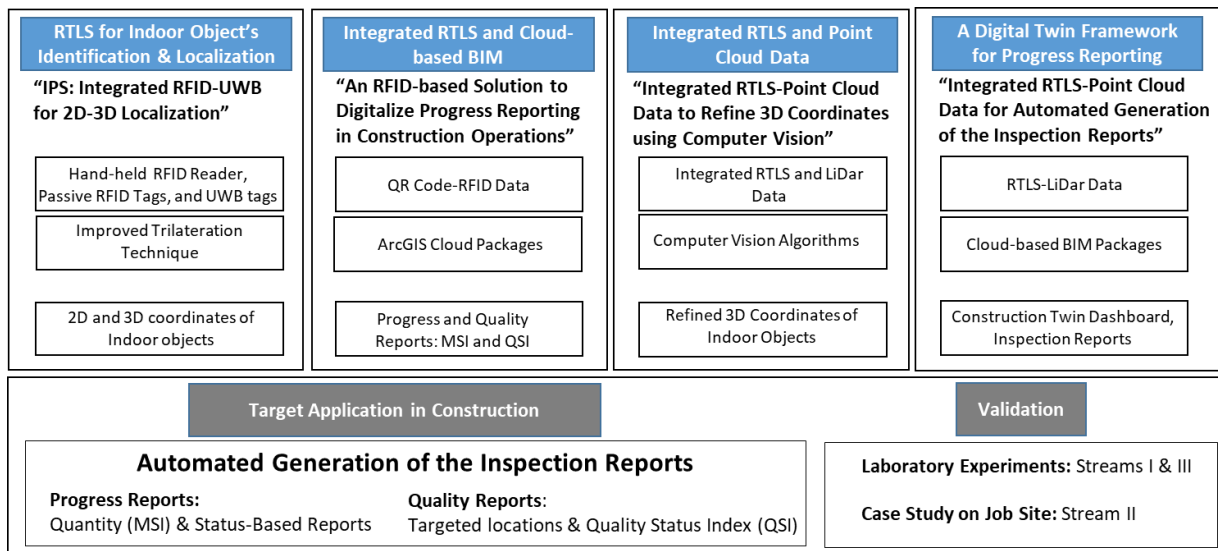


Figure 1.2: Overview of the reserach method.

1.4 Thesis Organization

This research is presented in five chapters. Chapter 1 introduces the research problem and motivation, outlines the objectives, and provides an overview of the method developed to achieve the defined objectives. Chapter 2 presents a review of the scientific literature in this domain, highlighting the identified gaps in the body of knowledge. The review focuses on RS technologies, computer-vision applications for PCD analysis, digital twin in construction, and automated progress reporting. Chapter 3 presents the methods developed in this study, focusing on the integrated use of RFID–UWB for indoor localization, integration of RS technologies with a cloud-based BIM platform, the integration of RTLS–PCD data to enhance 3D localization in indoor spaces, and the developed digital-twin platform for automated generation of the onsite inspection reports. Chapter 4 describes the experimental and case studies carried out to validate the developed methods, noting the limitations of each method. Finally, Chapter 5 outlines the conclusions drawn, the contributions of this research study, and opportunities for future work.

CHAPTER 2: LITERATURE REVIEW

2.1 Overview

A review of the relevant literature reveals that there is a range of different technologies for automating and enhancing onsite inspection and reporting. In the present study, the main focus is on the use of Real-Time Location system (RTLS) technologies, such as Radio Frequency Identification Device (RFID) and Ultra-WideBand (UWB) sensors, for indoor object localization. Moreover, the use of computer-vision techniques for the detection of 3D objects in Point Cloud Data (PCD) obtained using Light Detection and Ranging (LiDAR) technology is reviewed. The incorporation of Building Information Modeling (BIM) data is also reviewed in order to identify challenges related to progress reporting in construction. Despite the recent progress in this domain, there are still obstacles hindering the realization of a practical and comprehensive automated solution for onsite progress tracking. The integration of the above-noted technologies with a cloud-based BIM platform and digital-twin to enhance communication between sensors and physical assets is also reviewed. Finally, the application of these technologies for automated tracking and progress reporting in construction is investigated.

2.2 RS and Integrated RTLS Technologies in Construction

There is a wide range of Remote Sensing (RS) technologies for data acquisition on site. Each of these technologies has capabilities and drawbacks based on the domain of applications. The selection of one particular technology can vary depending on the type and accuracy of the information, and the environment in which the data will be acquired. Most previous attempts in this field were focused on single-sensor models, which are not usually applicable for the entire duration of a project. Table 2.1 provides a brief overview of these technologies, their capabilities, limitations, and accuracy.

Table 2.1: Capabilities and limitations of standalone RS technologies (Moselhi et al. 2020).

| RS Technology | Capabilities | Limitations | Accuracy |
|--|--|--|---|
| GPS, RTKGPS ¹ , and GNSS ² | (1) Global access in an outdoor environment (2) RTK GPS provides centimetre-level positioning accuracy in | (1) The acquired data are limited to position and time of objects, and not the identity or type of activities (2) Delays in data processing and | Almost 1 m for GPS and a few centimetres for RTKGPS |

| | | | |
|-----------------------------|---|---|--|
| | <p>real time over long distances</p> <p>(3) Flexibly and reacting quickly based on the needs in a construction site</p> | <p>transferring (an important issue specially for real-time operations such as equipment tracking or kinematic surveying)</p> <p>(3) Multipath errors in the congested environment</p> <p>(4) Signal blockage and building obstructiveness in an indoor environment</p> | |
| Robotic Total Station (RTS) | <p>(1) Enhanced tracking and automation capabilities in the positioning of objects</p> <p>(2) High positioning update rate</p> <p>(3) Higher vertical positioning (elevation) accuracy than unaided GNSS and GPS-based technology</p> | <p>(1) The high investment</p> <p>(2) Limited capability to track only one point at a particular time</p> <p>(3) Positioning errors will occur if the angles and distances are not captured simultaneously</p> | <p>Down to a few millimetres and arc seconds</p> |
| Barcode | <p>(1) Reasonable price</p> <p>(2) Straightforward usage with standard implementation protocols</p> <p>(3) Speeding up the computer data entry</p> <p>(4) Portability</p> | <p>(1) Very limited reading range</p> <p>(2) Sensitivity to the harsh environment³ (e.g., tags are not readable if covered by snow)</p> <p>(3) Low data storage capacity</p> | <p>N.A</p> |
| RFID | <p>(1) Longer range than barcodes (up to 100 m for Ultra-high frequencies)</p> | <p>(1) Lack of accuracy and difficulties for 3D positioning</p> | <p>Down to a few metres for 2D localization</p> |

UWB

- | | |
|---|---|
| <ul style="list-style-type: none">(2) Non-line-of-sight(3) Providing cost efficient location information(4) Tags are light and easy to attach(5) Unlike barcodes, RFID tags are durable in construction environments(6) Batch readability of tags making identification process much more efficient | <ul style="list-style-type: none">(2) Calibration difficulties (e.g., the need for a path loss model)(3) Affected by multipath effect(4) Problems associated with simultaneous identification of many tags(5) Active tags are fairly expensive.(6) Plus, relatively wide range may cause obstruction object detection(7) The need for battery replacement in active tags(8) Influenced by metal and high humidity specially in high frequencies |
| <ul style="list-style-type: none">(1) A longer range (up to 1000 m), higher measurement rate and positioning accuracy (less than 1 m) than typical RFID systems(2) Less influenced by metal and high humidity(3) Suitable for both indoor and outdoor environment(4) Not affected easily by other RF systems | <ul style="list-style-type: none">(1) Violation of line-of-sight can lead to the performance degradation specially in congested areas(2) Limited update rate(3) Multipath and radio noise effect in the case of metal occlusion(4) Some calibration difficulties (e.g., geometry and number of sensors) |
-

| | | | |
|----------------------|--|--|--|
| Infrared | <ul style="list-style-type: none"> (5) Relatively immunity to multipath fading (6) Reliable 3D localization even in harsh environment (1) High noise immunity (2) Low power requirement (3) Low circuitry costs (4) Higher security (5) Portability | <ul style="list-style-type: none"> (5) Tagging issues (e.g., battery replacement) (6) High cost (7) High missing data (8) Degraded range measurement as distance increases (1) Dependency on line-of-sight due to its inability to penetrate materials (2) Sensitive to light and weather condition (3) Low data transmission rate (4) Short range (5) Not passing walls unlike other RF wireless links (6) Limitation associated with scalability | Down to a few centimetres |
| Photo/Videogrammetry | <ul style="list-style-type: none"> (1) Straightforward configuration (2) Cost-effective field data collection (3) Portability (4) Provides information about the material, texture, and colour of the target object (5) High update rate (6) Well known internal geometry (7) Good interpretability | <ul style="list-style-type: none"> (1) Calibration difficulties (e.g., sensitive to the surrounding light condition, visual occlusions, and moving background) (2) Mirror effect caused by reflective surfaces (3) Less accurate than laser scanners in generating PCD (4) Problems associated with computing | Approximately 1% error in volumetric measurement |

Laser scanning

- | | | |
|---|--|--|
| <ul style="list-style-type: none">(1) High accuracy in generating PCD(2) Simple and well-defined internal coordinate system(3) Homogeneous spatial distribution of range points(4) Ability to scan actively in darkness and shaded areas(5) Ability to measure areas without texture(6) Ability to scan a large area | <ul style="list-style-type: none">depth in 3D modelling(5) Difficulty in identification of objects with unclear geometric configurations(6) Computational complexity of photogrammetric surveying(7) The need for another technology (e.g., RTKGPS or RTS) to provide the geo-referenced inputs for photo-based 3D modelling(1) High cost of laser scanners(2) Scanning is a time-consuming process(3) Occlusion problem and the need for a clear line-of-sight(4) More post-processing effort is required if the device moves(5) Limitations associated with modelling of edges and linear features(6) High storage capacity is needed(7) Not suitable for modelling moving objects(8) Not providing information | <p>Approximately 2% error in volumetric measurement and a few centimetres in ranging measurement</p> |
|---|--|--|

about material
type, texture,
and colour of the
scanned objects
(9) Eye-safety
distance
concerns

¹ Real-time kinematic GPS, ² global navigation satellite system, ³ extreme cold or hot weather in an outdoor environment.

RFID technology has been used in this respect with great capabilities for automatic identification and tracking of tagged objects on site. It applies to both built facilities and during construction activities due to its Non-Line-of-Sight (NLoS) capability, wireless communication, and on-board data storage capacities (Li et al. 2011). Besides identification-based applications, RFID technology is also used for localization of the tagged objects (Cai et al. 2014, Maneesilp and Wang 2012, Montaser and Moselhi 2014, Su et al. 2014). The main methods to localize an object using RFID sensors are trilateration, triangulation, proximity, and scene analysis. According to the literature, the former two techniques have been used primarily for tag localization. The proximity technique is conducted by using some reference points, where localization is based on a tag's closeness to each of these reference points. Scene analysis uses some algorithms, such as *k*-Nearest Neighbours (KNN) or probabilistic methods, to localize tagged objects based on the similarity of the received signal with a prior location fingerprint collected from the environment. In the range-based techniques mentioned above, the distance between a hand-held RFID reader and a tagged object is measured by converting Received Signal Strength (RSS) values to an experimental range value. Montaser and Moselhi (2014) investigated the application of the RFID technology for indoor location identification of the materials through a set of experiments. In this study, the roving RFID reader and tags' locations were achieved using a path-loss model and trilateration technique (Bardareh and Moselhi 2022, Moselhi et al. 2020). Wu et al. (2019) experimented using the RFID system for construction equipment tracking. They developed a positioning algorithm based on differential RSS while investigating the effect of environment and orientation between RFID tags and receivers on localization accuracy. Yoo and Park (2019) investigated RFID-based processes in a production plant of precast walls and beams. They found that the time required for locating materials was reduced from 25.23 min to 0.57 min compared with traditional manual methods. Besides identification-based applications, RFID technology is used to localize construction components to enrich the tracking of the materials (Cai and Andoh 2014, Maneesilp and Wang 2012, Moselhi and Azarm 2013, Su et al. 2014, Ta et al. 2017). Montaser and Moselhi (2014) experimented the application of RFID technology for indoor location identification of the

materials to track indoor materials. Yoo and Park (2019) evaluated an RFID-based solution for construction equipment tracking. They developed a positioning algorithm based on differential RSS while investigating the effect of environment and orientation between RFID tags and receivers on localization accuracy.

UWB technology is an RTLS that has a performance almost similar to an active RFID system. It uses very narrow pulses of radio frequency waves which are occupied in a wide bandwidth for communication between tags and receivers. Due to the advanced technology available in the UWB sensors for accurate time measurement in range of nanoseconds, different positioning techniques such as Time of Arrival (ToA) or Time of Flight (ToF), Angle of Arrival (AoA), Time Difference of Arrival (TDoA), and RSS-based techniques are used to localize objects by using this technology. Several researchers have investigated the use of this technology for location identification of the resources in the construction projects. Most of their efforts are focused on evaluating real-time tracking of workers, equipment and materials in an indoor and outdoor environment to improve productivity and safety on construction sites (Cheng and Venugopal 2011, Moselhi et al. 2020, Park and Cho 2016, Siddiqui et al. 2014), Masiero and Fissore 2017). Shahi et al. (2014) used UWB tags to localize and track the activities associated with the pipeline and plumbing system of a building in order to improve progress reporting of these operations. Other studies have investigated the effect of the UWB sensors' distribution geometry, employment of filters (i.e., Kalman Filter, particle filters and etc.), as well as the use of static reference tags to enhance the localization accuracy of these sensors (Almeida et al. 2005, Cheng and Venugopal 2011, Jimenez and Seco 2016, Nurminen and Ardeshiri 2015, Razavi et al. 2012, Siddiqui et al. 2014, Song and Tanvir 2015, Sun and Wang 2020, Xu and Shmaliy 2018, Zhue and Ren 2016).

The literature reveals that using a single source of sensory data does not provide sufficient information about the status of onsite construction operations. For example, the PCD captured by laser scanners require a direct line-of-sight, and they will become less effective as the project progresses and the site becomes obstructed due to increased congestion. In this way, the usage of another data acquisition technology could alleviate the drawbacks associated with individual usage of each RS technology in each of the project execution phases. That integration provides more timely and accurate information due to the complementarity and possible fusion of the captured data (Moselhi et al. 2020). Table 2.2 illustrates the integrated use of these RS technologies, capabilities, and limitations.

Table 2.2: Capabilities and limitations of the integrated RS technologies.

| Type | Integrated RS System | Capabilities | Limitations |
|---|--------------------------------------|---|--|
| Positioning systems integration with other sensory data | GPS + Barcode | <ul style="list-style-type: none"> (1) Relatively low cost (mainly goes for GPS receiver); barcode: Label ~ \$0.1, Reader ~ \$100–500 and GPS: Receiver ~ \$200 (2) High level of standardization and reliability (3) More scalable for projects of varying sizes (4) Straightforward implementation | <ul style="list-style-type: none"> (1) Need for free access to space for GPS system which makes it unsuitable for interior environment (2) Limitation of barcode tags in differentiating between items of the same kind (3) Not fully automated approach |
| | GPS + RFID | <ul style="list-style-type: none"> (1) Easier material identification due to non-line-of sight capability of the RFID tags (2) Providing both identification and localization data simultaneously | <ul style="list-style-type: none"> (1) The need for free access to space for GPS system (2) A large number of RFID readers are required which increases the cost; RFID Tag ~ \$1–50 and RFID Reader ~ \$1k–5k (3) Boundary constraint limitations in cluttered environments |
| | Sensor-aided GPS (SA-GPS) | <ul style="list-style-type: none"> (1) Stability to be used in various construction operations (2) Real-time tracking and reporting capabilities (3) Not sensitive to the ambient environment (4) Having both location/action recognition capabilities (5) Providing continuous update of the location estimates | <ul style="list-style-type: none"> (1) Obstacles associated with data fusion, coordination, processing, and reduction of data to produce meaningful conclusions (2) Requiring relatively more time for post processing (3) Drift inherent to sensors (4) Initialization and calibration difficulties |
| RFID integration with other sensory data | RFID + Wireless Sensor Network (WSN) | <ul style="list-style-type: none"> (1) Make it possible for tags to communicate with each other (2) Facilitating the negotiation of RFID readers together (3) Increased positioning accuracy | <ul style="list-style-type: none"> (1) Sensor does not provide any power until tag is not in the radio frequency field to communicate with reader |

| | | | |
|---|--|--|--|
| | | (4) Decreased energy consumption in comparison with an individual WSN ¹ system | (2) Reading range decreases as the system starts using energy |
| | RFID + LS | (1) Faster and more robust recognition and positioning of objects in 3D modelling (2) Alleviating the difficulties associated with the laser scanners object recognition specially in a crowded and full of furniture environment | (1) Poor positioning performance when the objects are in the corner of a room (2) Laser scanners are relatively expensive (a terrestrial laser scanner could cost more than \$60k) (3) Need for a facility management database of the available objects in advance |
| Integration of vision-based technologies together and with other RTLS | Photogrammetry + laser scanning | (1) Less number and time for scanning are required (2) Less number of digital photos are required which results in less computational effort (3) Better object recognition capabilities by adding depth information from laser data to the available digital photo planes (4) Convenient for modelling objects with unclear geometrical properties (e.g., excavation activities) (5) More accuracy in the localization of edge points (6) Providing more details about material, colour, and texture of the objects which improves the geometry and visual quality of the 3D modelling (7) Self-calibrating capabilities for cameras | (1) Expensive laser scanners (2) Problems associated with calibration and orientation of data acquired from two sensory sources, e.g., geo-referencing issues (3) Less effective when the site is crowded or covered by enclosures |
| | Photogrammetry + RTS (robotic total station) | (1) Enhanced scaling and 3D modelling capabilities (2) Better measurement accuracy (down to a few decimetres) rather than using individual | (1) High cost of RTS devices (2) Synchronization of digital cameras with RTS devices |

| | | |
|-----------------------------------|---|--|
| | photogrammetry techniques | (3) Limited capability for tracking multiple moving objects |
| Photo/video grammetry + UWB | (1) More reliability in positioning in comparison with individual use of each technology by replacing the data of one sensor with another in case of any failure in each sensor | (1) Calibration difficulties specially for large scale sites |
| | (2) More accurate and timely information are provided by proving more automation and decreasing computational effort in photogrammetry | (2) Error propagation phenomenon due to the intrinsic inaccuracy in each technology |
| | (3) Portability | (3) Less accuracy in comparison with other geo-referenced photogrammetry techniques (e.g., using a RTS or GNSS system) |
| Laser scanning + UWB | (1) Overcoming challenges associated with the presence of multipath, NLOS ² propagations and low visibility (e.g., occlusion, dust, fog, etc.) | (1) Discrepancy between the accuracy of the UWB mapping and that of LiDAR mapping |
| | (2) Less accumulated error in comparison with an individual usage of laser scanning technology | (2) High implementation cost |
| | (3) Ease of need for prior knowledge or control inputs | |

¹ Wireless sensor network, ² non-line-of-sight.

One group of these RS technologies includes RTLSSs such as GPS, RFID and UWB. Most of the technologies mentioned in the literature function based on signal measurement techniques such as the ToA principle, where a signal's propagation speed and propagation time directly lead to a corresponding distance. For instance, range-based localization is usually based on trilateration and triangulation techniques in which the Received Signal Strength Index (RSSI), phase-based indicator and ToA are used to measure the range distance from a tagged object (Moselhi et al. 2020, Montaser and Moselhi 2014). Moselhi et al. (2020) investigated the accuracy of the proximity and triangulation techniques for 2D localization of the RFID tags attached to a number of objects. They concluded the triangulation technique has better localization accuracy than other range-based measurement techniques. Su et al. (2014) developed a boundary condition trilateration technique for RFID tags' localization. It is based on selecting combinations of RFID reader locations from a boundary condition scenario. In

that scenario, a tag was localized if it appeared on the boundary circle, which has a radius equal to the maximum reading range of the RFID device. The combinations with location distribution that were more than a standard spatial dilution factor were selected to achieve better localization accuracy. Li et al. (2019) evaluated the use of range-free techniques, such as fingerprinting, in order to localize RFID tags. In this technique, the position of the target tag is obtained based on the coordinates of the dense reference tags, which in turn are selected via database matching. Researchers have also considered the use of optimization and machine-learning algorithms to improve the localization information acquired from the RS technologies. For instance, Ibrahim (2015) used the Particle Swarm Optimization (PSO) algorithm to enhance the path-loss model achieved from a WSN system for indoor object localization. Valero et al. (2016) investigated using a machine-learning algorithm to estimate the distance of the tagged objects by translating the signal strength received from the receivers. They used a BLE system in which a combined Convolution Neural Network (CNN) and Artificial Neural Network (ANN) was employed to localize the BLE tags.

Recently, there have been some efforts to localize and track people and objects using Wi-Fi, Bluetooth, and Bluetooth Low Energy (BLE) technologies for occupancy measurement. In fact, by installing some receivers in a target area, the location and number of detected items are estimated using smartphones, Bluetooth headsets, and smartwatches. It is done by tracking the changes in the received electromagnetic wave patterns, comparing them with calibrated models to count the number of workers or vehicles on site, and providing rough information about their location and behavioural algorithms. However, due to some legal restrictions for using smartphones on site and not entirely accurate results of this technology, its use in the construction industry is not common yet. In a different context, barcode and RFID are valuable technologies for material identification with applications in tracking resources for a supply chain management system. Vision-based technologies such as photo/videogrammetry and laser scanning have also found applications in the construction industry for making 3D as-built models of the site, providing sufficient information for automated progress reporting (Moselhi et al. 2020). Integrating GPS with RFID would provide a reasonable solution that benefits the localization and identification capability of both technologies. There are various scenarios for implementing such a system in order to have better outdoor resource tracking and management. In one scenario, the GPS receiver is attached to a roving RFID reader to provide information about the position of the RFID reader. By knowing the real-time location of the roving RFID reader, the 2D location of the tagged items is identified using the trilateration technique. Having

said that, this technology is not accurate enough for the localization of objects in elevation since GPS-based technologies cannot provide accurate information about height. As stated, accuracy is an important factor when deploying a system for data acquisition in a construction site. Therefore, integrating RFID with other positioning technologies like GPS-based systems is a solution to have higher accuracy in tracking tagged items. Having said that, GPS solutions present some drawbacks in specific environments, especially when it comes to building interiors. To avoid the limitations of RFID and GPS-based systems, the combination of ultrasound technologies and RFID can improve the positioning system (Moselhi et al. 2020).

The RTLS has many applications in construction for localization and tracking of the assets and equipment on site (Bardareh and Moselhi 2020, Montaser and Moselhi 2014). These technologies include RFID, UWB, BLE, GPS, and Wi-Fi sensors. The integrated use of these technologies to enhance the localization and tracking of objects on construction sites has been widely studied (Bardareh and Moselhi 2020, Moselhi et al. 2020). The localization information provided by the RTLS is used for 3D modelling and mapping of the materials on site. Knowing the location of the objects on site makes it much easier to manage the storage yard and construction site and have a more accurate and timely supply chain management system. These technologies usually use tags and receivers to communicate together. In this regard, a tag is identified by a specific ID written on it, and then objects are labelled with each tag. The receivers constantly communicate with the tags to acquire information about the site and to transfer the information to the server. In this way, the information about the objects' location and the object's presence in each zone is gathered automatically and in real-time for the associated applications. Many studies have investigated the use of various RS technologies to automate localization and tracking of the objects on site (Akhavian and Behzadan 2015, Andoh et al. 2012, Bardareh and Moselhi 2020, Ibrahim and Moselhi 2014, Jo et al. 2015, Kalikova and Krcal 2017, Labant et al. 2017, Li et al. 2013, Moselhi et al. 2020, Seo et al. 2013, Su et al. 2014, Ta 2017, Yoo and Park 2019). Chen et al. (2020) introduced a new method in which an integrated use of the Ultra-Wideband (UWB) and RFID helps to efficiently localize the objects in an indoor environment. This integration is aimed to overcome the high cost of sensors such as UWB and GPS for localization and tracking of large numbers of objects on construction sites. Moreover, the integrated use of the two technologies provides more accurate localization information not only in 2D but also in 3D object localization, which is essential for improving the BIM of the site. For this purpose, a sample number of objects labelled using inexpensive passive RFID tags are localized at the experimental level. The novelty of this

integrated system causes a more economical and accurate method for indoor material localization than the methods in the literature. In a set of experiments on these technologies, the performance of the developed method for object localization is validated. Table 2.3 provides a brief review on the capabilities, limitations and localization accuracy of the RFID, UWB and the developed method in this study, along with comparing approximate cost of each system with the developed method (Moselhi et al. 2020). The cost of operating each of these systems is based on the current price of the sensors and devices available in the market that are used in this experimental study (DecaWave 2016). The UWB used in the experiment is an off-the-shelf evaluation kit that is open source and not a final product. The cost of commercial UWB systems available in the market is much higher, making the developed method a rational choice to economically localize indoor objects.

Table 2.3: RS technologies for indoor material localization.

| Technology | Advantages and Capabilities | Limitations | Cost* | Localization Accuracy |
|---------------------|--|--|--------|---------------------------|
| RFID | <ol style="list-style-type: none"> 1) Inexpensive 2) Non-line-of-sight 3) Availability in market 4) Batch readability of tags 5) Straightforward usage | <ol style="list-style-type: none"> 1) Low localization accuracy 2) Calibration difficulties 3) Affected by multipath effect 4) Need for a roving surveyor | \$800 | Down to a few metres |
| UWB | <ol style="list-style-type: none"> 1) Long reading range (up to 100 m) of the sensors 2) Less influenced by metal and high humidity 3) Relatively immunity to multipath fading 4) Reliable 3D localization even in harsh environment | <ol style="list-style-type: none"> 1) High cost 2) Multipath and radio noise effect in the case of metal occlusion 3) Degraded range measurement accuracy as distance increases | \$50k | Down to a few centimetres |
| Integrated RFID–UWB | <ol style="list-style-type: none"> 1) Inexpensive with acceptable localization accuracy 2) Straightforward usage | <ol style="list-style-type: none"> 1) Data synchronization 2) Need for a roving surveyor | \$2.8k | Approx 1 m |

* Assuming the need for localization of 100 objects on site (the values are in Canadian currency).

2.3 Integrated Sensory Data and Cloud-based BIM Platform for Progress Monitoring

Joint use of tracking technologies with cloud-based construction platforms provides capabilities for digital transformation by facilitating access to onsite information. In case of a

Request for Information (RFI), updating the site status is possible through this integration. Furthermore, cloud-based platforms help to centralize information and enhance communication between parties to access the required information. A couple of cloud-based packages with BIM-based capabilities are available on the market. While they benefit from great capabilities for digitalizing the data acquisition and visualization on site, they still need to improve on limitations such as manual data entry and RFI options. Integrating the RTLS with cloud-based BIM platforms to address this issue has been widely studied and implemented in construction projects. In this integration, rather than using digital tools such as 4D BIM to improve the accuracy of material estimation or the visibility of material status, the integration distinguishes itself by adding capabilities to synchronize actual site progress with the material delivery status (Chen et al. 2020). An example of this integration is the use of RFID, which has many applications in construction for automated tracking and localization of objects. Integrating RFID technology and BIM creates a more systematic, automated, and intelligent job site. The application of the integrated use of BIM and RFID includes but is not limited to improving material tracking, automating and providing better visualization for site inspection, and a more effective workforce (Chen et al. 2020, Costin et al. 2015, Montaser and Moselhi 2014, Moselhi et al. 2020).

The integrated use of RFID technology and BIM has been studied to create a more intelligent and automated job site. This integration provides a digital link between the virtual models and the physical components in the construction process, which improves information exchange for construction and building management applications (Costin et al. 2015). Chen et al. (2020) investigated the joint use of RFID and BIM for look-ahead planning to improve material flow processes. In their research, the RFID tags were assigned to the materials from the supplier side, while the information about those materials was updated in the RFID-BIM platform and exchanged with the construction contractor through a central database. Li et al. (2017) showed that the integrated use of BIM and RFID technology decreases the lead time of the construction elements by approximately 15% due to the enhanced tracking of the delivery status. Wang et al. (2017) developed a BIM–RFID framework to ensure the location coordinates of the prefabricated concrete elements were read and compared with the expected location in BIM. Yin et al. (2009) developed a BIM cloud system based on the received RFID timestamps and the material geolocation. It was found that 15.23% of lead time was reduced given the increased efficiency of tracking the delivery status of individual prefabricated elements and sharing the information quickly among associated project participants. Xu et al. (2018) showed that using

the cloud-based BIM and RFID system facilitates real-time information sharing to reduce project time. Li et al. (2017) developed an RFID-enabled multidimensional BIM platform to alleviate schedule delay problems encountered in the construction of prefabrication housing. For this purpose, they developed a platform for real-time progress monitoring of a project and better progress visualization to identify any delay in precast fabrication and delivery. They also generated real-time data to produce leading indicators for safety and building protocol control and to enhance quality control by reducing rework or damage of the finished work.

Surveillance is a must to ensure that projects are progressing as planned and to plan for future actions during the execution period. In project control, it is essential to constantly track the project's schedule, cost, and quality. Earned Value Management (EVM) is a technique that addresses part of these needs by bringing cost and schedule variance analysis together to provide managers with more accurate project status and predict future project performance. Besides the outstanding capabilities of the EVM in project control, it has limitations, such as dependency on the project baseline and inaccurate schedule forecasts to estimate the end of a project. Some of these drawbacks are addressed by frequently reporting the number of consumed materials associated with various activities on site. Since the accuracy of EVM indices significantly depends on the frequency of actual data acquisition from the site, the use of innovative technologies helps to increase the data collection rate (Azarm 2013). Some researchers have argued that schedule measures of the EVM need to be revised since they deliver schedule variance and index in terms of monetary value (Khamooshi and Golafshani 2014, Moselhi and Azarm 2013). Moselhi and Azarm (2013) proposed focusing on critical activities rather than all activities, as non-critical ones may mask the project's actual performance. Balali et al. (2020), Khamooshi and Golafshani (2014), and Roghabadi and Moselhi (2020) introduced other versions of the EVM focusing on enhancing schedule measurements, such as Earned Schedule Management (ESM) and Earned Duration Management (EDM). Roghabadi and Moselhi (2020) developed a method to distinguish critical activities from non-critical ones while considering the effect of future risks to predict the project duration. A field study was conducted by Balali et al. (2020) to list various factors affecting the EVM cost estimations for road projects using a CNN, and the results were compared with those of conventional EVM and the regression method. Moselhi and Azarm (2013) insisted on the importance of onsite material management and how it affects schedule performance. Their work considered the interconnectivity between the material consumption and the schedule performance index to enhance project control. They developed a material-

based index to enhance the project control by improving the existing EVM and its indices by focusing on the critical activities to inhibit the effect of the non-critical activities on the project forecasting accuracy. Based on the literature, tracking consumed materials provides benefits over tracking the cost and schedule of the project. However, the quantity-based tracking of the materials does not indicate the progress in construction operations which are based on activities' status. Furthermore, having to tag all of the materials consumed in a project increases the technology cost and data collection effort, an issue that requires further investigation.

Quality is an essential aspect of a project, which is reported besides the project's performance in terms of schedule and cost. Two fundamental quality measures are considered in construction, including prevention and resultant measures. The quality of the project is reported in different ways. However, unlike other industries, in construction, the quality is affected by factors such as shortages of materials, design changes, lack of budget, and errors in cost estimation. Furthermore, it is possible to report the quality of the project through a regular quality assurance report (Rahman et al. 2017). Tracking the material soundness consumed in a project is essential to report the material waste and to highlight its effect on the project's progress, which needs further investigation.

2.4 3D Object Detection Using Computer Vision

There are advanced techniques in computer vision to detect objects with high accuracy from 2D data, such as images and video-frames in real time. However, using commercial cameras for photogrammetry may not provide adequate information about the location and distance between various objects on site. Moreover, concatenating the acquired image together increases the computational effort for extracting depth information about the scene. To address this issue, technologies that provide information about the scene's depth rather than 2D information are studied. These technologies include depth cameras and LiDAR devices. Depth cameras provide depth information about the scene, in addition to the RGB information. However, building scanning on a large scale has new challenges and opportunities that differ from the semantic parsing and segmentation of small-scale RGB-D images (Armeni et al. 2016, Armeni et al. 2018). LiDAR has been investigated in some studies as a prominent sensor that provides 3D information of the object, PCD, which has application in characterizing the shapes and localization of the objects on site (Adusumilli 2020). However, due to effects such as occlusions, noisy scans, discrete sampling, and cluttered scenes, point cloud-based object detection can be challenging, particularly in the case of large-scale data (Pang and Neumann

2016). Moreover, some characteristics of the PCD, such as being sparsely distributed in the 3D space and with unstructured storage, challenge its application for effective 3D object detection (Zhou and Tuzel 2018).

Using vision-based technologies such as photogrammetry, laser scanning, and their integration are appropriate choices to provide enough PCD to create 3D models of a site. More specifically, their integration enhances the PCD required for 3D reconstruction of the objects present on site. However, all these approaches have their limitations associated with their employment in a congested area and their drawbacks in modelling non-stationary and small objects such as furniture and project components. In this way, by integrating these vision-based technologies with RTLS technology, such as Robotic Total Station (RTS) and UWB, it is possible to overcome some of these problems. Table 2.4 compares these integrated systems over individual photogrammetry or laser scanning usage. They are different in terms of the level of automation in data acquisition, cost, reliability, and scalability to be used in various projects (Adusumilli 2020, Armeni et al. 2018, Bardareh and Moselhi 2022, Moselhi et al. 2020, Pang and Neumann 2016, Zhou and Tuzel 2018).

Table 2.4: Capabilities of individual and integrated vision-based technologies.

| Method | Data Acquisition Effort | Processing Time | Affordability | Data Accuracy and Reliability | Scalability |
|---------------------------------|-------------------------|-----------------|---------------|-------------------------------|-------------|
| Photogrammetry | √ | √√ | √√√ | √ | √ |
| Laser scanning | √√√ | √√√ | √ | √√ | √√ |
| Photogrammetry + laser scanning | √√ | √√ | √√ | √√√ | √√ |
| Photogrammetry + RTS | √√ | √ | √√ | √√ | √√ |
| Photogrammetry + UWB | √ | √ | √√ | √ | √√√ |
| Laser scanning + RFID | √√ | √√ | √ | √√ | √√ |

| | | | | | |
|-------------------------|----|----|---|-----|-----|
| Laser scanning + UWB | √√ | √√ | √ | √√√ | √√√ |
|-------------------------|----|----|---|-----|-----|

√: Low; √√: Medium; √√√: High.

Due to the computational complexity of photogrammetric surveying, construction management researchers have attempted to decrease the number of required photos by imposing geometric constraints and automating the modelling process based on pattern recognition and feature detection. Moreover, a solution based on integrating the photogrammetry data with the data acquired by a 3D laser scanner is also investigated to reduce the effort required for 3D modelling. In fact, due to the geometric stability of digital images, they are very suitable references for the inspection of the data acquired by laser scanners for 3D modelling. There are two approaches to integrating these two technologies. In one approach, the photos and scanned data are taken from the same positions, for example, the camera is installed on the laser scanner. In this approach, the additional process for coordinating different photos with scanned PCD is not needed. However, the photos are taken from the same distance and angle of view as scanning data, which would decrease the details in the photos. In another approach, photos are taken separately from scanned data but in a closer range and from different angles. This configuration requires an additional step to orient the digital images with the scanned data. This orientation can be done by choosing some common points or features in both data formats and then trying to merge them or by measuring the coordinates of several common points (tie-points) available in both data formats in different positions. According to the literature, the new capabilities provided by this integration have brought new applications in construction management. For instance, through a case study done by Ta (2017), the quantity of excavation work accomplished was rapidly tracked for automated progress reporting. By using this integration, they proposed a more robust and timely data acquisition procedure in which fewer images and less scanning time is required to produce acceptable results during the 3D modelling process. They could also overcome limitations in the photogrammetry technique associated with modelling objects with unclear geometrical shapes (e.g., excavation work). Another application for this integration is crack detection in an object or structure. In fact, this integration helps to improve the geometry and visual quality of the final 3D model. During the data collection phase, the information about the edges and linear features in the surface such as cracks are achieved based on analysis of the images, while the information about the object geometry is provided by scanning data. In this way, a more complete 3D model of the scene can be generated with sufficient and clear details about the colour, texture, and material of

various objects. Integrating a laser scanning system with photogrammetry would provide a timely, cost-effective, and accurate 3D model of a structure, which can decrease the human exposure costs and risk exposures caused by the lack of information during construction (Azarm 2013). More accurate visual information results in less rework and change orders, thereby improving productivity. Moreover, these 3D models are used to make accurate rehabilitation, maintenance, and renovation plans during the structure operation. However, the registration and alignment of these two sensory data matters. On one hand, both digital images and scanning PCD have internal errors that affect the registration process. On the other hand, factors such as the required accuracy, resolution and accessibility of the object may affect the chosen of the optimal method (Moselhi et al. 2020).

The LiDAR device and depth camera can create high-quality PCD (Nasrollahi et al. 2019). Various techniques have been studied to locate and segment building elements from the 3D PCD, such as slices comparing, region growing, p-linkage, Hough transform, Random Sampling and Consensus (RANSAC), and deep-learning techniques. These techniques are categorized as feature-based, geometry-based, and point cloud-based. Examples of feature-based techniques include but are not limited to region-growing techniques and P-linkage algorithms. Geometry-based methods such as RANSAC and Hough transform work based on segmentation and feature extraction to translate objects into shapes such as lines and circles (Amer 2020). In these techniques, the PCD is segmented into intrinsic object categories existing on the scene. Then, the classification algorithms are used to label each segment semantically. Bardareh and Moselhi (2022) and Armeni et al. (2018) argued that indoor space object identification by point cloud data is a detection problem rather than a segmentation task. They adopted a detection-based approach for element parsing in this regard.

CNN is a computer-vision technique for object-detection tasks. This network includes various stages to automatically translate the input data, including images and PCD, to the meaningful objects in the output. Feature extraction is an essential step in object recognition out of PCD, which includes extracting elementary geometric features, such as boundaries, edges, and corners, using local filters (Nasrollahi et al. 2019). In this regard, the significant changes in the distance of the surrounding PCD help to detect borders. However, it may be possible to identify borders by the impact angles of the sensor beam or changes in the normals (Munaro et al. 2016). The annotation, which is part of CNN for segmentation tasks, is usually manual and done by related software (i.e., Cloud Compare software package). During annotation, the number of

points in each part should not exceed a minimum and maximum value. The minimum value is important, especially for areas with a high density of PCD. Sometimes, the available PCD is augmented (i.e., flipped and rotated) in the pre-processing step to enlarge the training dataset. However, the augmented datasets are not used in the evaluation and testing. The evaluation and testing data are selected from the areas where the data are not used for training the model. An optimizer is also used to train the model (e.g., Adam optimizer). The CNN model's dropout layers are also used to improve the model's generalization.

Deep Neural Network (DNN), a kind of CNN with a deep forward network and many layers, has been recently used in this context for detecting 3D objects out of 3D PCD (Zhou and Tuzel 2018). However, many of these techniques must be revised to avoid the limitation associated with imbalance classes for object recognition out of PCD. Besides the generalizability of the deep-learning model on other datasets should be addressed, providing adequate annotated datasets for training the model could be challenging in case of changing the environment (Amer 2020, Nasrollahi et al. (2019). Furthermore, getting annotated data to train the classification algorithm for each new class of object is difficult. High computational time and processing effort are other issues of these techniques for object recognition (Nasrollahi et al. 2019).

Many advanced 3D object recognition techniques, such as VeloFCN, 3DOP, 3D YOLO, PointNet, PointNet++, VoxelNet, etc., have been proposed for 3D object recognition. They can be categorized as volumetric CNNs, multi-view CNNs, Spectral CNNs, and feature-based DNNs. Volumetric CNN is based on applying CNNs on voxelized shapes; however, data sparsity and computation cost of 3D convolution limits its resolution, especially for large-scale PCD. Multiview CNNs, in this respect, are based on rendering 3D PCD or shapes into 2D images and then applying 2D convolution nets to classify them. This technique applies to shape classification, not scene understanding or shape completion. Recently, spectral CNNs have been investigated using spectral CNNs on meshes. However, these methods are mainly used for organic objects rather than furniture meshes. Feature-based DNNs techniques are also used in this context in which the 3D data are converted into a vector by extracting standard shape features and then using a fully connected net to classify the shape (Adusumilli 2020, Qi et al. 2017). Most attempts in deep learning-based methods have been focused on regular input representations such as sequences, images, and volumes, while less attention has been on using point sets as inputs for the deep-learning algorithm. The main challenge of working with points is based on the sparsity of the points and the irregular set of inputs for DNN. A set of studies

have been done to address the issue associated with irregular inputs for DNN algorithms. However, most of these efforts are focused on generic sets and Natural Language Processing (NLP) applications, and they neglect the effect of geometry on the sets (Qi et al. 2017).

Based on data representation, CNN approaches can be classified into three main categories: voxel-based, pixel-based, and 3D point-based. These categories are further explained in the following sub-sections. In pixel-based approaches, 3D data are converted to 2D projections, such as images, while voxels are generated from the 3D points. Point-based approaches use 3D CNN to process PCD and implement 3D recognition tasks, including object classification, part and semantic segmentation (Nasrollahi et al. 2019, Qi et al. 2017). Table 2.5 illustrates these three groups, highlighting their capabilities, limitations, and overall accuracy. There are other metrics to evaluate the performance of the DNN algorithms, i.e., Intersection-over-Union (IoU), precision, and F1-score. However, the accuracy has been selected here for simplicity and to show the algorithms' overall performance.

Table 2.5: Deep-learning techniques for object recognition (Deng et al. 2021, Nasrollahi et al. 2019, Pang and Neumann 2016, Qi et al. 2017).

| Algorithm type | Input | Algorithms used | Capabilities | Limitations | Overall accuracy |
|--|------------|-----------------|---|---|------------------|
| Volumetric CNN algorithms (Adusumilli (2020), Zhou and Tuzel 2018, Qi et al. 2017) | Volumetric | 1) VoxNet | <ul style="list-style-type: none"> Replacing manual feature extraction | <ul style="list-style-type: none"> Computation cost Low resolution due to data sparsity | 1) 83.0 |
| | | 2) 3DShapeNets | | | 2) 77.3 |
| Multiview CNN algorithms (Pang and Neumann 2016, Deng et al. 2021) | Image | 3) Subvolume | <ul style="list-style-type: none"> Good performance for shape classification | <ul style="list-style-type: none"> Not applicable for scene understanding Many views of the environment are required Limited performance | 3) 89.2 |
| | | 1) LFD | | | 1) 75.5 |
| | | 2) MVCNN | | | 2) 90.1 |

and
complexity
of 2D
detection
algorithms

| | | | | |
|--|--------|---|---|--|
| Point cloud-based algorithms (Nasrollahi et al. 2019), Qi et al. 2017) | Points | <ol style="list-style-type: none"> 1) PointNet 2) PointNet++ 3) DGCNN 4) PointNeXt <ul style="list-style-type: none"> • Less computational cost • Space efficiency • Scalability • Potential for real-time applications • Robust algorithm to missing and corrupted data • Avoid falling in extremes (minimums) | <ul style="list-style-type: none"> • Missing some details of an object due to globally assigning features to local neighbouring points | <ol style="list-style-type: none"> 1) 89.2 2) 90.7 3) 92.9 4) 94.0 |
|--|--------|---|---|--|

2.4.1 Volumetric CNN Algorithms

The VoxelNet is a volumetric CNN algorithm for 3D object detection, outperforming some of the techniques mentioned above. The VoxelNet architecture has three modules: feature learning network, convolutional middle layers, and region proposal network (RPN). To extract descriptive features from a PCD voxel grid, a feature learning network is used in which the individual points in the voxel are processed to obtain point-wise features for the voxels containing more than a defined number of points. The point-wise features are then aggregated with locally aggregated features. Moreover, an element-wise max pooling is applied to obtain the locally aggregated features from the point-wise input features. The convolutional middle layer also reduces the feature map size, in which the voxel features are converted to dense 4D feature maps using convolution, batch normalization, and Rectified Linear Unit (ReLU). A modified RPN, a fully convolutional layer, includes three blocks. The output of every block is up-sampled to a fixed size and concatenated to construct a feature map with high resolution, while the feature map are further mapped to desired learning targets, including the probability

score map and regression map. The modified RPN provides the detection result by intaking the volumetric representation (Li et al. 2017).

This network has advantages such as: (1) avoiding the manual feature extraction, which is a typical workflow in using the PCD in pixel-based techniques. In the pixel-based techniques, the objects are detected by projecting the 3D PCD to the top view and then applying the image-based feature extraction methods. This workflow causes an information bottleneck, which affects the object detection out of the 3D information, (2) limiting the number of points available in a voxel to a defined value helps to enhance the computation and to address the memory constraints in the processing step, (3) the architecture of this technique helps to use the raw PCD for learning the feature representation simultaneously, meanwhile predicting accurate 3D bounding boxes (Li et al. 2017).

2.4.2 Multiview CNN Algorithms

Due to challenges associated with using 3D descriptor matching for object recognition of PCD, there is a need for a technique to avoid the complexity and time-consuming process of directly processing 3D data. One solution is to transform a 3D point cloud into 2D images by projecting the 3D PCD into depth information at multiple viewpoints and rotations (Bardareh and Moselhi 2022). This approach enhances the efficiency of object detection since it only relies on 2D CNNs for feature extraction. However, the reduced information in every view usually results in unsatisfied performance for distinguishing and localizing objects in 3D space (Yin et al. 2009). Moreover, producing many 2D detection tasks limits the appropriate 2D detection algorithm's choice and performance, and the increased processing time is another concern, especially for applications related to near-real-time object recognition (Bardareh and Moselhi 2022).

To reduce the amount of 2D detection tasks, Bardareh and Moselhi (2022) used a CNN in which multiple viewpoints and rotations were used for the same object class with a single pass through the network. Furthermore, they improved the detection efficiency by reducing the image sizes while using early rejection networks in a simplified architecture before starting the network of final multi-class detection. Yin et al. (2009) concluded that since LiDAR PCD is hollow-3D data, it can efficiently maintain the 3D representation by concatenating features from projected views and from the 3D spatial context. This could also result in a trade-off between precision and runtime latency. In this study, the PCD was sequentially projected into the perspective and bird's-eye views to extract the multi-view features. The perspective view

included features with rich information about the semantic context. On the other hand, the bird's-eye view addressed the highly sparse projected points, which are difficult to distinguish by semantic components. The features extracted from the bird's-eye view are used to predict the scales and locations of objects.

2.4.3 Point-Based CNN Algorithms

Due to certain characteristics of PCD, including its simple and unified structures, it is easier to train models with this data compared to the difficulties in dealing with other techniques using irregular and complex meshes. In a typical point cloud dataset, each point is represented by its three coordinates while additional dimensions may be added, such as normalized values and local or global features (Qi et al. 2017). As mentioned, due to the irregular format of PCD, most researchers prefer to transform the points data into regular 3D voxels and multiple images. This data transformation results in unnecessarily voluminous data, affecting the data's natural invariance (Nasrollahi et al. 2019, Qi et al. 2017). Working directly on the 3D point cloud datasets makes it possible to overcome the limitations associated with the techniques in which the PCD is transformed into pixel or 3D voxel grids (Nasrollahi et al. 2019).

PointNet is a novel type of CNN that provides a unified approach for 3D recognition tasks, including object classification, part segmentation, and semantic segmentation, by directly using n-dimensional tensors such as PCD (Nasrollahi et al. 2019). It was developed in 2017 to address the limitations of voxelization and rendering PCD. The Stanford 3D Indoor Scene (S3DIS) was used to validate the algorithm, including the scene semantic segmentation module for the scene analysis. This network has three parts, including classification, part segmentation, and semantic segmentation. The points in each part are sub-sampled by splitting the PCD into various areas, then divided into several parts inside. In the object classification part, the input point cloud results in outputs with k scores for all the k classes of objects. The segmentation network is an extension of the classification part. The semantic segmentation of PointNet is typically used to detect indoor building elements. In such cases, PointNet architecture concatenates both global and local point features and outputs per point score for object classification and semantic segmentation problems (Deng et al. 2021, Ma et al. 2022, Qi et al. 2017).

The PointNet algorithm has a pretty simple architecture, as each point is processed independently in the initial stages. Networks such as PointNet are more efficient in terms of computational cost, much more space efficient than multi-view-based methods in terms of parameters in the network, and much more scalable, showing great potential for applications

that need real-time object detection (Qi et al. 2017). PointNet is a robust deep-learning algorithm for addressing missing and corrupted data that normalizes the number of points in each block to a unique number (given that the surface point cloud density varies). This process requires down-sampling or up-sampling in which the block's density of the actual dataset is decreased and increased. This network is also invariant to input data permutations by using symmetry functions, such as max-pooling. It also considers neighbouring points' behaviour and does not isolate each point by using local and global features transformation. This network is invariant to data transformation or rotation by using a joint alignment network called T-Net. Imposing a regularization law prevents the situation of falling into extremes (minimums). Furthermore, data augmentation helps to increase the training dataset. Two commonly used methods for data augmentation of PCD are random rotations and random Jittering (i.e., adding noise). In a case study by Qi et al. (2017), randomly deleting 50% of data resulted in a 2% drop in accuracy which shows how robust this algorithm is in case of perturbation (i.e., missing or outlier data). This is because of the PointNet algorithm's capability to verify which set of input points has more contributions to achieve the final global features. These points, referred to as critical PCD, can be used to identify key features of each object. The Autoencoders are also used for shape completion and tasks associated with up-sampling of the PCD. This is useful since sometimes the quality of the acquired PCD is not high enough, or some data is missing.

Researchers have applied PointNet to classify PCD of various building elements. They also used PointNet for semantic segmentation purposes. For instance, PointNet was used in a study to semantically segment observed scenes in a robotic teleoperation system in a virtual reality environment. In another study, algorithms with architecture similar to PointNet, such as C-shapes and L-shapes networks, were used to segment PCD for industrial oil facilities. There are various variants of PointNet, which has improved the performance of its initial version by having an overall accuracy of 90.7%. Researchers have also investigated Dynamic Graph CNN (DGCNN), a modified PointNet version that uses edge rather than point features. DGCNN has relatively outperformed PointNet for object classification and semantic segmentation (Ma et al. 2022). The experiments by Ma et al. (2022) showed that the segment-based classification using PointNet performs better over DGCNN for furniture and other objects. However, for point-wise classification, the DGCNN showed better performance.

2.4.4 Dataset Benchmarks for Point Cloud Data

There are a couple of well-known benchmark datasets for PCD, such as ModelNet40, ShapeNet, Semantic3D, Stanford Large-Scale S3DIS Dataset, and 3DFacilities (Ma et al. 2022, Qi et al. 2017). ModelNet40 is used for classification tasks, while ShapeNet is used for part and semantic segmentation. The S3DIS is a large-scale point cloud dataset that includes information about the coordinates and colour features. The S3DIS is also annotated for 13 semantic classes of objects in an indoor scene. 3DFacilities, on the other hand, have been collected in an institutional environment and for 18 classes of objects (Ma et al. 2022). Figure 2.1 shows the defined class of objects in the S3DIS and 3DFacilities, along with the proportion of the objects in each class.

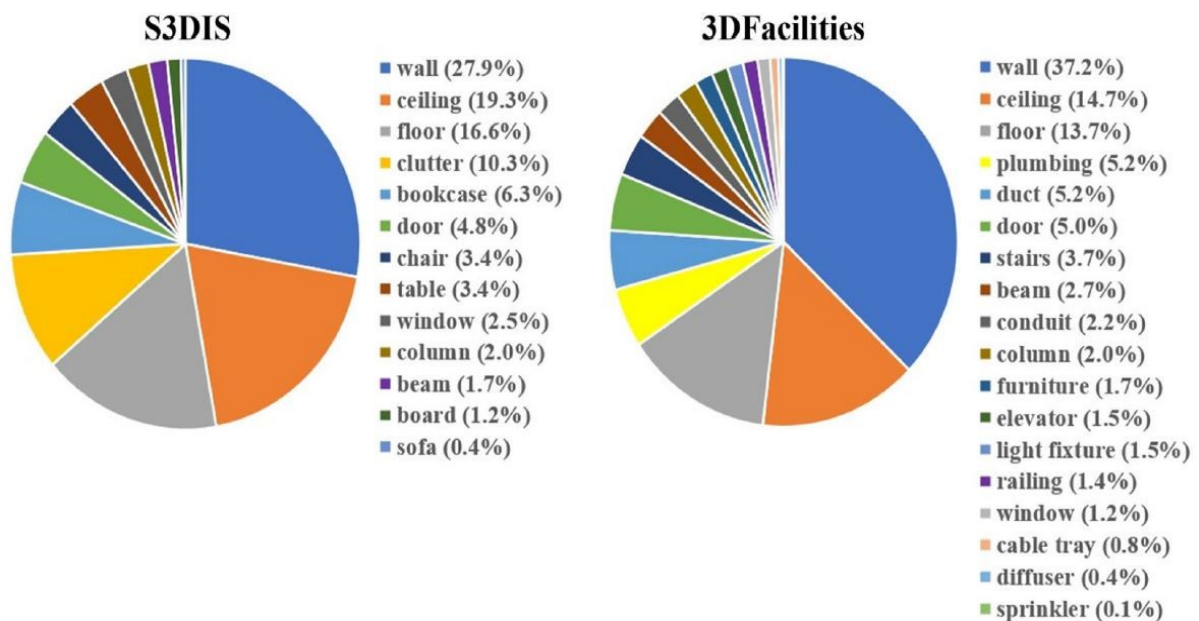


Figure 2.1: S3DIS and 3DFacilities point cloud-based benchmark (Ma et al. 2022).

2.5 Digital Twin in Construction for Automated Progress Reporting

There is no widely accepted conceptualization or definition of the term digital twins; however, numerous organizations have defined digital twins in terms of their functions and characteristics. The twin concept dates back to the NASA Apollo program in the 1960s, in which twins of some modules were replicated for a project's maintenance, support, and troubleshooting. According to the definition provided by the Centre for Digital Built Britain, a digital twin is "a realistic digital representation of assets, processes or systems in the built or natural environment" (Sacks et al. 2020). Digital twin refers to a virtual model or digital replica of living or non-living physical entities focusing on automation, connection, Internet of Things

(IoT), BIM, and big data analytics, which are closely linked to the same terms used in Industry 4.0 and smart manufacturing. A digital twin is not only the digital replica of an actual site but also includes the data and information about a physical asset or its environment. It also provides project teams with insights, scenarios, and representations associated with the asset or environment. Examples are using the IoT to track and monitor the assets in a target environment using sensors and data-sharing platforms. Sacks et al. (2020) argued that digital twin in construction should be viewed as a comprehensive mode of construction that prioritizes closing the control loops rather than an extension of BIM tools integrated with sensing and monitoring technologies. They proposed a digital-twin information system workflow—including information stores, information processing functions, and tracking technologies. They insisted on a digital-twin platform that comprises both product and process modelling rather than relying on BIM models.

The insights about the site condition, such as the assets' location, status, and other information about the temperature and humidity, can be transferred and updated through a cloud-based BIM platform. Furthermore, information about the scheduling of the activities and the objects assigned to each activity can be added to the BIM model to enrich the information about the onsite objects. Transferring all these raw data to a BIM-based model and updating the data in a defined time resolution, depending on the type of activities on site, perfectly fulfill the concept of a digital-twin project. Every change in the assets' location and environmental condition of the site is sensed and updated in the BIM model. This information is then processed, and the required actions are decided accordingly and reflected again on the BIM model (Tran et al. 2021, Huang et al. 2021). The constant communication between the physical environment and the digital model through the sensory data communication and the 3D representation of the site help to enhance the site inspection and progress reporting through a digital-twin platform. For this purpose, various RS technologies are used to obtain different types of information. For example, information about the location of the assets is acquired by the RTLS sensors attached to objects on site, including the equipment and materials, while the humidity and temperature sensors provide information about the site environment. Sensory data obtained by 3D imaging technologies such as laser scanners and depth cameras can also be used to enhance the project's Level of Development (LoD) through a digital-twin platform. Lean 4.0 and Industry 4.0 are two new concepts that can be implemented through a digital twin. The RTLS-based digital twin was investigated by Ruppert et al. (2016) to facilitate the practice of Lean 4.0 for asset tracking. In that study, three levels of digitalization and communication

between the physical and digital twins were introduced. In level 1, only a 3D representation model of the physical object or site is available. In level 2, a one-way data flow from the physical object (s) to the digital object (s) in the model is initialized. In level 3, an integrated and bi-directional connection between the physical object (s) in the field and digital object (s) in the model is fully automated. Sacks et al. (2020) identified a lack of a cohesive and integrated approach to production control in which multiple monitoring systems inform a project database, which can then support various management functions.

A digital twin can be used in the different life cycles of a project. Efficiencies identified using digital twin to compare as-designed with as-built conditions can benefit the entire facility lifecycle, from early capital planning to engineering and construction. The planning phase of a project is an area in the 4D simulation of a project, including the 3D model and schedule, which has been widely used. Planning must be proactive and requires increasingly detailed iterative planning actions to identify and remove constraints to prepare tasks for assignment to crews and execution. Planning depends on the availability of increasingly detailed process status information, which well-designed monitoring technologies can provide if they are embedded in a suitable digital-twin information system framework. Digital twins could also include the operation and maintenance phase after the project turnover. Some studies have widely investigated the application of the digital twin for sustainable construction and operation of projects. Because operation and maintenance are the longest phases of a facility's lifecycle, developing an accurate 3D BIM that reflects the asset's as-built condition is crucial. During the operating phase, it lights up the users and operators of the project with the data and information that are used to optimize the performance of the projects and for better decision-making. During the construction phase, digital twins would also enable the project user to better monitor and control the project, send and receive the data associated with assets in a project, and inform the users about the actual status of the assets. However, using a digital twin in the construction phase of a project for asset tracking and progress reporting has not been widely used and needs more consideration. Both industry and academia have widely adopted Scan-to-BIM to develop an as-built 3D BIM. The process begins with capturing the physical realities of the building environments in the digital form of imagery or 3D PCD (Shahi et al. 2014). However, using a digital twin in the construction phase of a project for asset tracking and progress reporting has not been widely used and needs more consideration. Sacks et al. (2020) identified three generations in development of the digital twin in construction. The first generation is described as an enhanced version of BIM on construction sites to date; the second generation introduces

semantics to enhance monitoring platforms with limited intelligence where a common web language framework is deployed to represent the digital twin with all its integrated IoT devices; the third generation, the apex of the digital implementation possible to date represents a fully semantic digital twin, leveraging acquired knowledge with the use of AI-enabled agents. Machine learning, deep learning, data mining, and analysis capabilities are required to construct a self-reliant, self-updatable, and self-learning digital twin. They argued that the term Project Information Model (PIM), as defined in ISO 19650 (ISO/DIS 19650, 2018), can and should include both product and process. Whereas most BIM tools only provide product modelling. The product information is stored in the design BIM model's objects, their properties, and their relationships. The process information is stored in the construction plans, including construction methods, schedules (tasks, activities, resources), budgets, and so forth. As-built BIM models or Facility Management BIM (FM-BIM) models are generally compiled reactively following execution, and their purpose is to provide owners with models for the operation and maintenance phase, called the asset information model (AIM) in ISO 19650. They are not intended to provide the short cycle time feedback needed for project control. Moreover, while critical path tools for master planning have been used in conjunction with BIM models to perform 4D CAD analysis of project schedules, these tools are not suitable for project control (Sacks et al. 2020).

A digital-twin platform can provide more integrated and accurate information, as well as a 3D representation of the project for the site managers or inspectors. In this way, by creating a more accurate as-built digital status of a project and comparing it with as-planned information, the project decision-makers can use it for applications such as automated clash detection, congestion management, problem diagnosis, and progress reporting. Cai et al. (2014) developed a risk twin to integrate risk with the cost and schedule of a project. The risk twin developed in their study was used for planning, construction, and operation phases. Modular construction, which gains increased market share, can benefit from this framework. Ruppert et al. (2021) developed an integrated RTLS and Monte Carlo simulation into digital twins to monitor production performance and predict the production status of a factory. In their work, a digitalized assembly progress report was generated in which the assembly components are tagged, identified, and tracked in the twin provides information about the progress of various activities in the modular or assembly projects while reporting the project's overall progress. In their digital-twin solution, the tagged components can be tracked over the project's life cycle

for maintenance of the building equipment in the operation phase, facilitating energy-efficiency planning.

Many studies have focused on the interface between laser-scanned data and a 3D model, such as BIM models, through a Scan-To-BIM workflow to automate progress reporting. For instance, Bosché and Ahmed (2015) used a 3D model as a prior source of information for detecting objects from the PCD. However, these approaches are unable to identify objects that are not in their exact locations pre-described by the as-designed model or located at a distance greater than a tolerance value specified in the object recognition software. Furthermore, they are incapable of providing sufficient information about non-structural activities such as the welding, inspection, piping system, etc.; however, BIM systems may help to facilitate these operations in future (Shahi et al. 2014). In another approach, Ibrahim (2015) designed a system based on SA-GPS for tracking and progress assessment of the earthmoving operations. They concluded a considerable decrease in average absolute percentage error in the project progress estimation compared to a system working only based on GPS from 12% to almost 3%. In a similar study by Akhavian and Behzadan (2015), a smartphone with sensor technologies such as GPS, accelerometer, and gyroscope were put inside construction equipment. Then, the time-stamped data for the equipment position, acceleration, and angular velocities were collected using commercial data logger applications available on the smartphone device. After a feature extraction process in which some features were defined based on the level of details required for an activity recognition process, a subset of originally extracted features were employed to train the supervised machine-learning algorithms (i.e., ANN, KNN and etc.) for activity classification. Finally, through an activity recognition step, the classified actions were defined as real actions on the site, and these data were used as input for a simulation model. El-Omari (2008) did a case study to rapidly track the quantity of excavation work accomplished for automated progress reporting. By using this integration, they proposed a more robust and timely data acquisition procedure in which fewer images and less scanning time is required to produce acceptable results during the 3D modelling process.

2.6 Summary

The literature review presented above examined the current state of RS technologies such as RTLS, 3D imaging, and their integration with BIM in construction applications, highlighting gaps in the body of knowledge. The use of RTLS technologies was investigated, and the integrated use of these technologies as a solution to compensate for the limitations of each

individual technology for applications on job sites, such as material tracking and progress reporting was identified. The use of RTLS technologies for indoor object identification, specifically for 3D object localization and for objects in elevation, warrants further study. Moreover, regarding indoor object localization and tracking of information for progress tracking, the mechanism and the requisite tools to ensure visibility is another gap that needs further investigation. The use of 3D imaging technologies such as LiDAR in applications such as automated Scan-to-BIM process and quality control was also investigated. Furthermore, the use of AI-based computer-vision techniques (i.e., DNN algorithms) for automated detection of objects on job sites was explored. The imbalance size of the datasets for various class of objects, especially in the PCD collected by the LiDAR devices, was identified as the main source of error in the studied algorithms for object detection. The imbalance arises from the inherent characteristics of point cloud data. The majority of the data collected by the LiDAR device pertains to elements such as slabs, walls, floors, and ceilings. In contrast, other categories of objects, including furniture and Mechanical, Electrical, and Plumbing (MEP), are represented by a significantly smaller portion of the point cloud data. Moreover, the use of PCD and DNN segmentation algorithms for indoor object localization in 3D format requires further investigation, particularly with respect to MEP equipment, which is highly complex and extensively linked with other components on site. Finally, the literature on digital-twin applications for project control in construction underscores the need for a digital-twin platform that can facilitate data acquisition on job sites through a bi-directional construction twin dashboard and that can automate the generation of onsite inspection reports.

CHAPTER 3: Research Methodology

3.1 Overview

The present study explores the use of Real-Time Location system (RTLS) and Light Detection and Ranging (LiDAR) technologies for 2D and 3D localization of objects in indoor spaces, as well as for automated generation of onsite inspection reports (see Figure 3.1). The RTLS used in this study is an integrated Radio Frequency Identification Device (RFID)–Ultra-WideBand (UWB) technology for indoor object identification and localization (Section 3.2). The integrated RFID–UWB is then combined with a cloud-based Building Information Modeling (BIM) platform to enhance asset tracking, inspection, and site reporting (Section 3.3). For this purpose, the RTLS data collected from the objects furnished with the RFID tags is used as input for the indices in the Earned Value Management (EVM), i.e., Material Status Index (MSI) and Quality Status Index (QSI).

In addition to using the RTLS for indoor object identification and localization, the 3D Point Cloud Data (PCD) collected using a TLS is used for automated object detection and localization. In this step, a few objects in a lab environment are selected as the target class of objects to be detected by a computer-vision Deep Neural Network (DNN) called PointNet. This network's classification and segmentation modules help to detect and localize objects. Further integration of the PCD with the RTLS data results in more accurate indoor localization for the tagged objects, as well as the capability to assign IDs to the detected objects via the point cloud and DNN algorithms (Section 3.4).

Section 3.5, finally, describes a digital-twin platform in which the integrated RTLS–PCD is transferred to a cloud-based BIM for the purpose of automated generation of the onsite inspection report using the 3D coordinates of the target objects. Figure 3.1 provides an overview of the methods developed in this study.

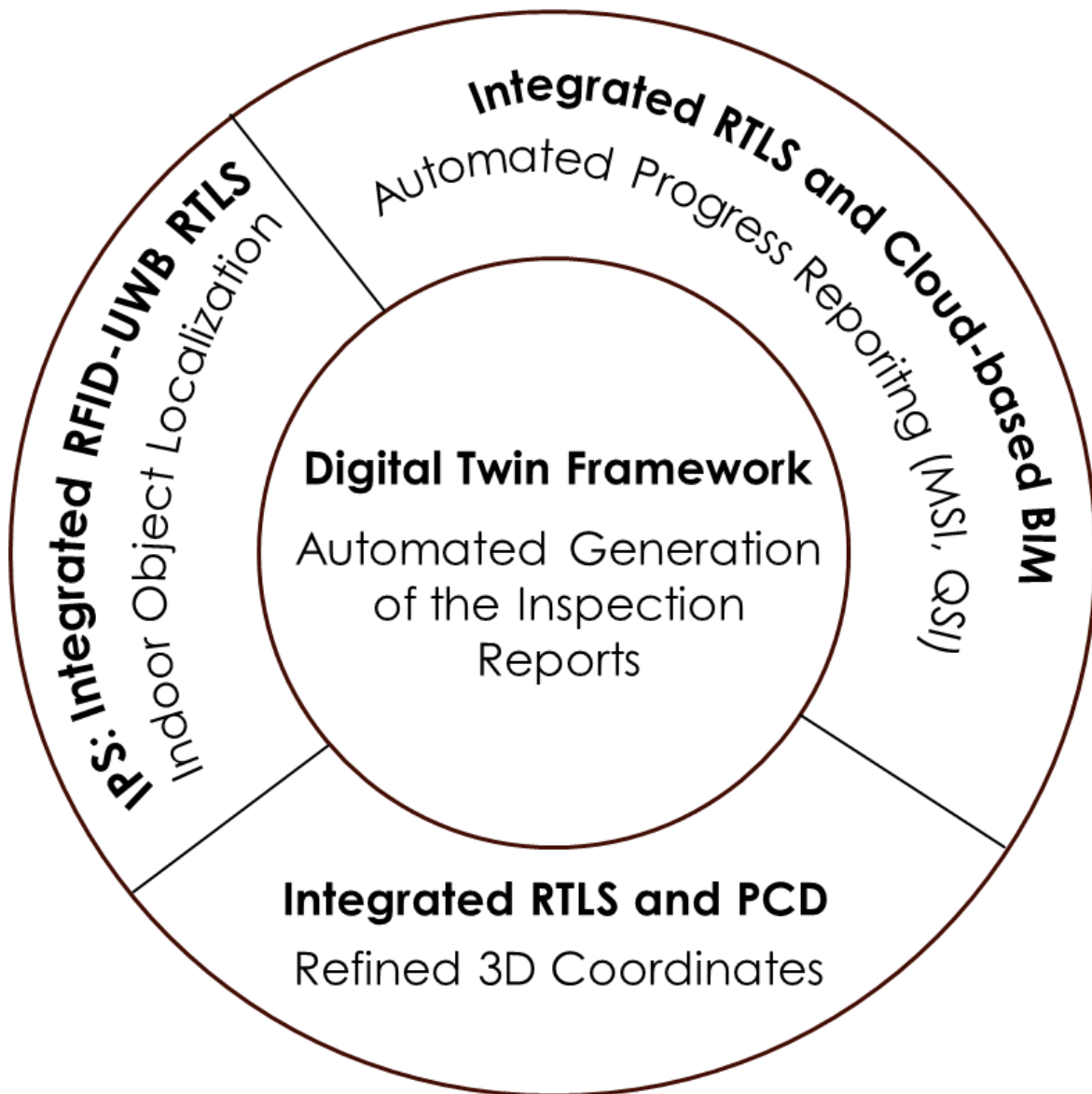


Figure 3.1: Overview of the developed method.

3.2 Integrated RFID–UWB for Indoor Object Localization

Indoor progress tracking has also been investigated recently by some researchers. However, in indoor tracking of resources and activities, there are notable challenges encountered if there is a wide range of materials and structural objects that need to be recognized. Moreover, available RS technologies with applications in indoor progress reporting (e.g., RFID, UWB, laser scanning, photogrammetry, etc.) have some limitations that may affect their performance in a confined area. In fact, vision-based technologies such as laser scanning and photogrammetry and their integration are good choices for generating PCD. However, they need post-processing steps for 3D modelling, which is manual and time-consuming. Georeferencing the system

during data collection is also important for more accurate data registration. In this way, using tracking technologies such as RTS and UWB with good localization accuracy can help facilitate these problems and create a more automated system for 3D modelling (Moselhi et al. 2020).

The fusion of the data acquired from various RS technologies and with other technologies has also been investigated as a solution to overcome the limitations of each technology. The activity-based approach for progress reporting is another area of interest in recent studies, which enables us to track activities related to moving objects and activities that do not have such traceable objects. Finally, registering the data acquired by various RS technologies with available building models (e.g., 3D CAD, BIM, etc.) also needs more investigation in the future (Moselhi et al. 2020).

Many studies have investigated the use of various RS technologies to automate localization and tracking of the objects on site (Tran et al. 2021, Wang et al. 2017, Xu et al. 2018). This section introduces a new method in which an integrated use of the UWB and RFID helps efficiently localize the objects in an indoor environment. This integration is aimed at overcoming the limitation of expensive sensors such as UWB and GPS for localization and tracking of a large number of objects on construction sites. Moreover, the integrated use of the two technologies provides more accurate localization information not only in 2D but for 3D object localization. In this regard, a sample number of objects labelled using inexpensive passive RFID tags are localized at the experimental level. This integrated system provides a more economical and accurate method for indoor material localization compared to the methods in the literature (Bardareh and Moselhi 2022).

The method is based on experimental work carried out in two phases, encompasses a set of experiments on the UWB and RFID separately in phase 1, followed by another set of experiments conducted on their integrated use for 2D and 3D localization of objects in phase 2. A schematic diagram of the developed method is illustrated in Figure 3.2. The novelty of this research lies in the integrated use of RFID and UWB to efficiently localize objects in an indoor environment and develop an improved trilateration technique. Using only UWB sensors to localize objects on site is not economically practical. To address this issue, the use of an inexpensive RFID system to facilitate object localization is investigated. However, the main problem of the RFID system is that the RSSI varies over time and is highly dependent on the site environment, especially for indoor sensory localization. Furthermore, there is no

conventional formula applicable for all use cases in different environments to accurately translate the RSS value to a range value, which results in low positioning accuracy. Moreover, using only RFID tags for localization of the objects in an indoor environment requires a large number of RFID reference tags to localize roving RFID reader and tags. In this regard, the integrated use of these two technologies is developed to benefit from the capabilities of each technology in localizing objects (Bardareh and Moselhi 2022).

Despite the use of GPS for outdoor applications, in an indoor environment, the performance of the GPS sensors is highly degraded since they need direct access to the sky to receive signals from satellites. To address this issue, the UWB sensors are used in lieu of GPS to localize the RFID reader. For localization of the RFID tags, there are various techniques which are mainly based on signal processing. Since, in this experiment, a roving RFID reader with a known location is used, the application of a range-based technique is investigated to localize stationary tagged objects. For applications associated with the localization of moving targets, such as workers and equipment, the UWB sensors are used to provide real-time location information. However, this experiment focuses on localizing indoor materials rather than workers (Bardareh and Moselhi 2022).

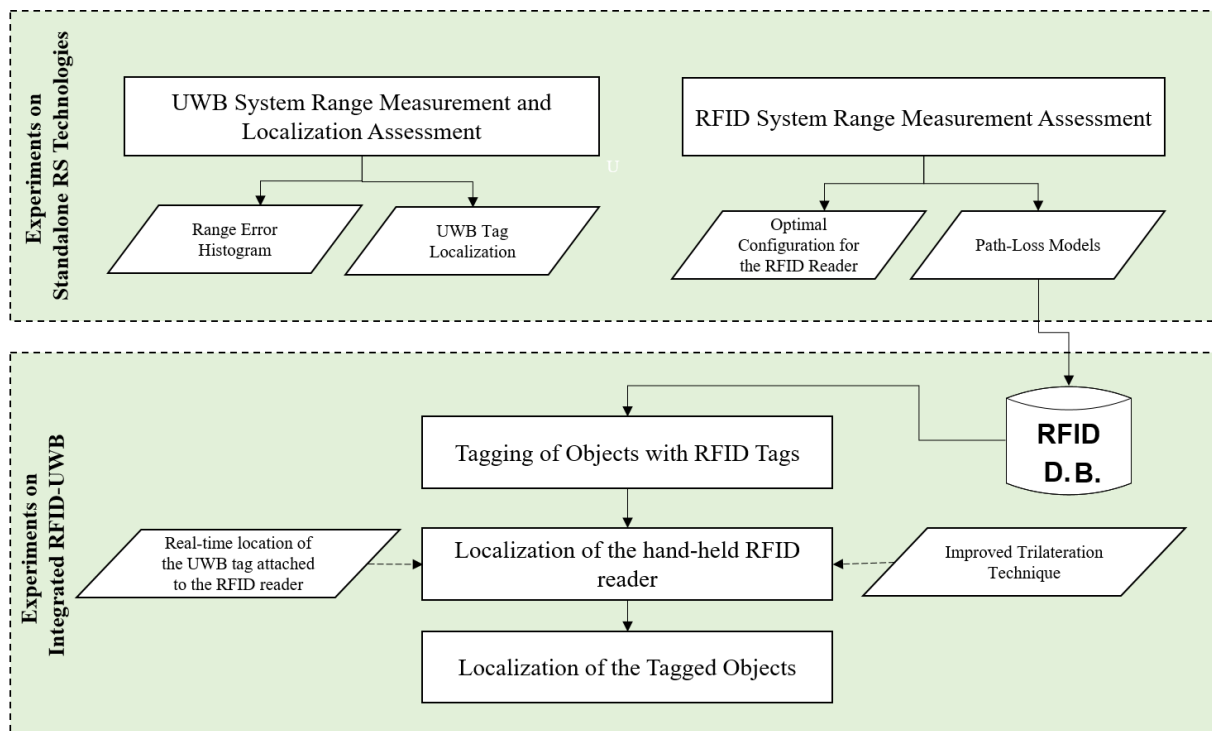


Figure 3.2: Schematic diagram of the developed method for indoor object localization (Moselhi et al. 2020).

In phase 1, the experiments on RFID and UWB are carried out to evaluate localization and range measurement accuracy of the UWB sensors used in this study and to search for optimal output power for a hand-held RFID reader to improve range measurement information provided by the RFID system used in this study. The UWB tests and the identified error histogram are provided in Section 4.1. With respect to the experiment on the RFID system, a path-loss model for four output powers of the hand-held RFID reader are developed and compared to identify the optimal output power, which are illustrated in Section 4.1 of this thesis. This value is identified by respecting maximum reading range of the hand-held reader and accuracy of the corresponding model. This optimal value is useful for applications associated with range measurement and proximity on construction sites (Bardareh and Moselhi 2022). To translate the distance between the hand-held RFID reader and the RFID tags various techniques are used; these techniques mainly capitalize on signal attenuation, although they are also governed by characteristics of the RFID system, such as the maximum reading range of the device (Cai et al. 2014, Montaser and Moselhi 2014, Su et al. 2014). In this experiment, an RSS-based method is used for range measurement which works based on a path-loss model. However, there are some factors that may affect the accuracy of the measurements; this includes factors associated with the RFID device such as operating frequency, the hand-held RFID reader output power and distance between the tags and the reader. The results of an experiment showed that if the distance of the reference tags from each other is half of the device reading range ($0.5RR$), then a better detection rate results (Shahi and Safa 2015). The factors associated with indoor environment, such as free space loss factor, multipath reflection, and interference effects also affect the RSSI signal (Omer et al. 2019, Tzeng et al. 2008). Some of these factors are addressed and evaluated in this experiment. Figure 3.3 illustrates various steps to achieve the path-loss models.

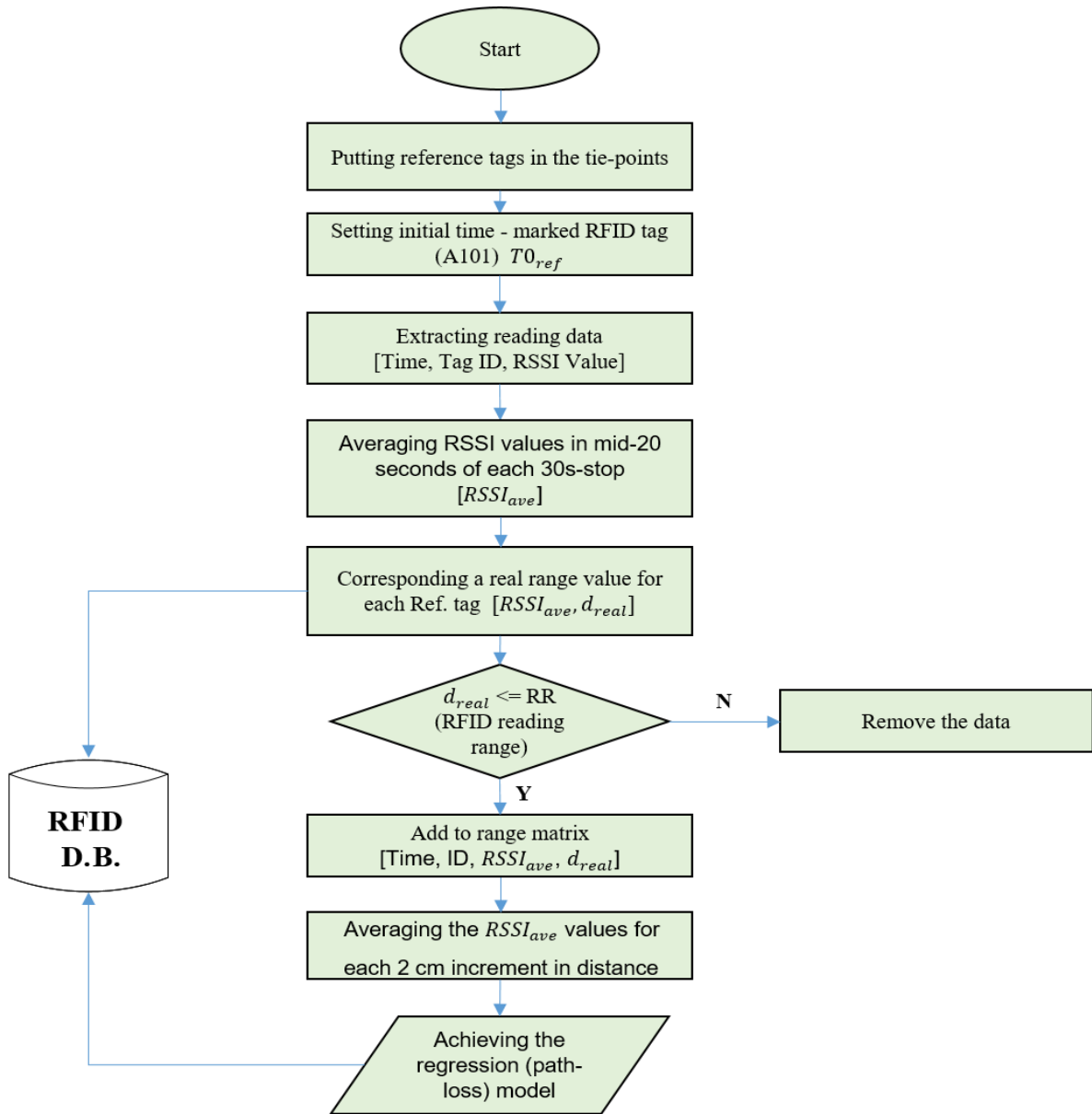


Figure 3.3: Various steps to achieve path-loss models.

In phase 2, inexpensive passive RFID tags are used together with the UWB sensors to provide localization information about a group of objects. To this end, a UWB sensor is attached to the roving hand-held RFID reader for its localization. Then, by knowing the location of the mobile RFID reader, the RFID tags attached to a set of identified objects are localized using the path-loss model and a trilateration technique, as explained later. The experiments conducted in the lab. validate the developed method in providing 2D and 3D information of the tagged objects (Bardareh and Moselhi 2022).

The integration of the acquired data, along with the mathematical concept, which is developed to improve the range-based trilateration technique, is described. Based on the location of the RFID reader, the RFID tags are localized using signal processing and a localization technique. Among various RSS-based techniques to estimate the tag's location, in this experiment, the DRVs are calculated using the path-loss models through Equation 3.1. In this equation, the constant values α and β are achieved for the RFID reader's three output powers, including o20, o22 and o25 dBm. In this study, the RFID tags' 2D and 3D localization are investigated. The RFID tag is localized by replacing these range values in the trilateration equations as provided in Equation 3.2 (Bardareh and Moselhi 2022).

$$DRV = \alpha \text{ RSSI} + \beta \quad (3.1)$$

$$DRV = [(x_i - X_{r_uwb})^2 + (y_i - Y_{r_uwb})^2 + (z_i - Z_{r_uwb})^2]^{1/2} \quad (3.2)$$

where $(X_{r_uwb}, Y_{r_uwb}, Z_{r_uwb})$ is the location of the hand-held RFID reader, which is measured by the UWB sensor attached to it; and (x_i, y_i, z_i) is the coordinates of the target RFID tag ($i = 0, 1, 2, 3$ for four different RFID reader locations in 3D localization) (Bardareh and Moselhi 2022).

Given that, in this experiment, the tagged objects are static, a small number of readers is sufficient for the localization of the tagged objects. However, in the case of localizing moving objects, a large number of RFID readers are required. To localize a tag in 2D and 3D, the data achieved for each tag are derived. Then, combinations of the three (four) from these data are selected to use the trilateration equations for 2D (3D) localization. Since the selection of these combinations affects the localization accuracy, the combinations with the highest value of Spatial of Distribution (SoD) are preferred. It is worth mentioning that the increase in the number of selected data for each tag greatly increases the processing time of the localization module, while the localization accuracy was not much improved. That is why in this experiment the number of the selected data is two times the required data for 2D and 3D localization (six and eight data with the highest SoD values, respectively) (Bardareh and Moselhi 2022).

The SoD value has a very close concept to a value called Dilution of Precision (DoP) which the GPS uses to enhance its localization. In fact, localization accuracy will increase when visible satellites are far apart, resulting in a higher DoP value with a stronger geometry (Xu and Shmaliy 2018). Saying that, unlike GPS, the RFID system does not work based on clock offset (using the time difference to measure distance). In this way, a new approach is needed

to consider the effect of RFID reader locations on localization accuracy. In this way, similar to the DoP factor in GPS, by calculating the mathematical variance of the various three (four) combinations of the reader locations, the best combinations are selected for the localization step. Equations 3.3 show the details of the SoD calculations which are used to select the initial data for the localization module (Bardareh and Moselhi 2022).

$$\begin{bmatrix} S_x \\ S_y \\ S_z \end{bmatrix} = \begin{bmatrix} \frac{(X_1 - \mu_x)}{(n-1)} + \frac{(X_2 - \mu_x)}{(n-1)} + \frac{(X_3 - \mu_x)}{(n-1)} + \frac{(X_4 - \mu_x)}{(n-1)} \\ \frac{(Y_1 - \mu_y)}{(n-1)} + \frac{(Y_2 - \mu_y)}{(n-1)} + \frac{(Y_3 - \mu_y)}{(n-1)} + \frac{(Y_4 - \mu_y)}{(n-1)} \\ \frac{(Z_1 - \mu_z)}{(n-1)} + \frac{(Z_2 - \mu_z)}{(n-1)} + \frac{(Z_3 - \mu_z)}{(n-1)} + \frac{(Z_4 - \mu_z)}{(n-1)} \end{bmatrix} \quad (3.3-a)$$

$$\mu_i = \frac{(X_{i1} + X_{i2} + X_{i3} + X_{i4})}{4}; \quad i = x, y, z \quad (3.3-b)$$

$$S^2 = S_x^2 + S_y^2 + S_z^2 \quad (m^2) \quad (3.3-c)$$

where (X, Y, Z) is the RFID reader coordinates obtained by the UWB sensor, (S_x, S_y, S_z) is the variances, and μ_i is the mean value of the coordinates of the reader locations in each combination (Bardareh and Moselhi 2022).

As mentioned, for locating the RFID reader the UWB tag provides the information about the reader location in a desired time span. However, the UWB data are recorded in millisecond accuracy (T_{uwb}), while the time resolution of the RFID system is in second (T_{ref}). In this case, first the location of the hand-held RFID reader in each time span is achieved from the UWB tag attached to it for a half-second before and after the time of the RFID tag reading time. Then, by using the path-loss models achieved for the RFID, the range of the tagged object from the hand-held RFID is calculated (Bardareh and Moselhi 2022).

Figure 3.4 shows the diagram of the localization module in which an improved trilateration technique is developed to enhance the localization accuracy. In each second, the information about the reference time, RFID tag ID, average RSSI for each tag, equivalent distance achieved from the path-loss models, and RFID reader coordinates are recorded ($T_{ref}, ID, RSSI_{ave}, d_{eq}, x, y, z$). Then, the data is re-arranged based on the identified tag ID. The novelty of the developed trilateration module is behind defining an adoptive radius for the trilateration equations and considering the spatial distribution of the RFID reader locations in the localization module. These improvements help to compensate for the errors in RFID reader range measurements obtained from path-loss models and to select the best combinations of RFID reader locations for the localization of each RFID tag. Additionally, using distributed

points in the trilateration circles helps to avoid solving non-linear and coupled trilateration equations (Bardareh and Moselhi 2022).

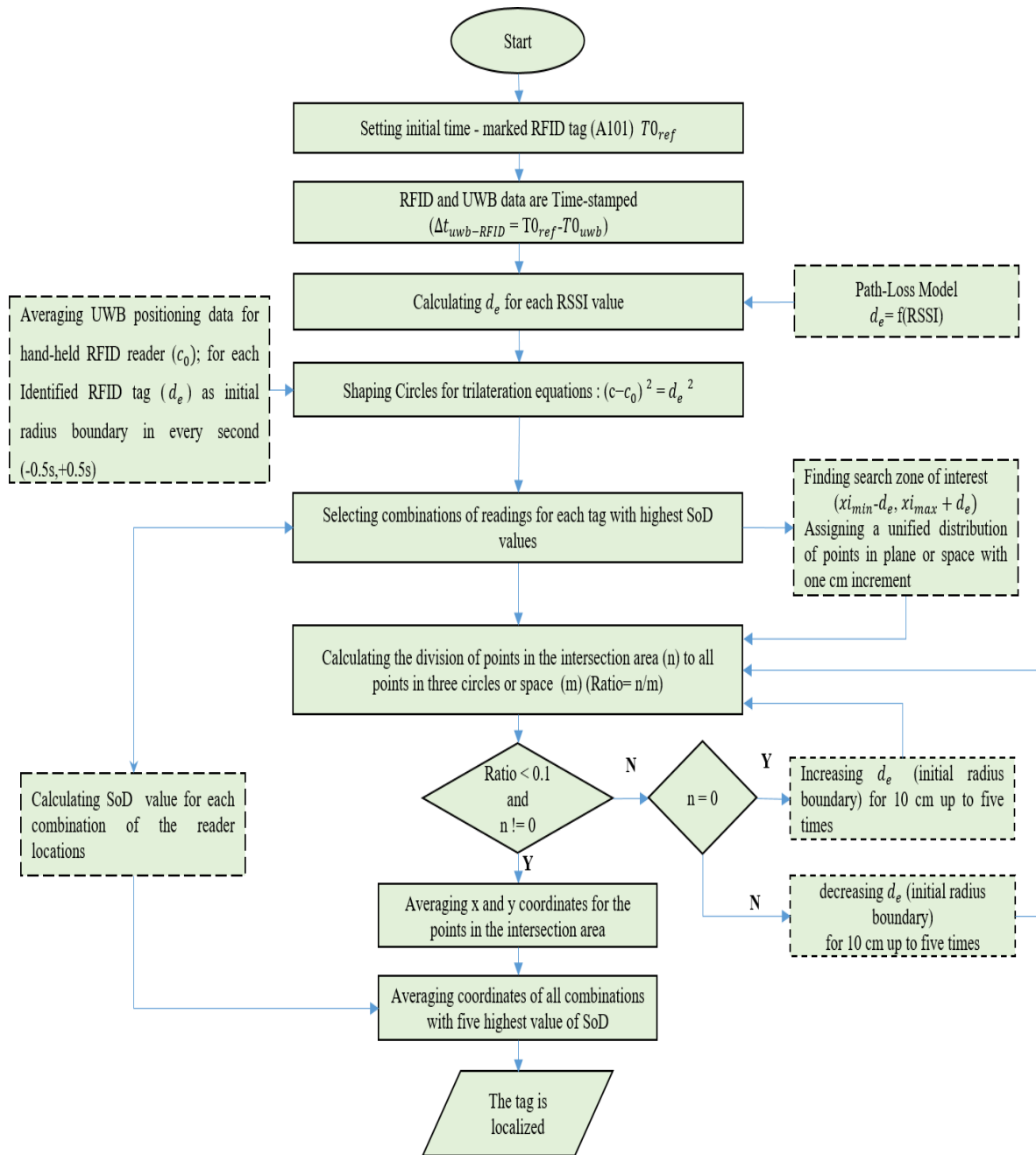


Figure 3.4: System localization diagram.

As mentioned, in order to use trilateration equations to localize a specific tag in 2D and 3D, at least three and four readings of that tag is required respectively. Each set of these readings makes a combination with a specific SoD value for the RFID reader locations. In the initial step of the module and for data selection, the set of data in the combinations with higher values

of SoD are selected to be used in the trilateration equations. In 2D localization, combinations of three out of six data, and in 3D localization combinations of four out of eight data are selected.

For each combination, the three (four) circles (spheres) by the centers in (x,y,z) coordinates and a radius of d_{eq} are drawn and a uniform distribution of points are assigned for each circle (sphere). Here a threshold value, Ratio, is defined which is the number of common points (n) in the intersection of the selected circles (spheres) to the total points (m) for each combination. If, by solving the trilateration equations (Equation 3.2), an intersected area with an acceptable number of points is achieved (e.g., ratio < 0.1), then the combination is accepted for the next step. But if there is no intersection between the selected combination (ratio = 0), or the intersection area is too large (ratio > 0.1) then an incremental increase and decrease for the circles (spheres) radius is implemented to achieve the desired number of common points. In fact, this incremental increase and decrease in the radius of the circles (spheres) is defined in the extent of the ranging error of the path-loss model for the identified optimal output power (o25 dBm), which is approximately 1 m. As such, 50 cm inside and outside of the initial radius (d_{eq}) of the circles (spheres) is considered, as this represents the extent of the error tolerance of the ranging measurement. Figure 3.5-a illustrates more details about this varying radius in 2D localization.

In the final step of the module, those combinations with higher values of the SoD are selected (Figure 3.5-b). As mentioned in the previous step, in this experiment the variance of the RFID reader location distribution in the Lab. is considered as an equivalent factor to calculate the effect of the geometry in localizing each RFID tag. Finally, the estimated location for each tag is calculated by averaging the coordinates of points available in the intersection area.

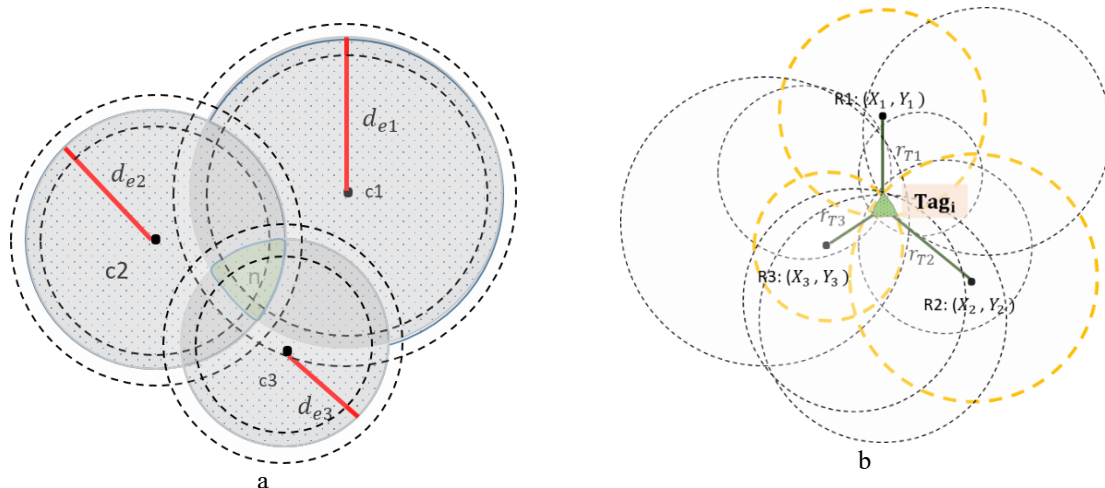


Figure 3.5: Improved Trilateration technique for 2D localization. (a) Radius variation in extent of the RFID system range measurement error (b) Combination with the highest SoD value (yellow dash-line).

3.3 Integrated RTLS and Cloud-based BIM for Tracking and Progress Reporting

The developed method in this section aims to improve progress reporting by providing more accurate and timely information about the materials used in a project and visualizing the information about the location and status of the materials through cloud-based 3D models. The materials in this study include the project components, such as HVAC, mechanical and electrical devices installed in the mechanical rooms of a project. The developed method distinguishes itself from previous efforts in this area by integrating material tracking with progress reporting by tracking the quality, status, and location of the materials consumed in a project. Moreover, in the present study, the control points for progress reporting are on materials which completes the interpretation of the scheduled-based indices. Despite the efforts in the literature that the Schedule Performance Index (SPI) and Cost Performance Index (CPI) are calculated at the activity level, the introduced MSI helps to overcome the limitations of the schedule and cost-based indices by taking critical materials into account in generating progress reports. MSI is augmented SPI and CPI, and BIM is used as a supplementary tool. For this purpose, a digitalized reporting method is developed to regularly monitor the material consumption in various construction activities broken down into the activities' zones. The quantity and status-based data collected are used to generate progress reports using the two introduced indices. The indices highlight the overall project status and the associated activities while reporting the quality of the consumed components. Customized terms, such as inspected and damaged, are also defined for both the prefabricated and the completed-in-place project components to report on their quality status. This quality status reporting provides more in-depth information about the project's performance beyond quantity-based reporting. The tracking and progress reporting method uses RFID-based technologies integrated with cloud-based Geographic Information System (GIS) platforms.

The developed method addresses the needs of the construction industry for two main applications: (1) Digitalizing material identification and localization, and (2) Site progress reporting. Integrated RTLS technologies and a cloud-based BIM platform are used for the first application to enhance the workflow for tracking construction materials in an indoor space

environment. For the second application, the developed method is used to digitalize site progress reporting and translate the data collected on site to prepare progress reports. Figure 3.6 provides an overview of the developed method for digitalized progress reporting on site, along with the technologies employed for this purpose. QR codes embedded on the RFID tags are used to collect the status of tagged components during site inspections, highlighting the predefined status of activities and identifying any damaged or broken components. Additionally, the integrated RFID–UWB method described in Section 3.2 is used for the location identification of components tagged with RFID tags. The PCD collected by the LiDAR device is used to calibrate the UWB system and to identify the coordinates of the UWB receivers on site. The project's planned documents are also used to identify near-critical activities and the critical components to be tagged. For data collection, two cloud-based platforms, Survey123 and OfficeEquip, are used to gather information using the QR codes and RFID tags.

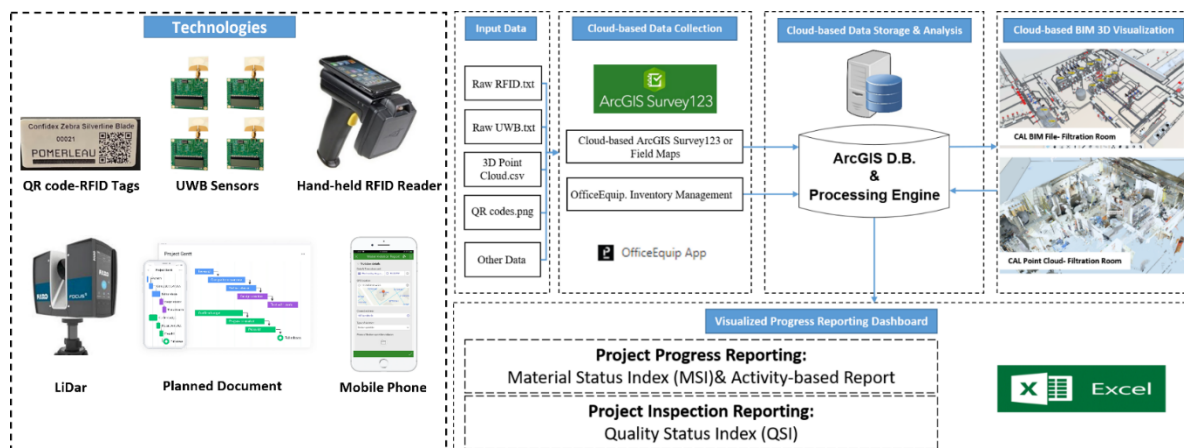


Figure 3.6: Overview of the developed method for digitalized site inspection and progress reporting.

The developed method comprises three main modules: surveying, material retrieval, and site inspection and progress reporting, validated through laboratory experiment and fieldwork. The site inspection includes reporting the materials with damaged or broken status, while progress reports capture the progress percentage based on quantities and the status of the materials consumed in the field. The experimented materials include automated tracking tools such as spot robots, drones, and depth cameras, which are available in the innovation group of a general contractor. The experiment focuses on indoor material surveying and retrieval and evaluates the performance of a cloud-based data collection and visualization platform for tracking. The

effectiveness of an RFID-enabled BIM platform in GIS cloud packages for tracking the experimented materials labelled with RFID tags has been evaluated. The materials tested in the fieldwork include the project components available in the mechanical rooms of a pool project. The fieldwork focuses on digitalizing progress reporting by validating two developed indices for reporting the progress and quality of onsite operations.

Figure 3.7 illustrates the developed method overview, and the three modules developed for enhanced tracking and digitalized progress reporting. As depicted in the figure, the first two modules are focused on object tracking and retrieval, while the third module insists on digitalizing progress reporting.

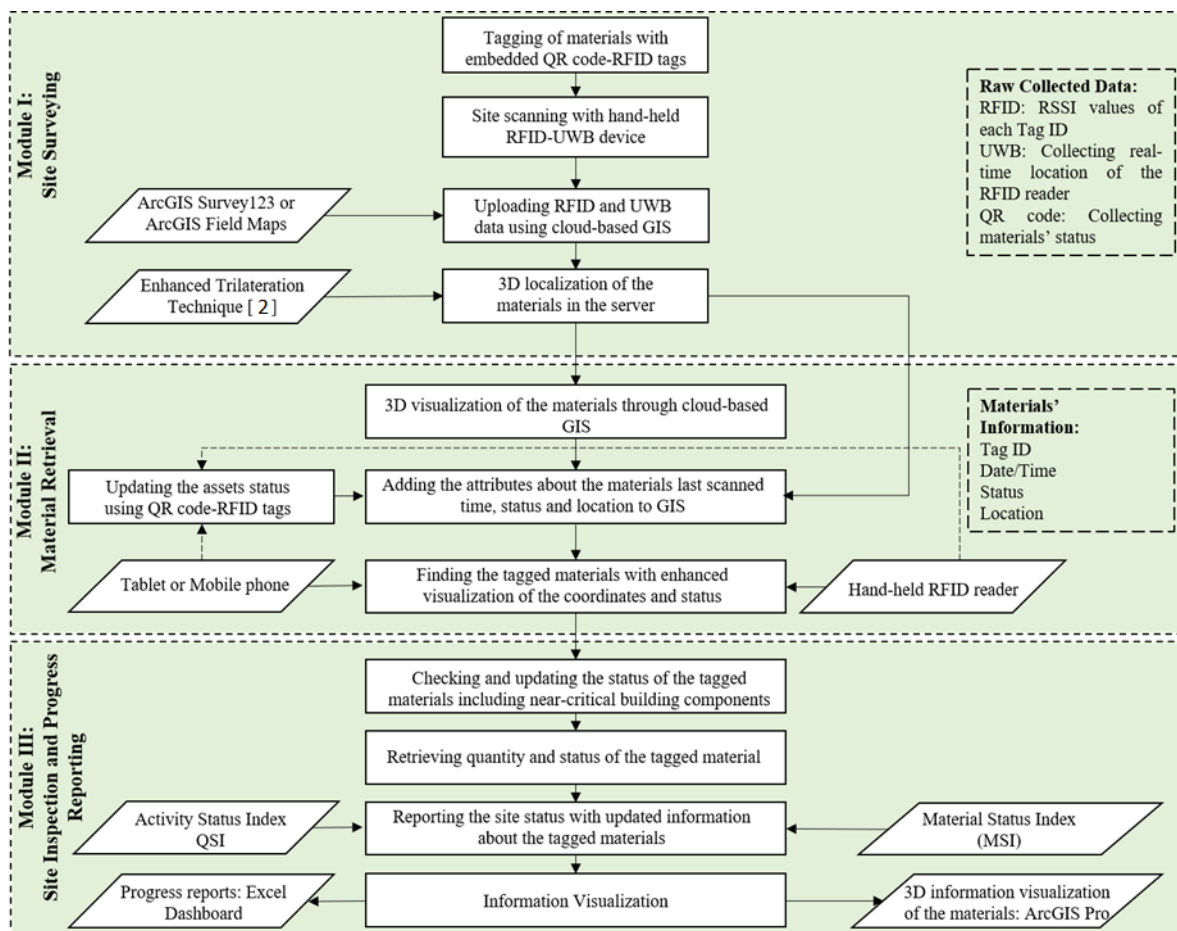


Figure 3.7: Overview of the developed method for tracking and site reporting.

The first module starts with data collection during site surveying using embedded QR code-RFID tags and cloud-based GIS platforms for data collection, including survey123 and ArcGIS Field Maps. The UWB system includes four UWB receivers, and one tag is embedded with an RFID system to shape the Indoor Positioning System (IPS) (Bardareh and Moselhi 2022).

ArcGIS Survey123 is used to design a customized survey for data collection and to transfer the collected data to the ArcGIS Pro. The collected data are then sent to the server for processing, in which the raw data are structured and clustered and used by a trilateration technique for indoor localization of the tagged objects.

The second module includes adding and updating the information required to facilitate object retrieval. In this regard, the object's localization information and the initial status are plugged into the GIS cloud platform. The object localization information and other associated attributes are automatically added to the ArcGIS. The attributes assigned to each RFID tag for each line of information including the tag ID, time of the data collection, the last status of the object, 3D coordinates of the objects, and an average localization error. The average localization error is calculated through Root Mean Square Error (RMSE) which is the actual versus estimated coordinates of the objects as provided in Equation 3.4. This information is used to help the site coordinator or site manager to retrieve the objects more efficiently. In this way, it is possible to find the tagged objects by selecting or searching items already created in the database with the associated attributes (i.e., querying based on RFID tag ID, status, object name, and location). Moreover, providing 3D visualization of the site and the objects associated with each zone is beneficial in retrieving the objects in the elevation or finding the hidden objects (i.e., in the ceiling, behind a wall, or inside a box).

$$\text{RMSE} = \sqrt{\frac{\sum_{i=1}^N (x_i^a - x_i^e)^2}{N}} \quad (3.4)$$

where N is the total number of target objects, x_i^a is the actual coordinates of object i , and x_i^e is the estimated coordinates of object i which is obtained using the developed method.

In the third module, the information associated with the tagged objects (i.e., components such as mechanical equipment in the field), is updated by scanning the QR code embedded on the RFID tag and overwriting the tag's information. By accumulating the information collected from the tagged objects, it is possible to report the overall status. For generating onsite inspection reports, two indices, MSI and QSI, are generated and used to report the progress of the site activities and the quality of the components used in each activity zone. The progress reporting information and the information associated with the components used are then visualized and reported in Excel software and the ArcGIS 3D platform.

Sections 3.3.1 and 3.3.2 elaborate on the first and second modules, respectively, while Section 3.3.3 explains the third module.

3.3.1 Indoor Material Tracking

To enhance the tracking of the materials by digitalizing the data entry and automating the information visualization, the QR code-RFID technology is experimented, and the localization and status information are mapped to the 3D model. The tagged materials' approximate location, status, and scanned time are updated and used to track the innovation group's tracking tools. The cloud-based ArcGIS packages for field data collection, Survey123 and Field Maps, facilitate the data acquisition process through digitalized surveys designed for data entry and transferring the acquired data to the cloud during data collection. At the same time, the 3D visualization of the tagged materials in the ArcGIS cloud facilitates material retrieval.

The experiments were conducted to track the materials available in the indoor space. During site surveying, inexpensive QR code–RFID tags are used in conjunction with the UWB sensors to provide localization information about a group of materials. An improved trilateration technique developed by Bardareh and Moselhi (2022) is used to localize the RFID tags with decimetre accuracy for 3D localization of the RFID tags attached to the target materials. For this purpose, a roving RFID reader equipped with a UWB sensor is used, while the UWB sensor captures the information about the real-time location of the RFID reader, and the hand-held RFID reader reads the tags. The raw data collected during the surveying phase is transferred to the server for further processing. Figure 12 shows the details of the data acquired through the QR code and RFID tags during data acquisition. As depicted in the figure, the QR code collects data about the time, zone and status of the components. The RFID is used to collect the time-stamped data about the time, ID, RSS of the tagged component. These data are used to estimate the tagged component's location and status in the site. During material retrieval, the updated information about the tracked material's last scanned time, status, and location are visualized in the BIM-based 3D model to retrieve the required materials. These information are then imported into the 3D model through ArcGIS cloud packages, in which the information are structured in compliance with the standard format defined in the ArcGIS Pro. The visualized information also facilitates site inspection and RFIs since the materials are annotated in the cloud-based BIM model, and the surveyor or the quality team instantly updates their information, whether by using the ArcGIS's field data collection applications on the phone or directly advising the 3D BIM models.

Figure 3.8 shows the 3D visualization of the scanned tags in ArcGIS Pro, along with geo-referenced coordinates and the status of the tagged components. These data are then used to

retrieve and trace the tagged components. To ensure accurate mapping of located components and associated information within the ArcGIS environment, it is necessary to georeference coordinates from the local system (using RTLS) to the global system (in ArcGIS). This process involves selecting tie-points from the project site that are visible in both interior and exterior spaces (e.g., entrance doors and window frames) and collecting their geocoordinates. Subsequently, components localized using the integrated RFID-UWB method are transferred to the global system by adjusting their coordinates based on the geocoordinates of the selected tie-points. For this study, this georeferencing process was performed manually using an Excel file. Appendix I provides more details of how RTLS data is mapped into ArcGIS.

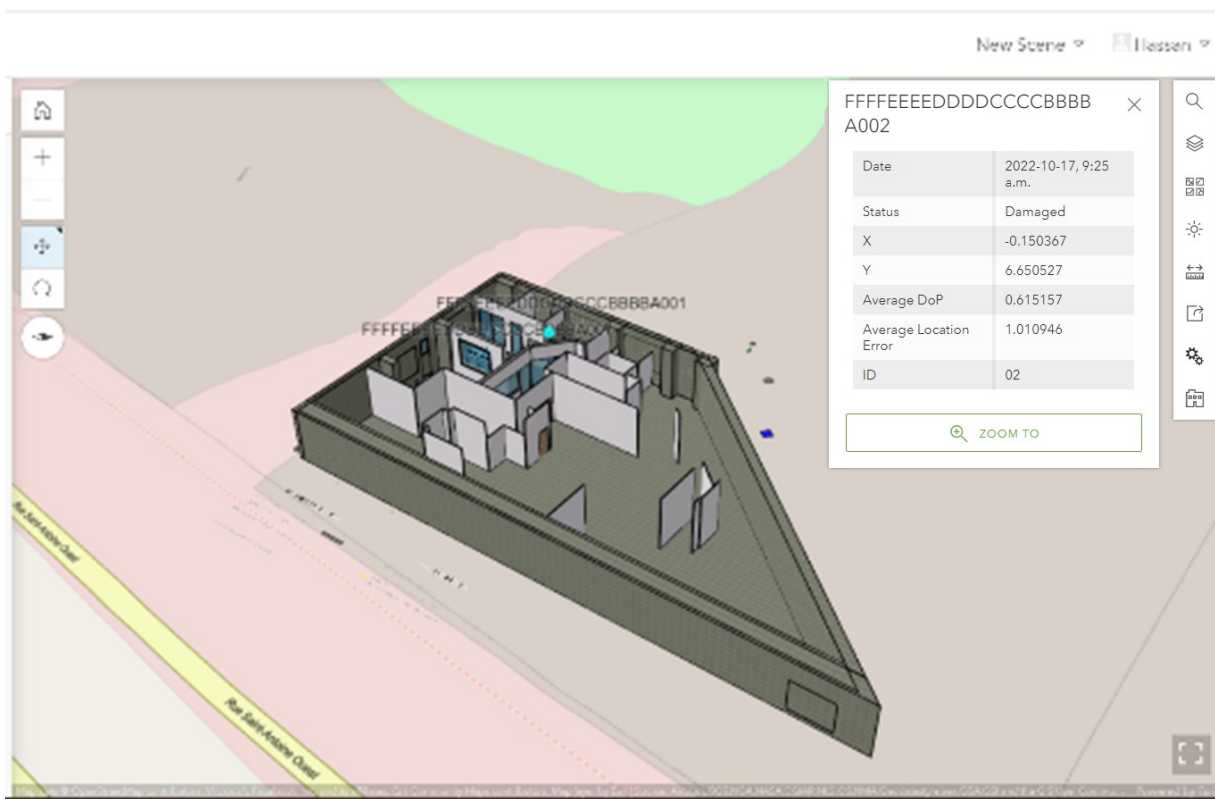


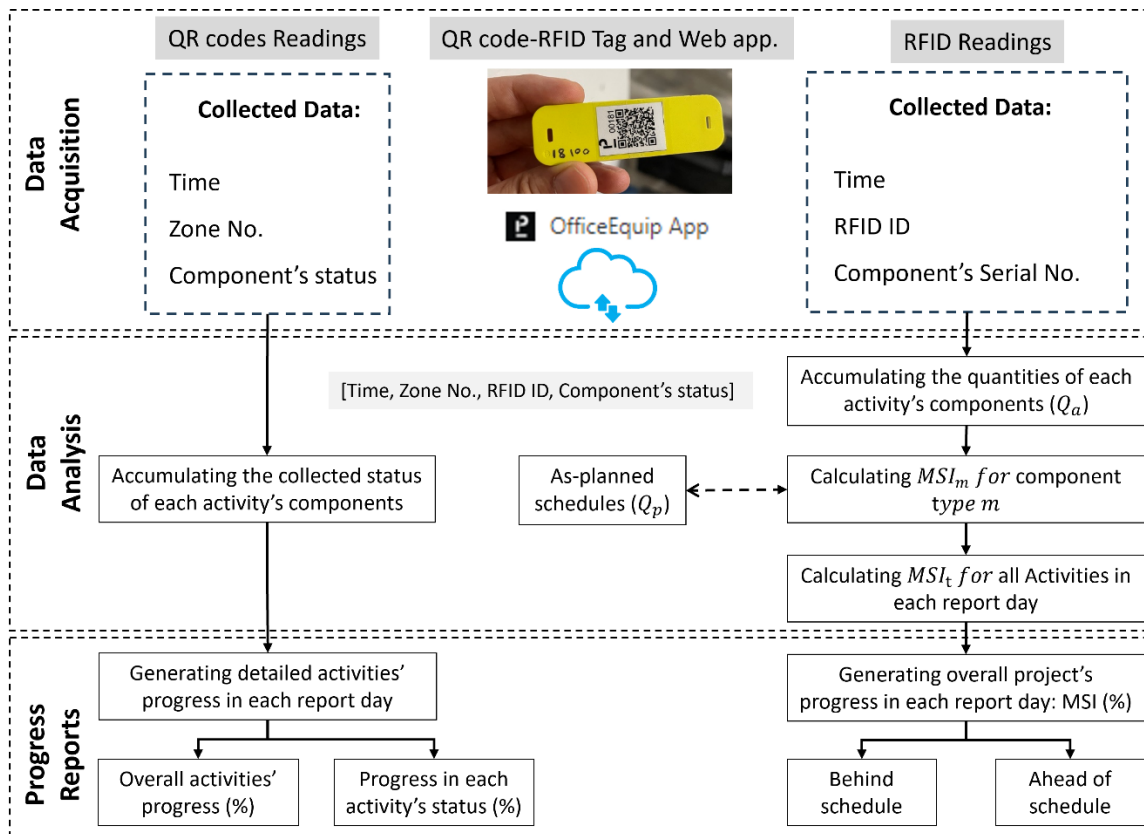
Figure 3.8: 3D visualization of the RTLS data.

3.3.2 Site Inspection and Progress Reporting

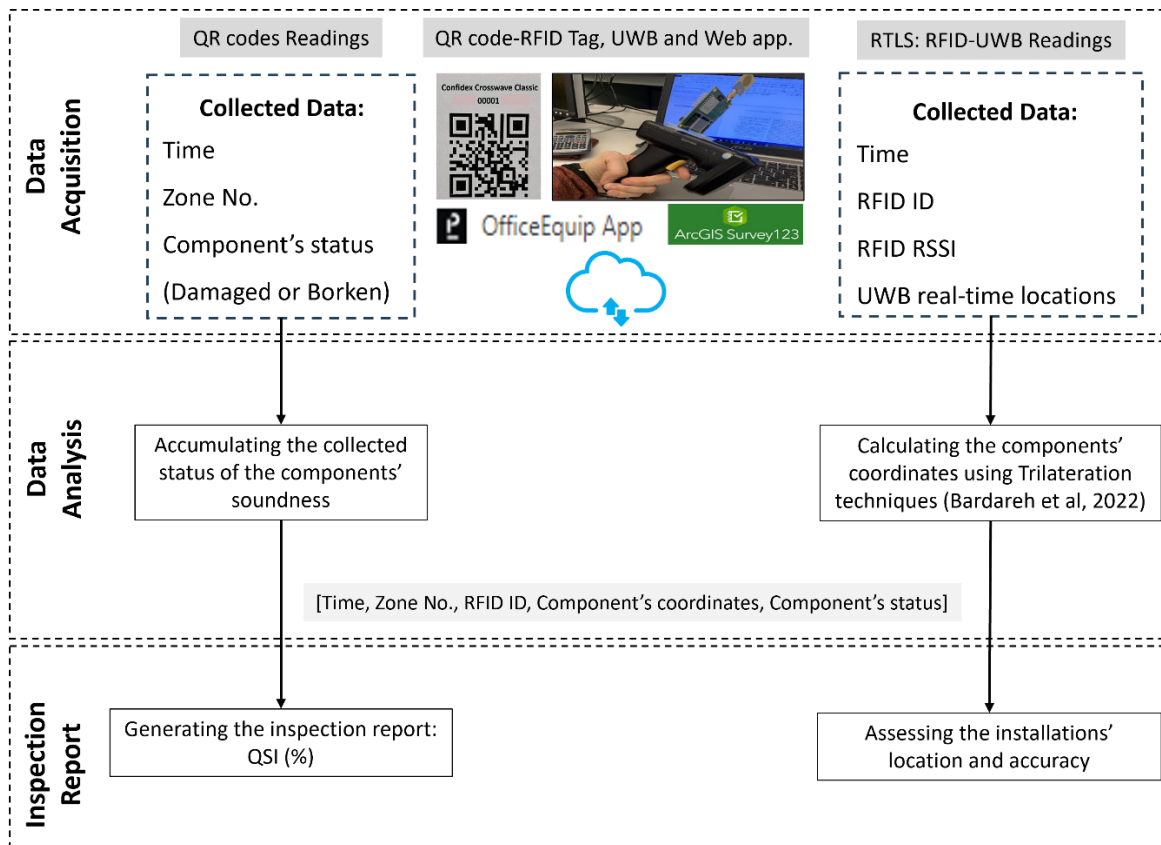
In the second part of this study, various activities on site are tracked to report the project's progress and quality. This includes reporting the quantity and status of the components and sub-components of near-critical activities. The criticality of the activity is defined based on the activity float time to its duration and by consulting with the site manager. For each activity, critical components are selected to be labelled by the QR code-RFID tags. The critical components are representative of all the components available in the project. Moreover, various

statuses, such as delivered, installed, and inspected, are defined through a survey to fill out for each activity during the site inspection. The quality of the components used in each activity is another area addressed in this study, as well as the progress in each activity. "Damaged or Broken" status reports the consumed components that need attention for maintenance or replacement.

Figure 3.9 illustrates the details of the developed method for generating onsite inspection reports. The project progress is represented by the introduced MSI and the percentage of progress in the activities' status collected during the site inspection. The QSI highlights the quality of the components (i.e., mechanical equipment) used for each activity and reports the project's physical progress.



(a)



(b)

Figure 3.9: The developed method to generate onsite inspection reports: (a) progress reports: MSI (quantity-based report) and status-based reports, and (b) QSI to highlight the quality of the components used, and their targetted location.

To generate the onsite inspection reports, various statuses are defined for each activity type, which includes the materials' tracking in different phases of the project, starting with material delivery to the installation and the quality inspections. For each status, a customized percentage was defined, representing the activity's progress by advancing in the phase-based status. The progress in each activity, including status-based progress and MSI, and the QSI are generated by accumulating the quantities and percentages for the materials consumed in each activity at the end of each reporting day. The MSI is calculated comprising the planned and actual schedules of the activities, accumulated for all activities to show the project's overall status on each reporting day. The actual quantity and quality status of the components on site are collected by QR code-RFID technology. Saying that, in obtaining the conventional SPI, calculations are on activity levels. However, in the developed method and in calculating MSI, control points are materials that augment the SPI and CPI indices (Chen et al. 2020, Moselhi

et al. 2020). The MSI calculation includes: (1) Critical components associated with near-critical activities are selected. The critical components are labelled with RFID tags' IDs, which are the same IDs defined in a planned model. The criticality of the components is implicit in the criticality of their associated activities. Two factors, including the total float time and the ratio of the total float time to the activity duration, are considered to assess the criticality of an activity. The latter one was considered since there is a higher chance for activities with longer duration to face delays, although they may have the same total float time. This ratio is quite project-specific. However, a default of 15% is suggested by Azarm (2013). This process helps to prevent tracking of unnecessary activities (and corresponding components), thereby decreasing the number of the tags required as well as the data collection effort required. Moreover, careful selection of the critical components helps to prevent overlaying of the project progress due to tracking of unnecessary components.

(2) Calculating individual MSI values for each component type. Equation 3.5 shows the MSI value calculated for each component type, where n is the total number of the near-critical activities that consumed component type m . The MSI value for each component type is the ratio of the actual quantity to the planned quantity of the components consumed or installed.

$$MSI_m = \frac{\sum_{i=1}^n Q_{ai}}{\sum_{i=1}^n Q_{pi}} \quad (3.5)$$

Here the Q_a is the actual quantity of the components used, while Q_p is the quantity of the components that are planned to be consumed by the reporting day.

(3) Calculating the total MSI involves summing the weighted MSI_m for each class of component. The weighted factor relates the criticality of various component classes to the associated activities. It also considers the interconnectivity between component types and their associated activities in highlighting the project's progress status. Equations 3.6 illustrate the formulas in this regard.

$$MSI_t = \sum_{m=1}^k MW_m MSI_m$$

$$MW_m = \frac{\left[\frac{FS_m}{\sum_{m=1}^n FS_m} \right] + \left[\frac{FDS_m}{\sum_{m=1}^n FDS_m} \right]}{2}$$

K = Total number of the class
of components
 MW_m = Material weight for
class of component, m
 n = Number of activities
 FS_m = Float score for material,
 m (3.6-a)
(3.6-b)

$$FS_m = \sum_{i=1}^n \frac{FS_{i,m}}{n}$$

$$FDS_m = \sum_{i=1}^n \frac{FDS_{i,m}}{n}$$

$$FS_{i,m} = Max_f - F_i$$

$$FDS_{i,m} = Max_{fd} - \frac{F_i}{D_i}$$

FDS_m = Float duration score

for material, m

$FS_{i,m}$ = Float score for activity

i using component m (3.6-c)

$FDS_{i,m}$ = Float duration score

for activity i using component m (3.6-d)

Max_f = The activity with maximum float (3.6-e)

Max_{fd} = The activity with maximum ratio of the float time to the duration (3.6-f)

The QSI is calculated by accumulating the number of components with the “Damaged or Broken” status in each activity during the site inspection. This can also compensate for the limitation of the MSI, in which the wasted components are not considered in the index, since they are omitted from the calculation of the Q_a .

3.4 Integrated RTLS and Point Cloud Data for Refined Indoor Object Localization

This section describes a newly developed method for the recognition and localization of objects on site, utilizing RTLS technologies such as RFID, UWB, and LiDAR device. The LiDAR device used in this study is a terrestrial laser scanner (TLS) which generates PCD for the experimented environment. In the developed method, the localization information obtained by the RTLS devices is refined by the localization information achieved from the PCD acquired, leveraging the object detection and segmentation capabilities of a computer-vision algorithm. For this purpose, the information obtained is merged to enrich the recognition and localization of the identified objects on the scene. In this thesis, the main emphasis is on the integration of computer vision with RTLS to refine 3D object localization. The improvement of the computer vision algorithm used for semantic segmentation of the collected PCD is not the primary focus of this study. Figure 3.10 illustrates the schematic overview of this integration, and how the RTLS data are exchanged with the detected PCD.

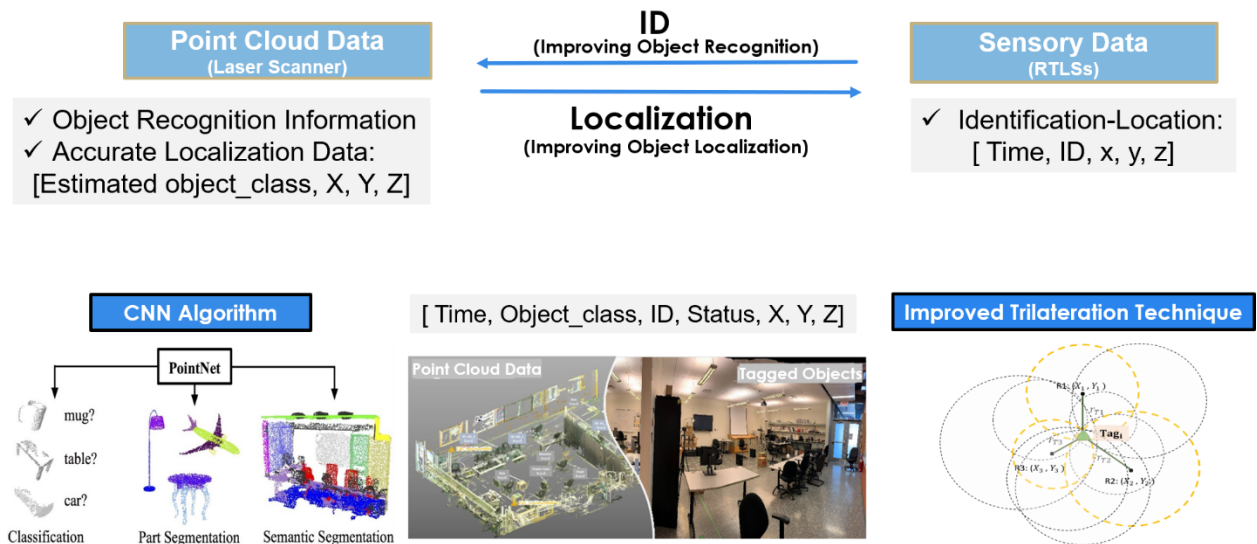


Figure 3.10: Schematic diagram of the developed method for indoor object recognition and localization (Bardareh and Moselhi 2023).

This study uses a point cloud-based algorithm, PointNet, to detect and localize objects. PointNet, which is a point-based algorithm, is used to alleviate the limitations associated with voxel-based and pixel-based algorithms. As depicted in Figure 3.11, the algorithm comprises two main modules, classification and segmentation. The semantic segmentation module of the algorithm makes it possible to label each point cloud with the defined class of object. The developed method mainly focuses on using the segmentation information achieved from the PointNet algorithm and integrating it with the RTLS information. This helps to localize the recognized objects on site while enhancing the localization information of the tagged object obtained by the RTLS sensors. The hyperparameters are set based on the suggestions of the algorithm's founders (Qi et al. 2017). The Adam optimizer is used to adjust the learning rate, which is set to 0.001. In this study, a certain class of objects, including furniture and slabs, is used to train the algorithm. The number of epochs is set to 25. Additionally, the batch size is set to 32, and the dropout rate is 0.3.

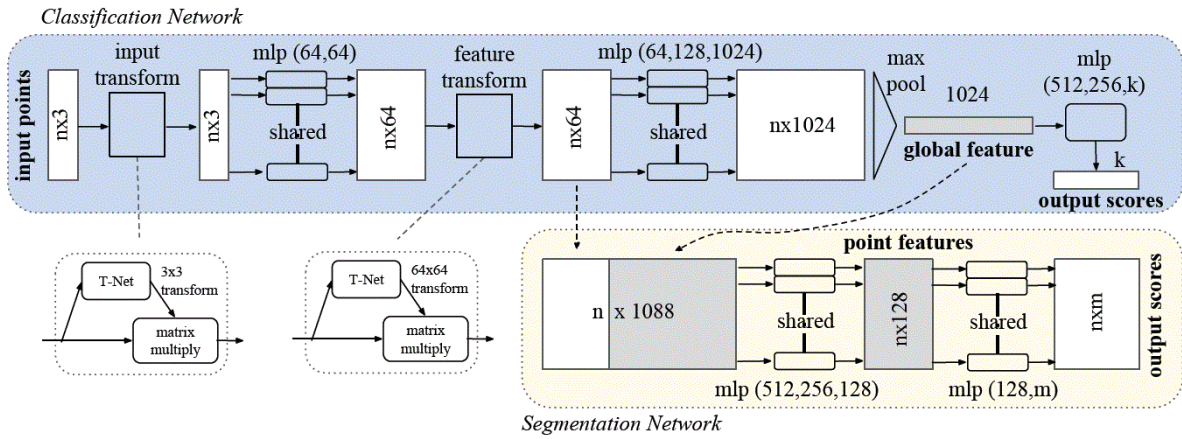


Figure 3.11: PointNet algorithm (Qi et al. 2017).

The main focus of this research study is on using PCD to recognize and localize objects. The identified gaps in the literature limit the performance of the DNN techniques for onsite object recognition and localization. One of these gaps is the generalizability of the developed models for various object recognition tasks in different environments. In this regard, this study investigates the performance of the available PointNet algorithm to recognize one class of the object, chairs, available in the experimental environment's scene point cloud. This class of object is already available in the benchmark datasets used in this experiment to train the DNN model. However, the model's capability to recognize the objects available in the experimental environment and the information about the objects' location are evaluated in the first phase of the experiment. In the second phase of the experiment, an integrated RFID-UWB system is used to identify and localize the RFID tags attached to the objects in the experimental environment. Some of the chairs are tagged with RFID tags, while the information about their identification and location are obtained using a trilateration technique. In the last phase of the experiment, the possibility of using these tagged objects as the ground-truth information for enhancing the information obtained using the PCD is investigated. The information exchange between these two groups of information helps enhance the recognition of the information obtained using the PCD. Meanwhile, the accurate localization of the PCD helps improve the RFID-based system's localization accuracy.

The information exchange between RTLS and PCD helps enhance object recognition through computer vision. Meanwhile, the accurate localization information of the point cloud data helps improve the RFID-based system's localization accuracy. Three scenarios are experimented with through the developed method to validate the results. The first scenario includes the

application of the PCD acquired by a laser scanner to do object recognition and localization using a DNN technique. The second scenario involves experimentation with the use of RTLS for object identification and localization. Here, some objects are tagged with RFID tags, while the information about the object is assigned to it using an ID. The third scenario involves the integrated use of these technologies to enhance both the recognition and localization of the identified objects. The information achieved in each scenario is used for various purposes. For instance, the objects and assets with RFID tags can be localized and tracked using the ID assigned to each tag. However, the PCD provides information about the number of objects available in each room for each class of object, along with information about the accurate location of each object. The integrated approach developed in this study helps to enhance the information provided by each type of technology by exchanging the information between the first two scenarios. The developed method in this section helps to enhance object localization on site, which has applications for improving site inspection, asset retrieval, and automated 3D modelling of the site. In the following sections of this paper, the techniques for implementing these technologies are elaborated on, focusing on the CNN for using PCD for indoor object recognition and localization. Then, the method developed in this study is validated through various experimental scenarios.

The point cloud coordinates—as well as its additional feature channels, such as intensity, colour, and normals—represent specific statistical properties of the points and are designed to be invariant to certain transformations (Qi et al. 2017). Despite the excellent information provided by the point cloud instead of images, including coordinates and features, some intrinsic limitations related to using the PCD should be addressed. These limitations include the degraded quality of the PCD in case of having unorganized, noisy, and missing data that may be caused by occlusion, reflective or transparent surfaces in the building elements. Furthermore, the large volumes of point cloud files demand a larger storage area in the server while requiring high computation processing performance for applications associated with 3D model reconstruction and automated object recognition. Moreover, the PCD acquired by laser scanners does not include material type and texture information, which is needed for some applications in building engineering.

The developed method is coded in Python, using the TensorFlow library for the object recognition of the PCD. Three experimental scenarios are tested in a laboratory environment to validate the developed method, including RTLS, LiDAR and their integrated use. The results

for the individual use of the RTLS sensors and LiDAR device (first and second scenarios) are confirmed with the object localization and recognition proposed in the literature studies. In the third scenario (i.e., the integrated scenario), 90% accuracy is achieved for object detection, while localization is found to be accurate to within a few centimetres (this is further explained in Section 4.3).

In the present study, Stanford 3D Indoor Scene (S3DIS) is used to train and test the PointNet algorithm (Tran et al. 2021, Qi et al. 2017). However, the PCD collected by the LiDAR device in the laboratory environment is used to evaluate the trained algorithm in detection of the selected class of object (i.e., chairs in the laboratory). The algorithm used has an acceptable classification accuracy. However, the results for 3D scene object segmentation and detection, which is required for detecting the target objects in the scene, are unsatisfactory. Only four out of ten target objects are correctly detected by the network. However, the localization accuracy of the detected objects increased to a few centimetres in 3D format. This problem was reported by Qi et al. (2017) and is compensated for by integrating the RFID technology in this study. Moreover, for comparison purposes, object segmentation and detection are carried out using a ready-to-use platform in the market, Vercator Cloud, thereby improving the 3D scene object segmentation and detection (Vercator 2024).

3.4.1 Evaluation Metrics

Intersection Over Union (IoU), Equation 3.7, is applied to the results as an evaluation metric to assess the performance of the point cloud-based classification algorithm. It is used to evaluate the performance of the PointNet, by quantifying the overlap percentage between the target mask and our prediction output (Qi et al. 2017).

$$IoU_c = \frac{|P_c \cap G_c|}{|P_c \cup G_c|} \quad (3.7)$$

P_c refers to the set of points the trained model predicted to be of the class- c , G_c denotes the ground truth set of points that belongs to class- c . Accuracy is also used to evaluate the detection accuracy of the PointNet scene semantic segmentation based on the number of correct predictions to the overall number of objects.

Moreover, to evaluate the localization accuracy of the RFID–UWB, the RMSE is used as suggested by Bardareh and Moselhi (2022). The same metric is used to evaluate the localization accuracy of the coordinates assigned to each object through semantic segmentation of the PCD.

3.4.2 Integrated PCD and RTLS Data

Figure 3.12 shows the overview of the research methodology and how these two groups of sensory data can communicate together to enhance object recognition and localization on site. As depicted in the Figure, the identification assigned to each object labelled with the RFID tag is used to localize and identify each object. While the PCD contains information about the number of objects in the scene, along with the exact location of each object. For objects identified by both the RFID system and the PCD, more accurate information about the ID and location of the object is achieved through this information exchange.

Integrating the identification and positioning data acquired by a tracking system, such as RFID or UWB, with the PCD acquired by a laser scanner could provide additional capabilities in the 3D reconstruction of various elements in a job site. As such, not only structural elements (e.g., floor, ceiling, wall, windows) but also small objects and equipment in a job site can be recognized, localized, and modelled using the integrated RTLS data and PCD. This helps to create a more accurate as-built 3D model of construction projects, which can be used for inspection, progress reporting, and productivity analysis of various activities varying from structural to equipment and facility installations (Cai et al. 2014, El-Omari 2008, Munaro et al. 2016, Roghabadi and Moselhi 2020, Shahi et al. 2014).

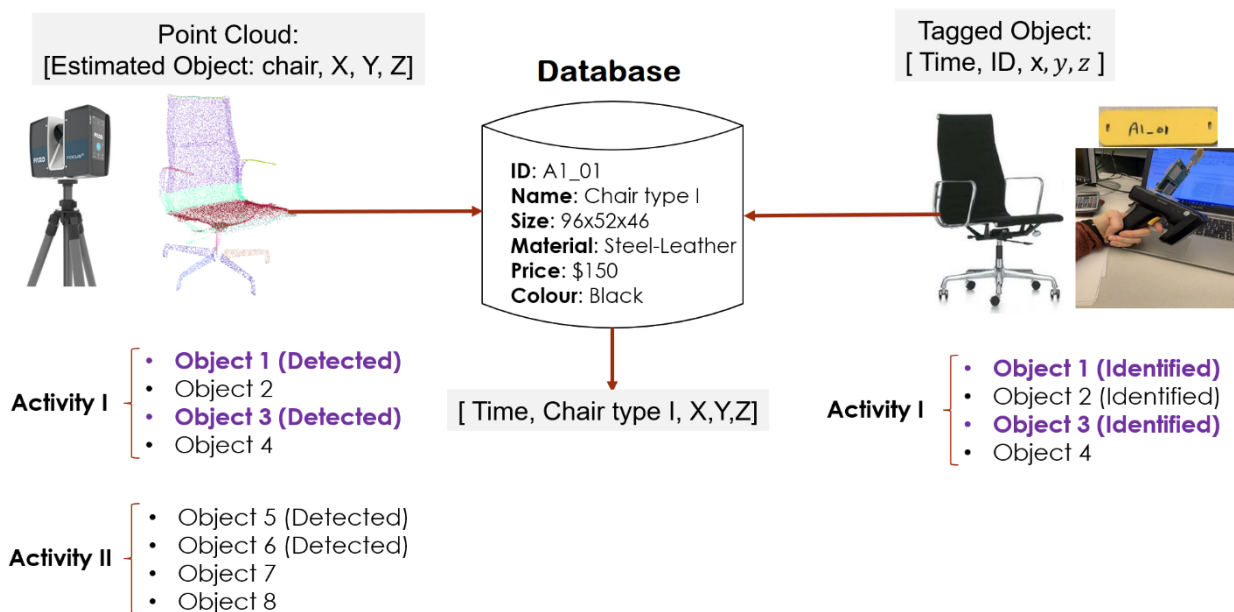


Figure 3.12: Joint RFID-based and point cloud data (Bardareh and Moselhi 2023).

3.5 Digital-twin Platform for Automated Generation of Onsite Inspection Reports

This section introduces an innovative framework for the automated generation of onsite inspection reports, leveraging the integrated use of Real-Time Location System (RTLS), 3D digital imaging, and web-enabled computer-vision technologies. The aim underlying the framework is to enhance the efficiency of construction project delivery by boosting productivity and facilitating timely decision-making through an improved inspection process.

A sensory-based framework is developed to identify and localize onsite installations as the basis for generating onsite inspection reports that contain both installation progress information and targeted coordinates. Figure 3.13 illustrates the framework, including the data collection technologies employed, data processing algorithms, and the resulting onsite inspection reports. The framework comprises three methods: (1) an RTLS-based tracking method that utilizes a joint application of RFID and UWB technologies to improve the localization of tagged objects, (2) a 3D object detection and localization point cloud-based method that utilizes a computer-vision algorithm, PointNet, and a user-friendly cloud platform (i.e., Vercator Cloud), and (3) an integrated method that combines the outputs of the first two methods comprising the use of RTLS and analyzed PCD through computer vision algorithms.

The first method, described above in Section 3.2, provides information about indoor objects' locations. The second method, described above in Section 3.4, detects and localizes objects using a computer-vision algorithm and 3D PCD (Xu et al. 2018). These two types of data are then integrated to improve the 3D localization of the RTLS while assigning IDs to the objects detected by the computer-vision algorithms. As illustrated in Figure 3.13, the integration is achieved by mapping the coordinates of the objects realized by these two technologies, comprising RTLS and LiDAR technologies. For this purpose, each of the objects identified by the RTLS is assigned an ID and coordinates. Each type of object detected and localized by the computer-vision algorithm is also assigned to a dedicated class of objects, which is chair here, and assigned 3D coordinates. To obtain the coordinates of a detected object, the PCD labelled by the algorithm's segmentation module is averaged for each detected object. To refine the 3D coordinates of the identified objects with RTLS, the accurate 3D coordinates (obtained from the averaged PCD) are replaced with the RTLS coordinates. The selection of the detected PCD in the vicinity of the identified object is explained in Section 3.5.3, along with various scenarios related to this integration. Since the RTLS has a 3D localization accuracy of approximately 1

m, the vicinity threshold for assigning the detected objects and their labelled PCD to the identified objects via RTLS is selected within this range.

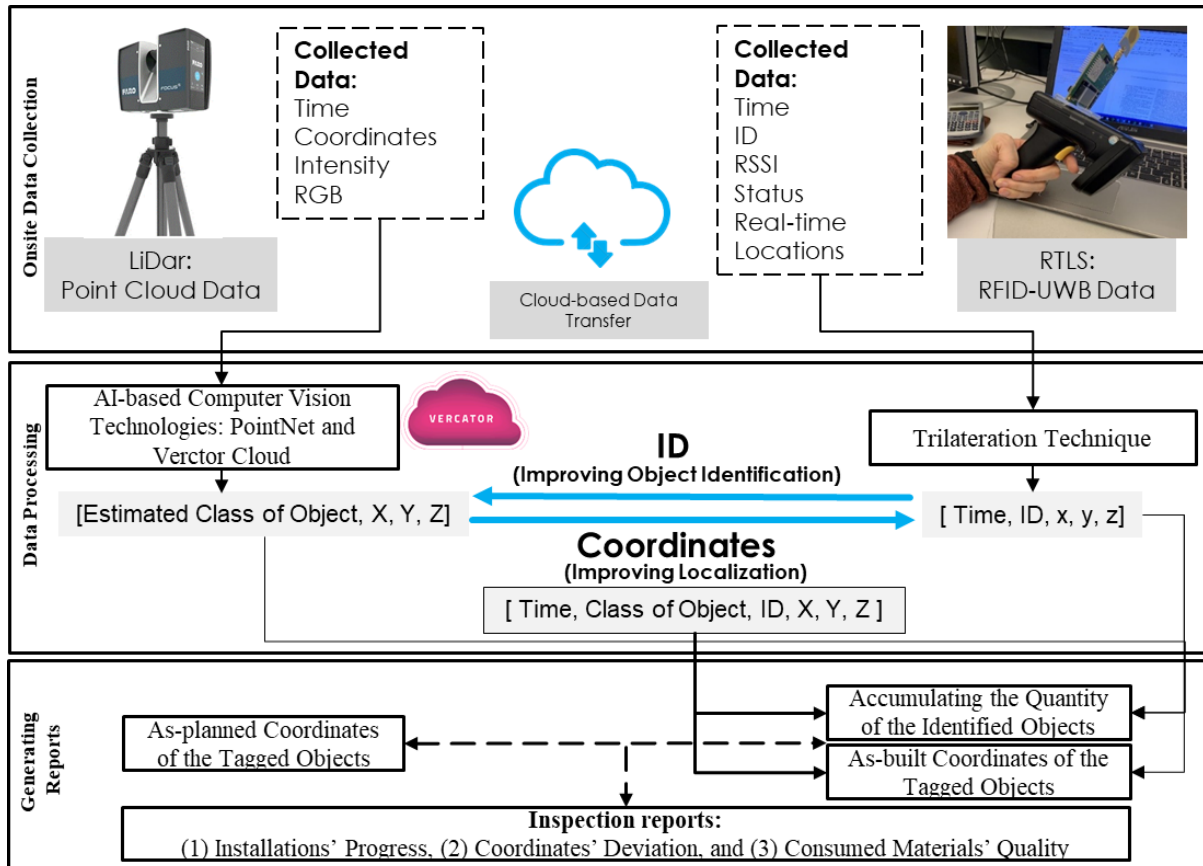


Figure 3.13: Developed framework for data collection and integration using RTLS and LiDAR data.

Integrated technologies are used in the framework to enhance the accuracy of the identified object (i.e., chair) coordinates, as well as the accuracy of the information about the quantity of the objects. Onsite inspection reports are then generated using the collected data mapped to the digital environment, considering the quantities and locations of the objects, where deviations in the coordinates represent differences between as-built and as-planned locations of installations, including the \pm localization error of the integrated RTLS and 3D imaging technologies. The as-planned coordinates are derived from the tie-points on the floor in the laboratory.

The RTLS module is based on the RFID-UWB system, developed in an earlier work to provide location identification information about indoor objects' locations accurate to within a few decimetres (Bardareh and Moselhi 2022). The AI-based computer-vision module employed is

also drawn from an earlier work, the module having been developed to detect and localize objects and provide information about the number of objects using a deep neural network algorithm and 3D point cloud (Bardareh and Moselhi 2023). The last module is progress reporting, in which the integrated use of the RTLS and point cloud-based computer vision is used to automate object detection and localization. This integration is achieved by mapping the coordinates of the objects obtained by these two technologies. The objects tagged using the inexpensive RFID system are more accurately localized using the PCD, as depicted in Figure 3.13.

In the experiment, a few activities are selected to represent the project's progress, with these activities being monitored by tracking objects present in the two mechanical rooms of a project. It should be noted that, while other studies have used the same concept for activity recognition of related tasks on site (Huang et al. 2021), the present study focuses on object recognition and localization, integrated within the digital-twin platform to enhance onsite inspection and progress reporting.

Integrated technologies are used in the framework to enhance the quality of the data collected and to achieve more accurate location identification information on project components, along with information about the status, quantity, and availability of these components. These technologies include a terrestrial laser scanner and a Real-time Location System (RTLS) enabling automated recognition and localization of tracked objects. This recognition and localization information, together with BIM, are embedded in a digital-twin platform.

Progress reports are then generated using the collected data mapped to the digital environment that contain the quantities and locations of the identified objects. These reports are also visualized a construction twin dashboard to provide project managers with accessible and timely information. As shown in Figure 3.14, the front end of the dashboard includes information about the project's overall status, represented by the MSI. The localization error, moreover, reflects the accuracy of the integrated RTLS in providing as-built visuals of the localized objects on site. The activity overall progress in each report day is presented in the form of a graph, while the pie charts provide detailed resolution on each activity's progress for the defined statuses (i.e., the percentage of objects delivered, installed, inspected, and damaged or broken).

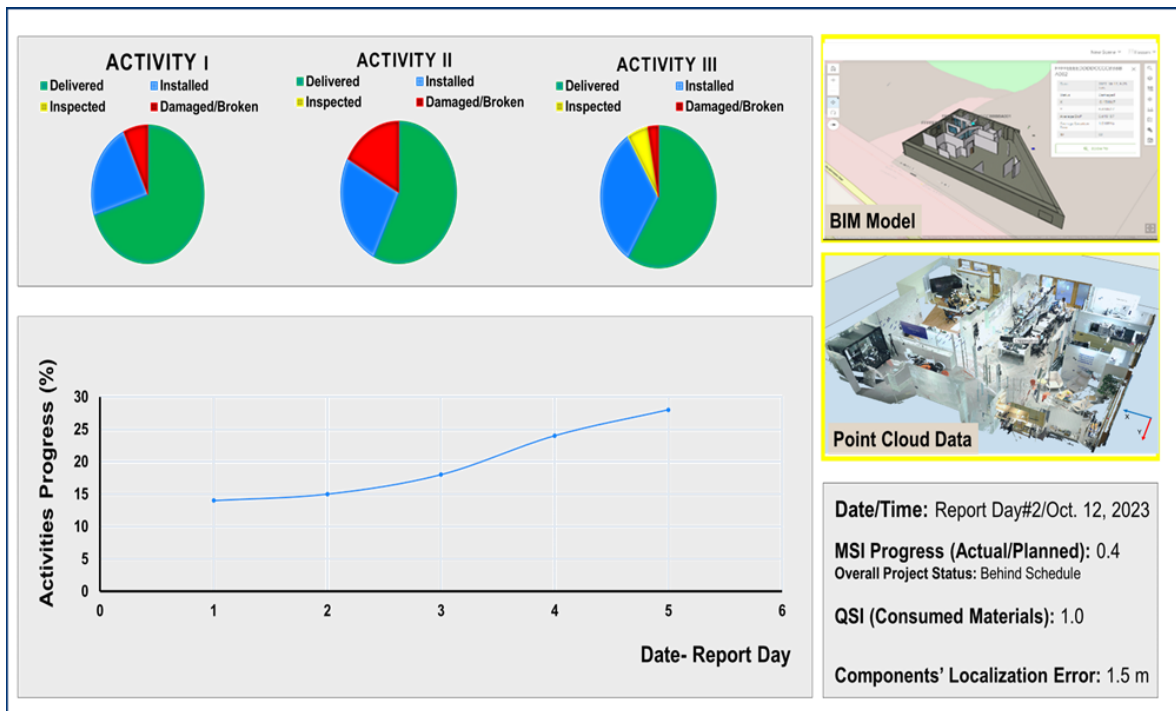


Figure 3.14: A construction twin dashboard to visualize progress reporting.

3.5.1 RTLS in a Digital Twin

While the reasonable cost of RFID technology makes it a good choice for indoor object localization, when it is employed as the sole technology for localization of objects in an indoor environment, a large number of RFID reference tags is required to ensure localization accuracy (Cai et al. 2014). In outdoor applications, RFID has been integrated with GPS-based sensors to eliminate the need for RFID reference tags (Cai et al. 2014, Su et al. 2014). These methods essentially find the location of the RFID reader(s) using a GPS receiver and then determine tag locations through a trilateration technique. However, in an indoor environment, the performance of GPS sensors is degraded since they rely on signals from satellites. In this regard, the UWB system can replace GPS as the means of localizing the RFID reader in each time span.

Accordingly, in the present study, a system integrating RFID with UWB sensors is employed. This integration helps to avoid the high cost of full-scale UWB implementation for object tracking while taking advantage of the medium-range capability of low-cost RFID technology (Ruiz and Granja 2017). This integrated module, which provides near-real-time IPS data on the project components present on site, benefits from the accurate positioning capability of UWB sensors for localizing the hand-held RFID reader in an indoor environment (Bardareh and Moselhi 2022, Bardareh and Moselhi 2020), as noted above. As such, it is capable of

localizing the tagged objects using inexpensive passive RFID tags while updating the status of project components using cloud-based data collection tools.

3.5.2 PCD and Computer Vision in a Digital Twin

There are a number of different Scan-To-BIM approaches for implementing PCD to facilitate 3D modelling of the components available in a scanned scene. There are also various levels of automation for generating the models from the PCD. In a manual approach, PCD is used to manually model the objects based on visual inspection. In this approach, supplementary tools for 3D modelling (i.e., as-built modeller) are used to facilitate the modelling of objects. In semi-automated approaches, AI-based supervised modelling is implemented in which the as-planned 3D model of the project on site corresponds to the acquired PCD. In these techniques, the supervised classifiers or AI techniques are used to relate every object in the generated model to a corresponding element in the planned model. The planned model, in turn, is used as a reference to help identify the objects in the PCD. Although semi-automated are more advanced than purely manual approaches, they still rely on manual inspection of the generated models, and they errantly assume that the as-planned 3D model is sufficiently accurate (Bardareh and Moselhi 2023).

AI-based and DNN techniques have been used to model the objects represented in PCD. These techniques directly use the PCD and are capable of detecting and segmenting various classes of objects present in the tracked scene based on just one round of training. While these techniques are fully automated, they can be lacking in terms of accuracy (Bardareh and Moselhi 2023, Ma et al. 2022).

In this study, a point cloud-based network is used to detect and localize objects. For this purpose, an available benchmark is used to train and test the model (Bardareh and Moselhi 2023, Qi et al. 2017).

3.5.3 Integrated RTLS and PCD for Automated Generation of Onsite Inspection Reports

Integrating RTLS data with PCD enhances object localization and identification by leveraging the capabilities of both types of data (Tran et al. 2021). The RTLS component ensures accurate identification by assigning IDs to identical objects, a function computer-vision algorithms are not capable of due to their limitations in differentiating between identical objects from the same class. RTLS is also beneficial in NLoS scenarios, where the LiDAR device is not able to collect

PCD (i.e., if an area is covered or objects are hidden behind a panel). The point cloud-based computer-vision component, meanwhile, provides highly accurate (within 1 cm) localization information, which is crucial in many applications on job sites, such as automated inspection of Mechanical, Electrical, and Plumbing (MEP) installations.

To achieve the integration, all objects recognized and localized by the RTLS and PCD are first derived. Then, for any object with an RFID tag, the objects detected by the PCD in the vicinity of the tagged object that belong to the same class of object are selected. For example, if an object (i.e., a chair, in the case of this study) is tagged and identified with the RFID tag, the PCD identified by the DNN algorithms as representing a chair is then assigned to that chair. The coordinates of the objects detected in the PCD are then replaced with the location information of the RTLS. Figure 3.15 shows the flowchart of the steps for the individual deployment of these technologies and their integration for generating onsite inspection reports.

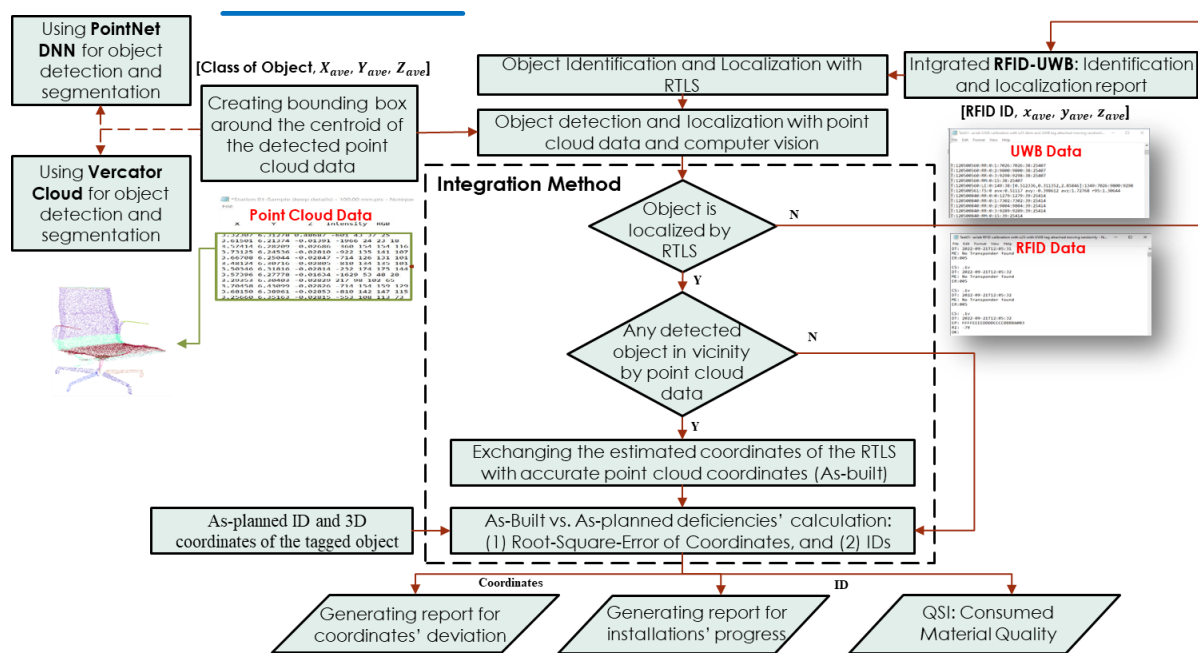
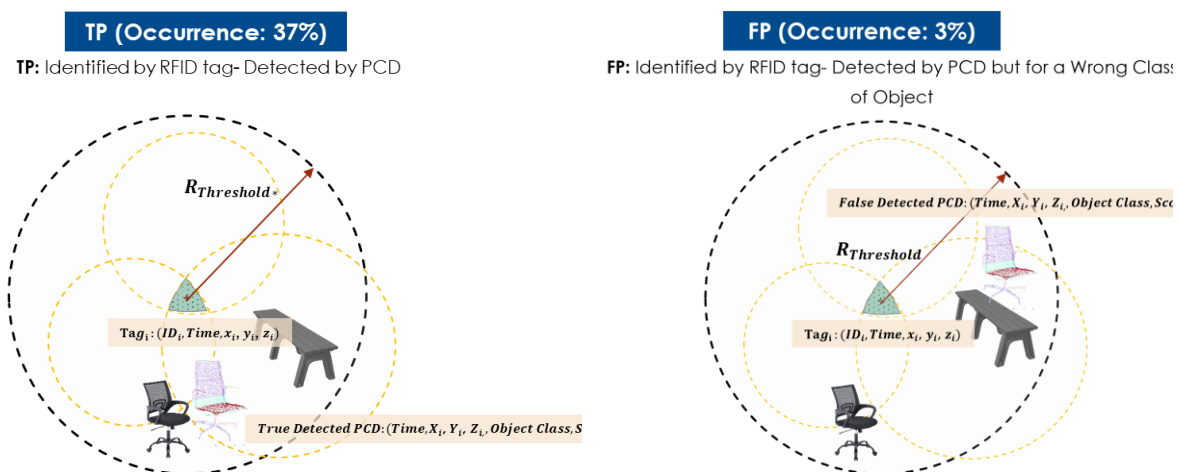


Figure 3.15: Flowchart of the developed method for integrating RTLS and point cloud data.

The integration enhances the localization accuracy of the RTLS as well as the accuracy of the coordinates in the PCD. However, the experimental results show that the occurrence rate for this improvement is only 30–40% of the tagged objects when using the PointNet algorithm and available datasets as a benchmark (Tran et al. 2021). For the other 60–70% of the tagged objects, it is the raw identification and localization information obtained by the RTLS that is

used to generate the onsite inspection reports. In the present study, the computer-vision results obtained using PointNet are compared with those obtained by the Vercator cloud platform. It should be noted that Vector Cloud uses optimized computer-vision algorithms to detect objects from PCD and for various classes of objects. It also allows the labelled PCD to be exported for further analysis and integration with RTLS data (Vercator 2024).

Figure 3.16 illustrates various scenarios for integrating RTLS and PCD to detect chairs in the laboratory. The integration of the RTLS data with computer-vision data ensures higher accuracy of the objects' 3D coordinates while also providing a means of assigning IDs to the detected objects for the purpose of generating onsite inspection reports. As depicted in the figure, the predominant scenario, the false negative (FN), is the situation in which a chair is labelled and identified by an RFID tag but not detected by the PCD. True positive (TP) is when the PCD detects the tagged chair. Finally, in false positive (FP), the RFID tag correctly identifies the chair, but the chair is not assigned to the correct class of object in the PCD. In the FP scenario, the object's location as detected by the RFID tag is errantly replaced with the location of another object(s) in the vicinity. This is a rare scenario, and the information about the object's ID is still valid in such cases. Although further experiments with other types of objects would be required to fully validate the results, RFID information can still be used as the primary source of information for object recognition, resulting in a robust identification rate for objects labelled with RFID tags and improved localization information in TP situations.



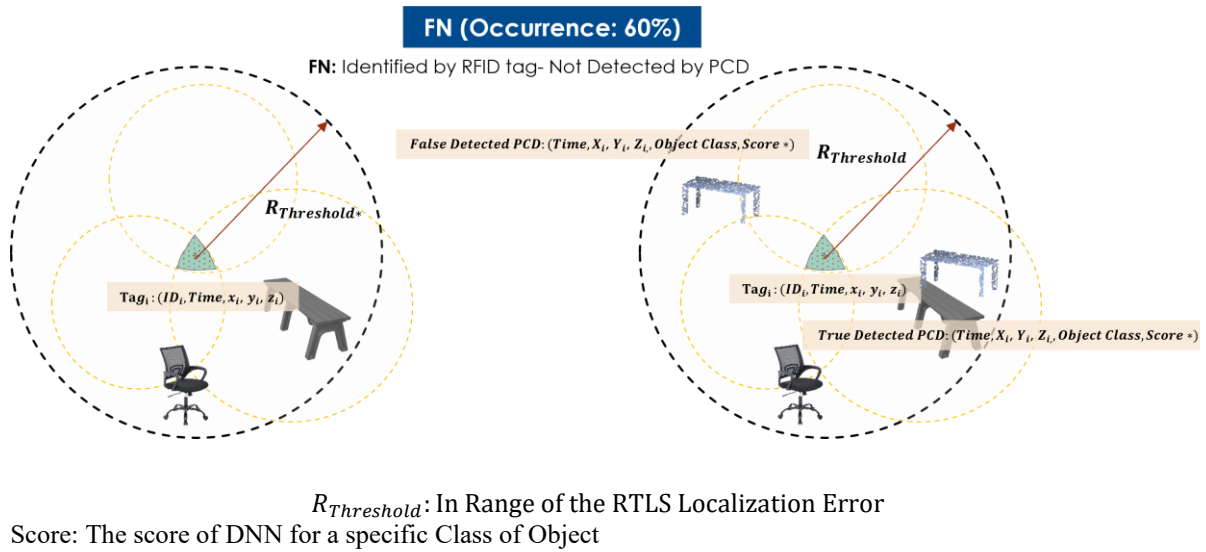


Figure 3.16: Various scenarios in integrating RTLS and point cloud data.

ArcGIS packages are used for data collection and for mapping the information in the BIM model for visualization purposes. The objects identified using the RTLS, PCD, and integrated RTLS–PCD data are counted and added as inputs to the material status index developed by Moselhi and Azarm (2013) in order to achieve automated generation of progress reports.

3.6 Summary

This chapter described the methods developed for indoor object identification and localization and their application in generating progress reports and visualizing the tagged objects in an indoor environment. The first method is a cost-effective and practical RTLS based on integrated RFID–UWB technologies. The method provides 2D and 3D localization of the objects on the floor and at elevation, as well as the ID and status of the tagged objects, and is capable of handling even the most challenging objects to track on job sites, such as mechanical equipment and other MEP installations. This information is then mapped to the cloud-based BIM platform (i.e., GIS packages) to facilitate data collection and visualization of component installation progress and status. The object ID, location, and status are used to generate two developed indices, MSI and QSI, which capture the progress of the installations and identify any damaged or broken objects.

Computer-vision data is integrated with the RTLS data to refine the 3D coordinates of the target objects identified by the RTLS and by the DNN algorithms. This is achieved by capitalizing on the detection and segmentation capabilities of the DNN algorithm, PointNet, as well as those of a commercial platform on the market, Vercator Cloud, in detecting and localizing the PCD

assigned to the target objects. The highly accurate 3D coordinate information acquired using the integrated RTLS–computer-vision data, in turn, is used to automate the generation of onsite inspection reports through a digital-twin platform. The onsite inspection reports in this study, it should be noted, are documents that monitor and record the progress of component installations and their targeted locations. A bi-directional construction twin dashboard is also developed to visualize the reports, and to facilitate data collection on site.

CHAPTER 4: Method Implementation and Results

4.1 Overview

This section describes three case studies carried out in both laboratory and site environments to evaluate the methods developed in this study. The laboratory case studies validate the methods described in Sections 3.2 and 3.4, comprising: (1) an experimental study on the integrated Radio Frequency Identification Device (RFID) and Ultra-Wideband (UWB) to develop a Real Time Location system (RTLS) for indoor identification and localization of objects in 2D and 3D formats, and (2) an experimental study on integrating the RTLS data with point cloud data, leveraging computer vision capabilities to refine the 3D localization of objects. The case study on site validates the method described in Section 3.2 to generate progress reports by integrating the RTLS data with cloud-based Building Information Modeling (BIM) packages. The mechanical rooms of a pool project are selected for the study, and the results are visualized through a dashboard.

To localize the objects with the RTLS devices, the hand-held RFID reader equipped with the UWB attached acquires data associated with the RFID tags attached to the objects. The UWB tag attached to the RFID reader provides the reader's real-time location, while the RFID tags' location is identified using the trilateration technique and the distance of the tags from the RFID reader. Figure 4.1 shows the technologies used for data collection in this study.

The device used for 3D Point Cloud data (PCD) acquisition is Faro Focus 3D X 130. This device has a maximum reading range of 130 m. It covers the entire horizontal angle. However, the vertical angle's field of view (FOV) is 300°. The ranging error of the laser scanner is ± 2 mm. This device scans stationary stations. The final PCD is generated by registering the various stations and aligning the axis and origin. In this experiment, the laser scanner is set to resolution = 1/4, quality = 4 \times , vertical angle of view -60° to 90° , horizontal angle of view of 360° , scan size 10,240 \times 4,276, scanning rate = 43.7 Mpts, and number of scans = 5. The approximate time for each scan is 11.5 min.



QR code-RFID Tags



UWB Sensors



Hand-held RFID Reader



Light Detection and Ranging
(LiDAR)



Mobile Phone

Figure 4.1: Technologies used for data collection: RTLS and LiDAR.

4.2 Experimental Study for Testing RFID and UWB Devices

4.2.1 Laboratory Layout

The experimental work was carried out over an area of $13\text{ m} \times 8\text{ m}$ in a laboratory environment. The area was divided into a $90\text{ cm} \times 90\text{ cm}$ grid marked as shown in Figure 4.2. The grid defines 65 ground-truth tie-points, including Line-of-Sight (LoS) and NLoS situations. Extending the tie-points to the NLoS situation helps to evaluate the UWB system accuracy for situations in which obstacles such as walls and furniture may affect localization accuracy. Four UWB sensors are located at the four corners of the area used for the experiments, and 10 RFID tags are located, as shown in Figures 4.3 and 4.4. A fifth UWB sensor was located on the mobile RFID reader. The receivers are located at a height of 1.65 m, except one at a height of 2.15 m. Putting one of the receivers at a different height allows the UWB system to localize the roving tag (mounted on the mobile RFID receiver) even for elevations above the surface of the other three receivers. However, in this experiment, the roving UWB tag is at a height of 1.35 m. Three experiments were carried out on the UWB, RFID, and integrated use of both technologies. These experiments are subsequently described in sections 3.3, 3.4 and 4.1, respectively (Bardareh and Moselhi 2022).

The objects are located at tie-points already marked on the ground to validate the localization information obtained from the experiment. For data acquisition, a laser scanner is used to collect PCD from five different stations in the lab. Meanwhile, the surveyor roves around the lab with a hand-held RFID reader to capture RFID data. To enhance localization information, the surveyor stops moving when triggering the RFID reader. However, the UWB tag attached to the RFID reader can capture real-time localization information at a frequency of approximately 4–5 Hz, or every 200–250 ms, even when the surveyor is moving.

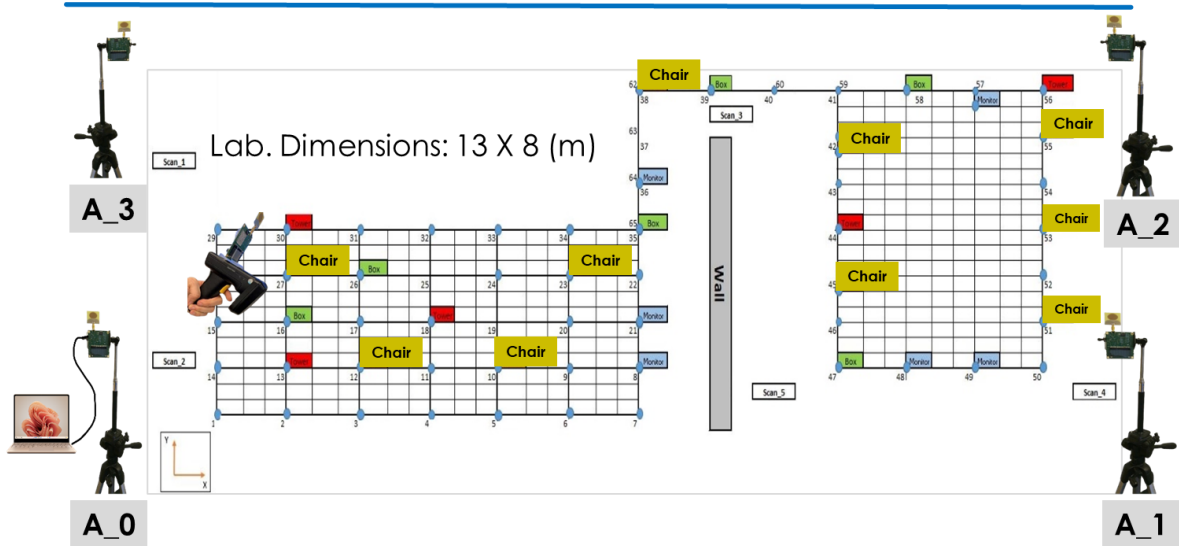


Figure 4.2: Layout of the tie-points in the lab.



Figure 4.3: Experiment environment in the lab.

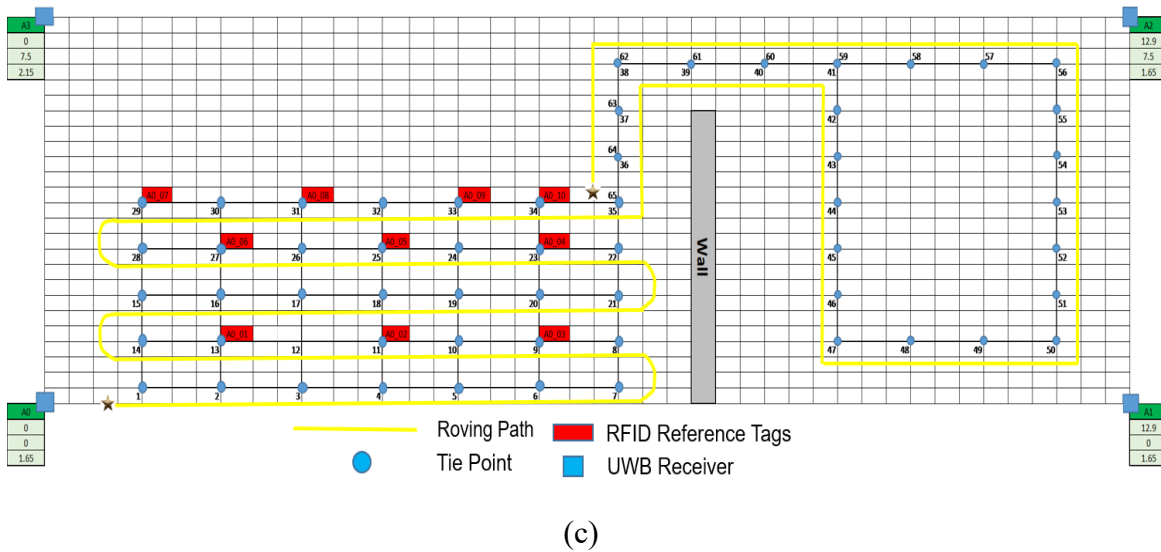
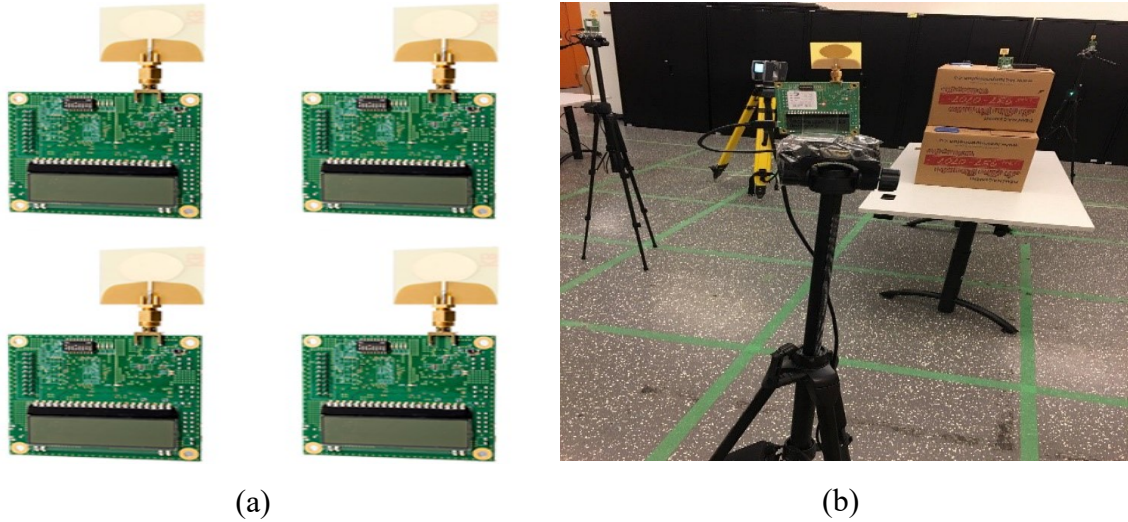


Figure 4.4: Experiment environment: (a) UWB sensors (b) UWB receiver (c) Layout of the UWB sensors placement, RFID reference tags and tie-points.

As outlined in Chapter 3, the experiments consist of two phases. Phase 1 focuses on testing the UWB and RFID systems. Phase 2 focuses on the integrated use of RFID and UWB for object localization in both 2D and 3D formats.

4.2.2 Experimental Study on UWB

The experiment consists of moving the mobile UWB tag along the movement path shown in Figure 23, to the 65 different ground-truth locations. For each tie-point, a time interval of 30 s is considered, so each test lasts 32.5 min. The data rate of the system is set on 110 kbps and Channel 2 (3.993 GHz) which is the recommended configuration defined by the manufacturer for longer range measurement. Ten (10) seconds before and after each displacement is removed

in order to guarantee a good ground-truth data. With this configuration, in each second between three to four localization data are recorded which is still suitable for real-time data acquisition. However, to increase the rate of data acquisition applicable for moving tags with higher speed, the data rate of 6.8 Mbps is available. The impact of a moving sensor on the localization accuracy of the UWB sensor has been evaluated in the integrated RFID–UWB experiment, following the data acquisition workflow outlined in Section 4.2.1. More details about the experiment are found in (Jimenez and Seco 2016, Ruiz and Granja 2017).

The UWB sensors used in this study utilize an atomic timer embedded in their PCB board that provides a high positioning accuracy in the range of a few decimetres. These are open-source sensors that are just an eighth of the cost of commercial sensors, but do not have a protected enclosure (DecaWave 2016). The experimental work aimed to study: (1) the range measurement accuracy of the UWB System, and (2) its localization accuracy.

With respect to range measurement, the real-time ranging distance of the UWB tag from the stationary UWB receivers are measured. One way to improve ranging measurement is to remove outlier data from our estimation. In this experiment, first any outlier ranging values in NLoS situation with the absolute error value more than 0.8 m from the mean range error in each stop are removed from the initial data. Then, the ranging data are split into three 5-m intervals (0–5 m, 5–10 m, 10–15 m). After removing the ranging data in the first and last 10 seconds of each stop, the distance of the roving tag from each receiver is obtained by averaging the remaining ranging data in the middle 10-s for each tie-point.

Figure 4.5 shows the good performance of the experimenting UWB in which the measured ranging values against real ranging values are depicted. As expected, all data points are above diagonal line which indicates the positive aspect of error due to the NLoS dispersion. In other words, the measured range values are larger than the real values due to the factors such as multipath effect and signal deviation.

Figure 4.6 and Figure 4.7 illustrate error histogram, and mean ranging error and standard deviation (SD) values in each ranging interval with and without omitting initial outliers in NLOS situation. Figure 4.7 shows how removing outliers improves the mean ranging error, especially for longer range intervals. However, it results in missing the data for 4 out of 65 tie-points. For instance, in the third range interval (10–15 m), removing outliers shows the improvement of approximately 10 cm, while this value for the first range interval (0–5 m) is approximately 1 cm.

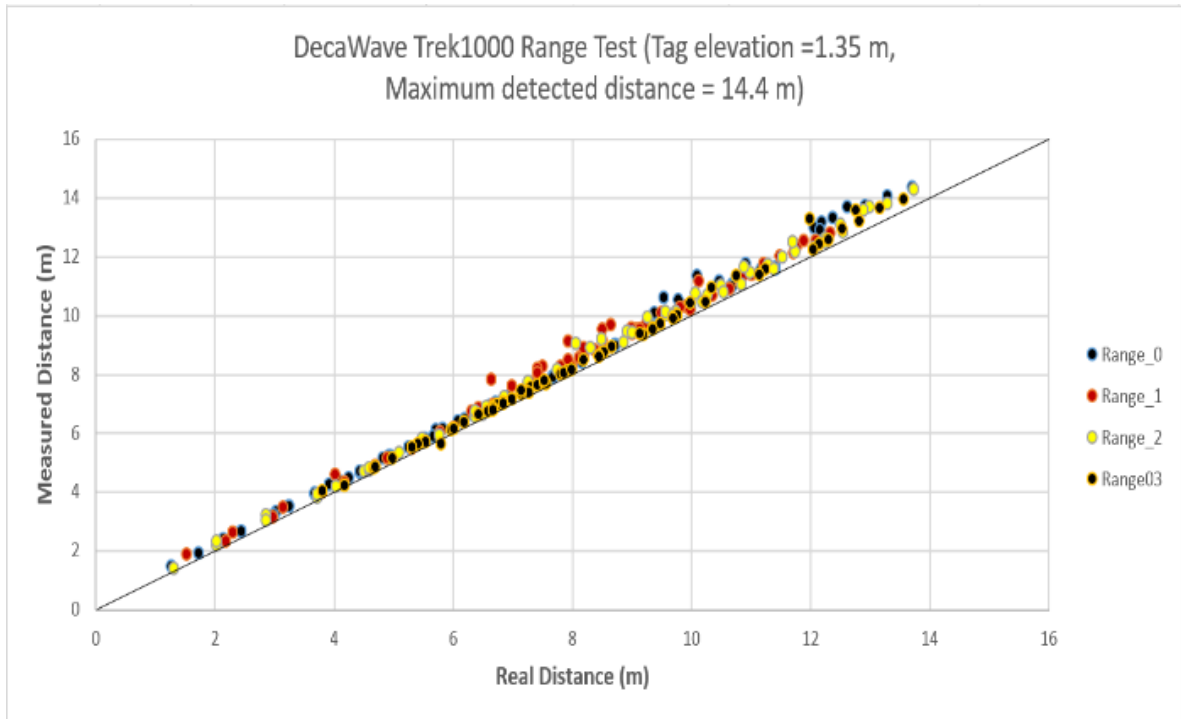


Figure 4.5: Real versus measured ranges.

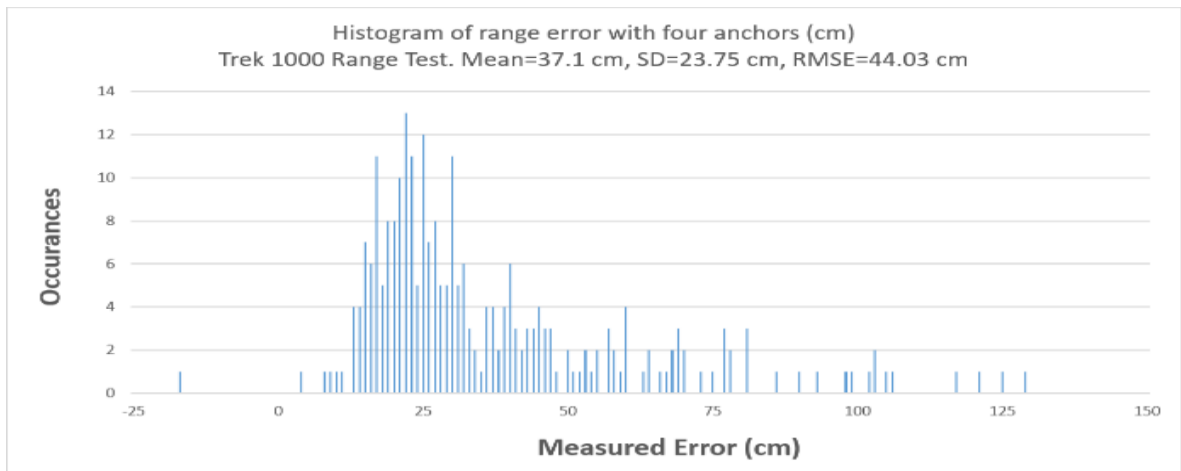


Figure 4.6: Error histogram in NLoS scenario.

| Initial Mean Error and SD values | | |
|----------------------------------|----------|--------|
| Range | Mean (m) | SD (m) |
| 0_5 | 0.2258 | 0.0915 |
| 5_10 | 0.3259 | 0.21 |
| 10_15 | 0.5216 | 0.256 |

| Mean Error and SD values without outliers | | |
|---|----------|---------|
| Range | Mean (m) | SD (m) |
| 0_5 | 0.2143 | 0.07311 |
| 5_10 | 0.3004 | 0.1426 |
| 10_15 | 0.4298 | 0.1752 |

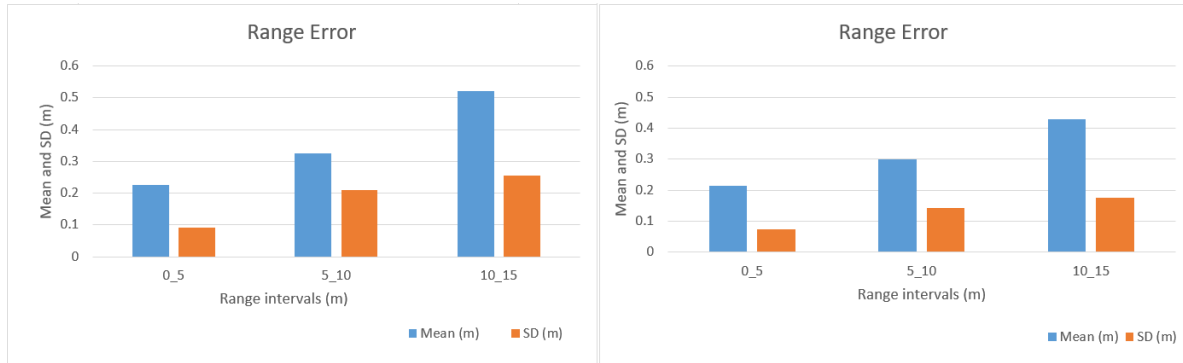


Figure 4.7: Mean and SD error values with outliers (left), and without outliers (right).

As to localization accuracy, the 3D localization information provided by the UWB are used to localize the hand-held RFID reader. A comparison of the methods to mitigate localization error associated with NLoS scenario and the situations in which they are employed were discussed in (Jimenez and Seco 2016, Ruiz and Granja 2017).

The final results in the Lab show an Root Mean Square Error (RMSE) of approximately 20 cm for 3D localization, while the results without removing the outliers and for all 65 tie-points show the error of approximately 30 cm in 3D localization.

4.2.3 Experimental Study on RFID

To achieve the model for range measurement, 10 reference tags with known locations are located in some of the tie-points at the height of 1 m from the floor level (Figure 4.4). The model is developed for the RFID system based on a dataset of approximately 1,200 readings in each set of the experiment. Each dataset consists of the information about the tags reading time, ID and signal strength which are acquired while moving on 35 tie-points in LoS situation.

The RFID device is experimented for four RFID reader output powers including o20, o22, o25 and o29 decibel-milliwatts (dBm), which are equivalent to minimum, conventional, proposed and maximum outputs equal to Effective Radiated Power (ERP) of 0.1, 0.16, 0.32 and 0.8 watts. Saying that, the maximum reading range of the RFID reader is increased by rising the output power of the reader. For each of these scenarios, after removing the data acquired in the first and last 5 s in each tie-point, the data in the range less than maximum reading range of the RFID reader are selected (e.g., below 3 m for o20 dBm or 6 m for o25 dBm). By achieving the

initial regression line for each set of data, the outliers (error exceeding 1 m) are removed. Finally, the data are averaged for increment of 2 cm and the final regression model is achieved. Figure 4.8 illustrates the path-loss models for the four RFID reader outputs. The figure depicts the RSSI value versus, the distance between the reference tags and the reader in each tie-point. In this experiment, the linear regression models are selected; however, more details about the best regression models and their accuracy are available in (Montaser and Moselhi 2014, Razavi et al. 2012).

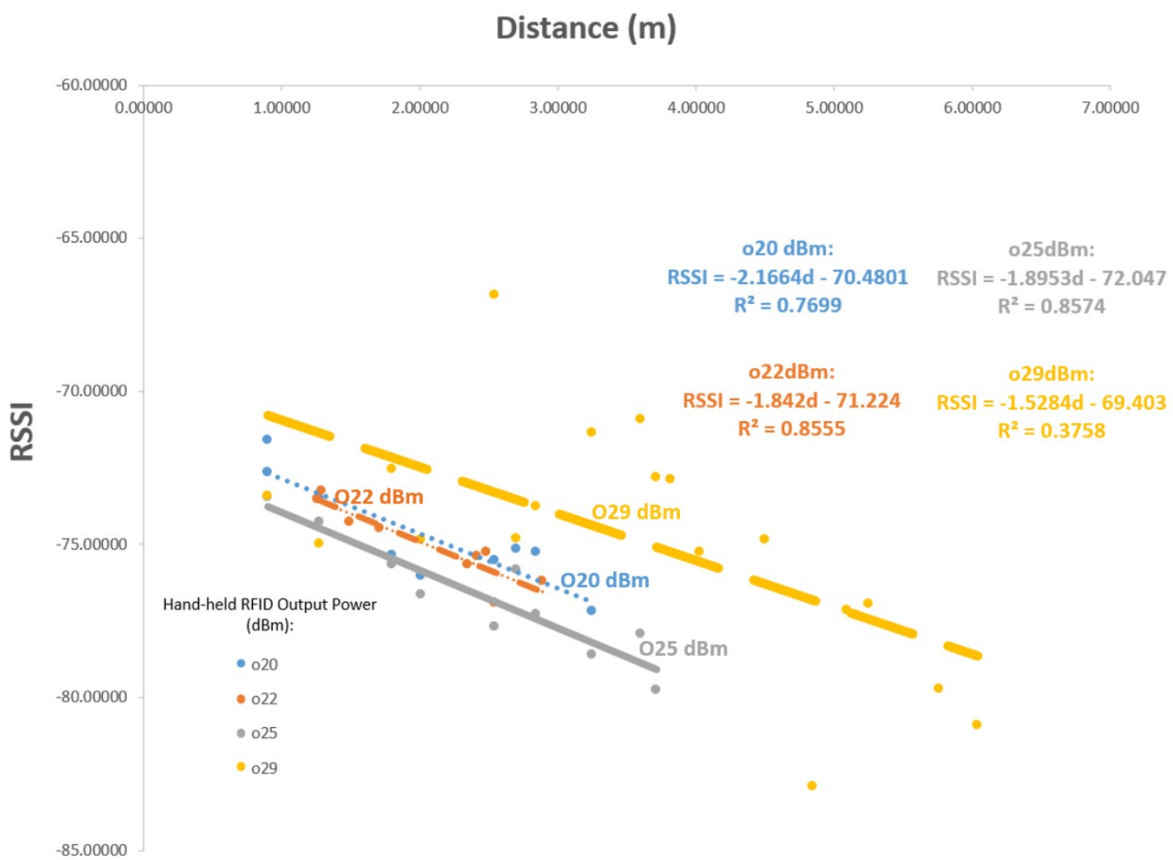


Figure 4.8: RFID system path-loss models.

Table 4.1 illustrates the results for these scenarios detailing the linear path-loss equations to achieve the distance range value (DRV), R2-value for each regression model, RFID reader maximum range and absolute error in range measurement. Based on the results achieved, the best performance of the RFID system is for the output of 25 dBm in terms of the device maximum reading range and ranging accuracy parameters. This output is proposed for applications associated with range measurement (i.e., proximity warning system) that were mentioned in the literature. More investigation is needed to optimize the RFID output power

by considering the two parameters. Other factors such as the environment and multi-path effect can bias the accuracy of the achieved path-loss models.

Table 4.1: Results for path-loss models.

| Scenario | Distance Equation | R ² | Range (m) | Error (m) |
|----------|--|----------------|-----------|-----------|
| o20dBm | $-0.4616 \times \text{RSSI} - 32.5333$ | 0.77 | 3.0 | 0.79 |
| o22dBm | $-0.5429 \times \text{RSSI} - 38.6667$ | 0.86 | 3.5 | 0.94 |
| o25dBm | $-0.5276 \times \text{RSSI} - 38.0135$ | 0.86 | 6.0 | 0.91 |
| o29dBm | $-0.6543 \times \text{RSSI} - 45.4089$ | 0.38 | 6.5 | 2.17 |

4.2.4 Experimental Study on Integrated RFID and UWB

For the integrated RFID and UWB, the data acquisition is based on the experimental work described above, and considering the characteristics of each technology in order to enhance the localization accuracy. The data acquisition for evaluating the developed system is similar to the steps used in developing the path-loss models of the RFID system. However, this time the location of the hand-held RFID reader is measured by a UWB tag. Figure 4.9 shows the developed device for this purpose in which the UWB tag attached on top of the RFID reader provides real-time location of the reader during data acquisition. Ten sample RFID tags are labelled and placed at the height of 1 m on the optional tie-points. One tag is labelled as the time reference tag (A1_01 in Figure 4.9) for data synchronization in which the start of the data acquisition for RFID and UWB data is set in the Python code as this tag is read. A surveyor is requested to start roving in the lab; however, to enhance the accuracy of the UWB system in localizing the RFID reader, the surveyor stops moving when triggering the hand-held reader. In each stop, the RFID reader acquire the data from the RFID tags in the vicinity, depending on the maximum reading range of the reader (varying from 3 m to approximately 6 m). Since the surveyor moves arbitrarily in the lab, a time-step of one second is considered for matching the RFID and UWB data; which is in extent of the time resolution provided by the RFID reader. In this set of experiments a total of approximately 3,500 lines of data are acquired for the integrated RFID-UWB. This includes the data acquired for three different output power of the RFID reader, and for 2D and 3D localization.

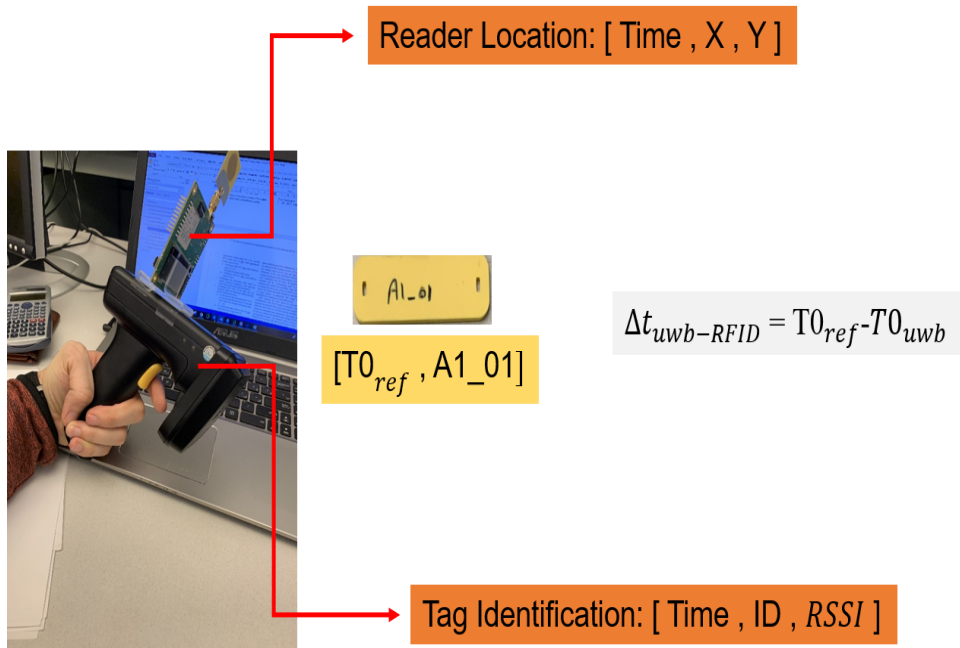


Figure 4.9: Integrated RFID–UWB device.

The results for various scenarios in which the RFID reader output is set to 020, 022 and 025 dBm, and its effect on the localization accuracy of the integrated method are shown in Table 4.2. Error1 illustrates the localization error before SoD analysis, while Error2 shows improved accuracy after considering the reader spatial distribution in which the data with the highest values of SoD are selected and averaged.

Based on the results, an increase in the RFID reader output power decreases the localization accuracy; however, the maximum reading range of the device increases. While in the experiments on the sole RFID device, the 025 dBm was identified as the optimal output power for applications associated with range measurement, but the 2D-localization error with this output power is almost two times more than the error for the conventional RFID reader output (022 dBm). This is due to the fact that the developed 2D (3D) localization algorithm depends on the intersection of the circles (spheres). As the RFID output power increases, a larger area of plane (space) is occupied by the circles (spheres), and the localization algorithm's capability to adjust the radius and control the Ratio value decreases. Moreover, the processing time of the algorithm greatly increases the RFID optimal output power, particularly for 3D localization.

Table 4.2: Results of the various techniques for onsite material localization.

| Technique | RFID–UWB 2D Localization | | | RFID–UWB 3D Localization | RFID (Montaser et al. 2014) | RFID + GPS (Hubo et al. 2014) | | | RFID (Wu et al. 2019) |
|-----------|--------------------------|-------|------------|--------------------------|-----------------------------|-------------------------------|----|----|-----------------------|
| | Error | Error | Confidence | Error 2 | 2D | 2D | 3D | 2D | |
| Scenario | | | | | | | | | |

| | r 1 (m) | r 2 (m) | e 95% for Error 2 | (m) | Localizatio n Error (m) | Localizati on Error (m) | Localizatio n Error (m) | Localizatio n Error (m) |
|--------|------------|------------|----------------------|------|-------------------------------|-------------------------------|-------------------------------|----------------------------|
| o20dBm | 0.48 | 0.47 | 0.38–0.56 | 1.04 | | | | |
| o22dBm | 0.65 | 0.52 | 0.34–0.7 | 1.15 | 1.9 | 2.48 | 2.59 | 1.25 |
| o25dBm | 1.25 | 1.01 | 0.32–1.7 | 1.8 | (+1.38) * | (+1.95) * | (+1.44) * | (+50.75) * |

* Improvement of the localization error in the developed method as compared to the previous studies.

The results also show that the idea of using varying radius and SoD analysis improves the localization accuracy more for the longer maximum reading range of the RFID reader or with the higher output power. The longer maximum range of RFID reader is valuable since less surveying time and effort is needed for data acquisition. In this way, the absolute 2D localization error improves for approximately 24 cm in o25 dBm, while this number for o22 dBm and o20 dBm are only thirteen and 1 cm (Bardareh and Moselhi 2022).

The developed method also shows good performance in 3D localization of the tagged objects on site. For instance, in the conventional output power of the RFID reader, the results show an RMSE of approximately 1.15 m, while this value for the methods based on RFID alone and integrated RFID and GPS technologies, investigated in the literature, are, respectively, 1.9 m and 2.59 m. As shown in the table, by projecting the 3D localization information on the plane, the RMSE is approximately 0.52 cm for 2D localization, which illustrates a localization error of approximately 1 m in the elevation. Comparing the localization error with the available UWB system, the error value of the developed method is over two times more than the standalone UWB system. However, the cost of the developed method for object localization is much less costly than the individual UWB system (Bardareh and Moselhi 2022).

It should be mentioned that the localization errors in Table 4.2 are the cumulative error of the UWB system localization, RFID system path-loss model, and the localization module, which affect the localization of the objects labelled by RFID tags. The use of particle filters and removing more outliers from UWB localization data could be the topic of future studies which enhance the localization data required for the RFID reader location. Furthermore, a sensitivity analysis on the threshold values defined in the localization module, such as Ratio and the number of acceptable data with higher SoD values, may also improve the localization accuracy, which needs more investigation. The main constraint for such an analysis would be the high processing time of the algorithm and the mathematical effort required to solve the non-linear trilateration equations, particularly in the case of 3D localization (Bardareh and Moselhi 2022).

The developed method provides objects localization in the indoor environment by using low-cost RFID tags. In this way, a larger number of objects are localized, while the individual use of expensive sensors such as the UWB and GPS is identified as the main limit for object localization. Moreover, the integrated use of the UWB and RFID solves the problem of using a large number of RFID reference tags for localization of the roving hand-held RFID reader, mentioned in previous studies. The integration method developed in this study for indoor material localization can be easily extended for outdoor applications, while the long-range UWB or accurate GPS-based technologies are used to localize the equipment and workers on site (Bardareh and Moselhi 2022).

The thorough investigation of the RFID system results in identifying the optimal output power for the hand-held RFID reader, which results in a better performance for range measurement applications in terms of accuracy and higher reading range of the reader. The developed trilateration technique also improved the 2D and 3D localization accuracy of the RFID tags over the accuracy reported in the previous studies (Bardareh and Moselhi 2022).

4.3 Onsite Case Study for Progress Reporting using MSI and QSI

This section describes the fieldwork conducted to validate the method in Section 3.3. The mechanical rooms of a site are selected to validate the progress reporting module in this study since components are installed in these spaces. Components in this study includes the mechanical equipment required in the mechanical room of a pool project. The data collection rate depends on the type of activities, but for the sake of this study, the data are collected and reported weekly. In this regard, a coordination meeting with the site coordinator is needed to identify the various activities and to define customized statuses for each activity. Information about the quantity of the components planned to be installed up to the report date is also needed to calculate the Material Status Index (MSI) and compare as-planned with as-built status. The planned schedule for the activities also helps to identify near-critical activities defined in this study and to tag the critical components associated with near-critical activities. Near-critical activities are identified by defining a threshold ratio of each activity's float to duration time. This ratio is defined as 10% for this study, which the site manager confirms. Appendix II provides a guideline for applying this method on job sites, along with a detailed, step-by-step process for implementing this digitalized progress tracking.

The fieldwork has three main operations: (1) localization of the tagged components with hand-held RFID reader and the attached UWB sensor, and to transfer them to the cloud-based

Geographic Information System (GIS) platform along with a 3D representation of the site as done for material tracking, (2) site surveying and assigning status to the tagged components, and report any issue for damaged or broken component during site inspection, and (3) generating the progress reports on the status of the overall project (using MSI) and that of each activity.

The four UWB receivers are installed on the side of the room, while 40 critical project components associated with near-critical activities are labelled with RFID tags. Tagging the critical components helps avoid tagging all components with RFID tags, which reduces the tagging effort and cost while reducing the data collection time.

Figure 4.10 shows a 3D model of the mechanical rooms in the fieldwork. For data collection, the site surveyor starts roving on site and updates the components' status. Moreover, the surveyor reports any issue automatically through the GIS cloud-based platform. By knowing the updated status of the components associated with each activity, it is possible to report the progress of each activity automatically. The 3D visualization of the information also allows for a tagged material to be quickly retrieve using the latest localization information updated in ArcGIS's database. Furthermore, the information about the components' location, time, and status is automatically updated in the database during surveying. At the same time, any issues are reported or marked for further action during the site inspection and RFI. Figure 4.11 illustrates a sample component tagged with the RFID tag and the associated information embedded in each tag.



(a)

(b)

Figure 4.10: Site layout for digitalized progress reporting: (a) Filtration room, (b) Boiler room.

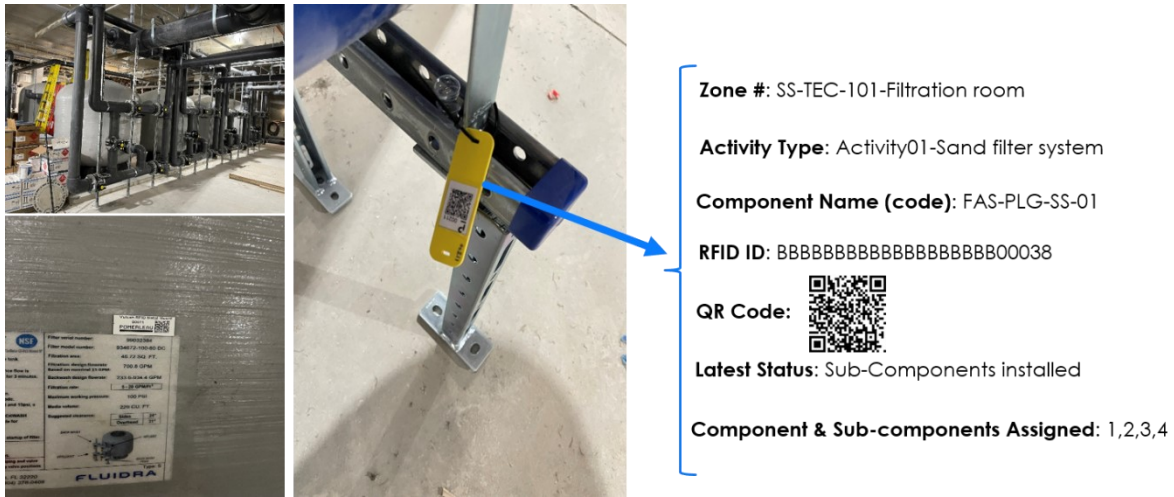


Figure 4.11: Sample tagged component on site for progress reporting.

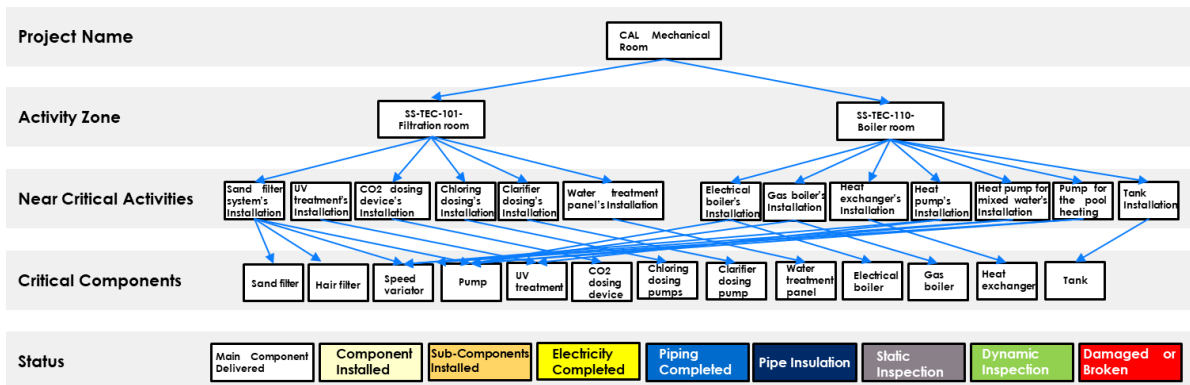
The infrastructure provided for material tracking is used for site reporting and progress tracking of the installations in the mechanical room. Two indices are developed to highlight the installation's progress and quality. The developed MSI and Quality Status Index (QSI) are used to report the progress and quality of the activities. The quality of the activities is defined based on the number of damaged or broken materials in each activity.

Table 4.3 shows the tagged components of 13 near-critical activities in 13 classes of components associated with the activities. These components are tagged with QR code-RFID tags to track their quantity, status, and location from delivery to completion. Figure 4.12 illustrates the reporting hierarchy in this fieldwork and the relation between the components, activities, and the data collected for each reporting information. As depicted in Figure 4.12.a, the mechanical rooms have been broken down into two zones, and the near-critical activities in each zone are identified to be tracked. For each activity, a set of consumed components with tagged IDs is tracked through defined statuses. Figure 4.12.b shows how the progress reports and visualized models are generated automatically from the collected data (i.e., ID, status, and location of the tagged components). In this study, data collection to identify the status of the tagged components is conducted manually. However, the identification of the tagged components, their IDs, and their locations on each reporting day is automatically achieved through the developed method in Stream I.

Table 4.3: Near-critical activities and tagged components for site progress reporting.

| Zone # | Activity Type | Component Name (code) | RFID ID | Duration (days) | Float (days) | Float/Duration |
|-----------------------------|--|-----------------------|---------|-----------------|--------------|----------------|
| | | FAS-PLG-SS-01 | ID00038 | | | |
| | | FAS-PLG-SS-02 | ID00039 | | | |
| | | FAS-PLG-SS-03 | ID00037 | | | |
| | | FAS-PLG-SS-04 | ID00036 | | | |
| | Activity01- Sand filter system's installation | FAS-50M-SS-01 | ID00060 | | | |
| | | FAS-50M-SS-02 | ID00059 | 90 | 5 | 0.06 |
| | | FAS-50M-SS-03 | ID00058 | | | |
| | | FAS-50M-SS-04 | ID00057 | | | |
| | | FAS-50M-SS-05 | ID00056 | | | |
| | | FAS-REC-SS-01 | ID00011 | | | |
| SS-TEC-101- Filtration room | Activity02- UV treatment's installation | FAS-REC-SS-02 | ID00012 | | | |
| | | UV-PLG-SS | ID00211 | | | |
| | | UV-50M-SS | ID00206 | 90 | 10 | 0.11 |
| | | UV-REC-SS | ID00110 | | | |
| | Activity03- CO2 dosing device's installation | CO2-PLG-SS | ID00111 | | | |
| | | CO2-50M-SS | ID00112 | 90 | 10 | 0.11 |
| | | CO2-REC-SS | ID00113 | | | |
| | Activity04- Chloring dosing pumps' installation | PO-CHL-PLG-SS | ID00114 | | | |
| | | PO-CHL-50M-SS | ID00115 | 90 | 10 | 0.11 |
| | | PO-CHL-REC-SS | ID00116 | | | |
| | Activity05- Clarifier dosing pump's installation | PO-CLA-PLG-SS | ID00117 | | | |
| | | PO-CLA-50M-SS | ID00118 | 90 | 15 | 0.17 |
| | | PO-CLA-REC-SS | ID00119 | | | |
| | Activity06- Water | CTR-PLG-SS | ID00120 | 90 | 15 | 0.17 |
| | | CTR-50M-SS | ID00121 | | | |

| | | | | | | |
|------------------------|---|------------|---------|----|------|------|
| SS-TEC-110-Boiler room | treatment panel's installation | CTR-REC-SS | ID00122 | | | |
| | Activity07-Electrical boiler's installation | CHEL-1 | ID00183 | | | |
| | Activity08-Gas boiler's installation | CHEL-2 | ID00184 | 88 | 5 | 0.06 |
| | Activity09-Heat exchanger's installation | CHGA-01 | ID00182 | | | |
| | Activity10-Heat pump's installation | CHGA-02 | ID00194 | 88 | 5 | 0.06 |
| | Activity11-Heat pump for mixed water's installation | EEE-PIS-1 | ID00208 | | | |
| | Activity12-Pump for the pool heating's installation | EEE-PIS-2 | ID00189 | 88 | 10 | 0.11 |
| | Activity13-Tank's installation | EEE-PIS-3 | ID00195 | | | |
| | | POEC-CH1 | ID00188 | | | |
| | | POEC-CH2 | ID00207 | 88 | 10 | 0.11 |
| | | POCT-CH3 | ID00123 | | | |
| | | POCT-CH4 | ID00124 | 88 | 10 | 0.11 |
| | | POEC-CP-1 | ID00193 | | | |
| | POEC-CP2 | ID00196 | 88 | 10 | 0.11 | |
| | RENPI | ID00013 | 88 | 5 | 0.06 | |



(a)

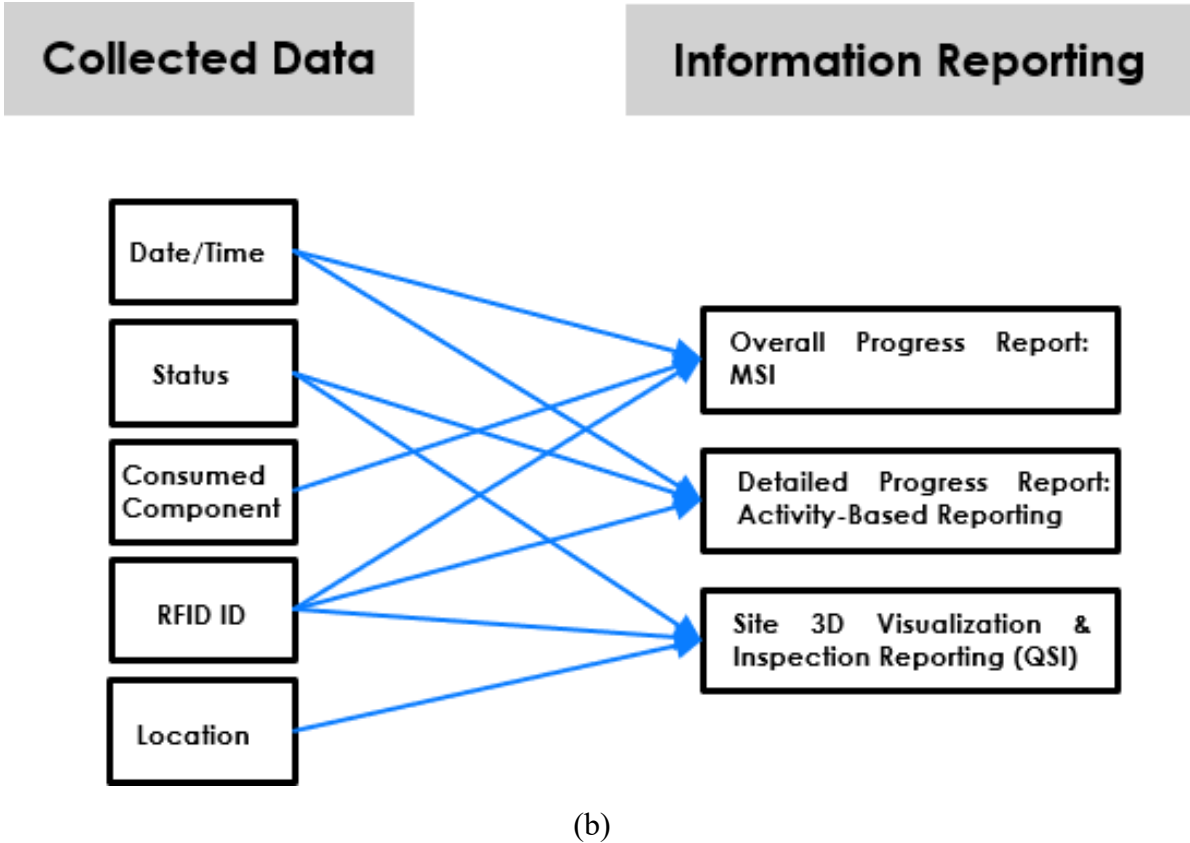


Figure 4.12: Overview of the site reporting hierarchy: (a) reporting hierarchy, and (b) data collected for each type of reporting information.

Once the tags attached to the components on site have been read, their status is updated via cloud-based GIS platforms. For this purpose, the surveyor updates the status of each component by selecting the predefined statuses defined in the Survey123 application on the phone. The MSI is calculated for progress reporting based on the number of tags identified for each activity type, representing the actual number of installed components. The activity-based reports include the progress of each activity, obtained by adding up the progress percentages corresponding to the status assigned to each activity type. The quality of the components used in each activity is determined by calculating the ratio of damaged or broken components to the total number of components used for that activity.

Table 4.4 provides the results for the generated site progress report for five reporting days in two months. The reason that MSI does not show the project progress on the first day of data collection lies behind the fact that MSI depends on the interconnectivity of the components used in various activities. The index cannot show the overall project status since each component is used in only one activity on the first report day. However, the activity level

progress reporting based on the assigned status still shows the progress of the activities on that day.

Table 4.4: Material-based and activity-based reporting.

| Parameter | | Project Timeline | | | | |
|---------------------------------|---------|--------------------------------------|------------------------------------|------------------------------------|------------------------------------|-------------------------------------|
| | | Report Day01 (September 27, 2023) | Report Day02 (October 12, 2023) | Report Day03 (October 18, 2023) | Report Day04 (November 7, 2023) | Report Day05 (November 15, 2023) |
| MSI | | 0.30 | 0.40 | 0.40 | 1.08 | 1.01 |
| Overall Status | Project | Behind Schedule (MSI<1) | Behind Schedule (MSI<1) | Behind Schedule (MSI<1) | Ahead of Schedule (MSI>1) | Ahead of Schedule (MSI>1) |
| QSI (%) | | 100.00 | 100.00 | 100.00 | 100.00 | 100.00 |
| | | Activity Status Reporting | | | | |
| Main component delivered (%) | | 100.00 | 100.00 | 100.00 | 100.00 | 100.00 |
| Component Installed (%) | | 32.50 | 37.50 | 42.50 | 55.00 | 62.50 |
| Sub-Components Installed (%) | | 0.00 | 10.00 | 15.00 | 45.00 | 57.00 |
| Electricity Completed (%) | | 0.00 | 0.00 | 0.00 | 0.00 | 5.00 |
| Piping Completed (%) | | 0.00 | 0.00 | 0.00 | 22.50 | 22.50 |
| Pipe Insulation (%) | | 0.00 | 0.00 | 0.00 | 0.00 | 0.00 |
| Static Inspection (%) | | 0.00 | 0.00 | 0.00 | 0.00 | 0.00 |
| Dynamic Inspection (%) | | 0.00 | 0.00 | 0.00 | 0.00 | 0.00 |
| Overall Activities Progress (%) | | 14.42 | 15.73 | 18.3 | 24.97 | 28.62 |

4.4 Experimental Study on Integrated RTLS and PCD Data

This section describes the validation of the developed framework for integrating RTLS data with PCD to refine 3D object localization through an experimental study conducted in a laboratory environment, in which identical chairs are used as the sample class of objects to be identified and localized. The chairs are labelled with passive RFID tags (placed at the top of the chair-back at a height of 1 m) and positioned on the targeted tie-points on the floor (Figures 4.13 and 4.14). The laboratory is also scanned with a LiDAR device to calibrate the RTLS and collect the PCD required for the Deep Neural Network (DNN) algorithms. For a total of five

scan stations, 22.5 Mpts are collected. Table 4.5 shows the as-planned coordinates of the chairs on the designated tie-points on the floor, along with the ID assigned to each chair. Ten tie-points are selected from a total of 65, and each of chairs is located on a tie-point.

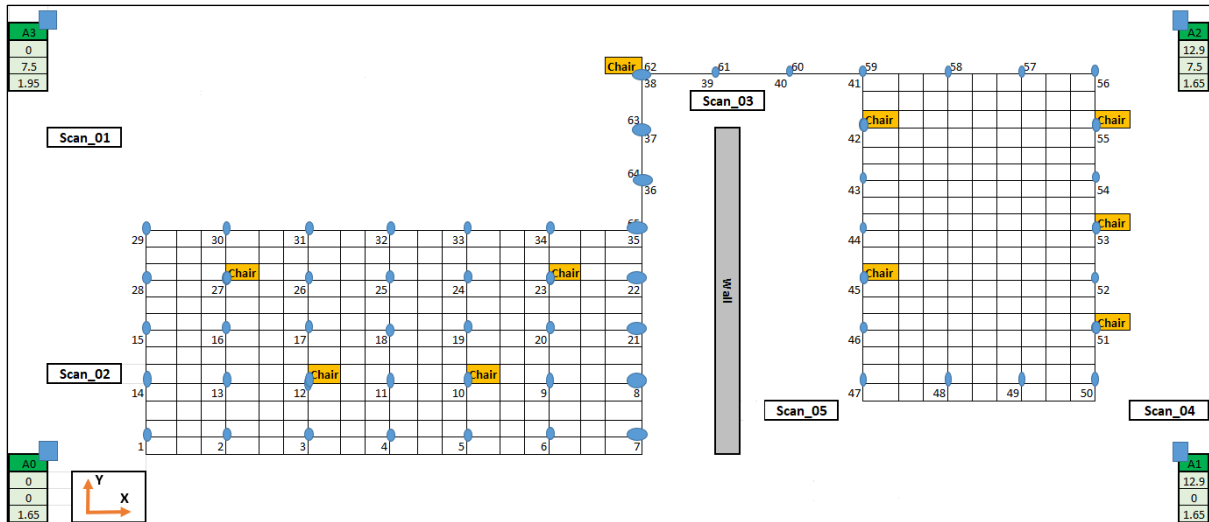


Figure 4.13: Layout of the tie-points in the laboratory with scanned stations.



Figure 4.14: Registered point cloud data of the laboratory.

Table 4.5: Targeted coordinates in the tie-points (as-planned status).

| No. | Tie-point | ID | X_p (m) | Y_p (m) | Z_p (m) |
|-----|-----------|------|-----------|-----------|-----------|
| 1 | 10 | A001 | 4.8 | 1.2 | 1 |
| 2 | 12 | A002 | 3.0 | 1.2 | 1 |
| 3 | 23 | A003 | 5.7 | 3.0 | 1 |
| 4 | 27 | A004 | 2.1 | 3.0 | 1 |
| 5 | 38 | A005 | 6.6 | 6.6 | 1 |
| 6 | 42 | A005 | 9.3 | 5.7 | 1 |
| 7 | 45 | A007 | 9.3 | 3.0 | 1 |
| 8 | 51 | A008 | 12.0 | 2.1 | 1 |
| 9 | 53 | A009 | 12.0 | 3.9 | 1 |
| 10 | 55 | A010 | 12.0 | 5.7 | 1 |

Table 4.6 provides a summary of the initial results for three experimental scenarios defined in this study for object recognition and localization using RTLS data, PCD-based object detection using PointNet, and the integration of these two technologies. The locations of the objects detected in the PCD are obtained by averaging the coordinates assigned to each object class through the PointNet semantic segmentation process. Meanwhile, the RTLS provides details about each tagged object's ID and location. The assumption in the integrated RTLS–PCD scenario of the experiment is that, while the RFID tags have the primary role in identifying the objects, the information provided by the PCD helps to enhance the localization accuracy of the identified tags. To achieve this, the averaged coordinates of points labeled as chairs within the radius of the RTLS error in 3D localization are assigned to the tagged chair. As shown in Table 4.6, since the point cloud data provides accurate coordinates of the segmented components, replacing their coordinates with those acquired by the RTLS will enhance 3D localization accuracy.

Table 4.6: Preliminary results of the integrated RTLS and point cloud data using PointNet algorithm for object detection.

| Parameter | PCD | RTLS | PCD+RTLS |
|----------------------------------|-------|-------|----------|
| PCD Detection (IoU) | | | |
| RTLS Identification (%) | 41.00 | 90.00 | 36.90 |
| 3D Localization (RMSE in metres) | 0.45 | 1.54 | 0.45 |

Table 4.7 shows the estimated coordinates of the chairs as determined by the integrated method using the Vercator cloud platform for object detection and localization in comparison to the results achieved using the PointNet algorithm to refine RTLS coordinates. The deviation in coordinates is calculated by obtaining the RMSE between the as-built coordinates and the as-planned coordinates of the chair in each tie-point. In a real scenario on the job site, this value would be a sum of the deviations from the as-planned coordinates and the integrated method's error in estimating the chairs' coordinates. However, in the experiment, all chairs are precisely located on the as-planned coordinates in order to identify the integrated method's error in estimating the as-built coordinates (see the right-most column of Table 4.7).

Additionally, to calculate the progress of the chair installations, the number of identified chairs is divided by the total number of planned tie-points. There is found to be only one instance of the integrated method failing to identify and localize a chair. Since all the chairs are present at the targeted tie-points, the integrated method achieves a 10% error.

Table 4.7: Tagged chairs' estimated coordinates and their deviations from as-planned status using Vercator Cloud for object detection.

| No. | Tie-point | $X_e(m)$ | $Y_e(m)$ | $Z_e(m)$ | Coordinates' deviation (RMSE) |
|-------------------------------|-----------|----------|----------|----------|-------------------------------|
| Using PointNet Algorithm | | | | | |
| 1 | 10 | 3.5 | 1.9 | 1.8 | 0.97 |
| 2 | 12* | 3.2 | 1.4 | 1.5 | 0.33 |
| 3 | 23* | 5.9 | 3.3 | 1.2 | 0.24 |
| 4 | 27 | 3.5 | 3.2 | 2.6 | 1.23 |
| 5 | 38 | 6.1 | 7.4 | 1.9 | 0.75 |
| 6 | 42 | 8.5 | 6.9 | 1.7 | 0.46 |
| 7 | 45* | 9.1 | 3.1 | 1.2 | 0.17 |
| 8 | 51 | - | - | - | - |
| 9 | 53* | 11.7 | 3.6 | 1.5 | 0.38 |
| 10 | 55 | 13.4 | 4.8 | 1.7 | 1.04 |
| Average Deviation (m) | | | | | 0.62 |
| Estimated Progress | | | | | 90% |
| Using Vercator Cloud Platform | | | | | |
| 1 | 10* | 4.6 | 1.1 | 1.2 | 0.17 |
| 2 | 12* | 3.1 | 1.2 | 0.9 | 0.08 |
| 3 | 23* | 5.5 | 3.2 | 1.0 | 0.16 |
| 4 | 27* | 2.2 | 3.1 | 1.2 | 0.14 |
| 5 | 38* | 6.7 | 6.5 | 0.8 | 0.14 |
| 6 | 42 | 8.5 | 6.9 | 1.7 | 0.46 |
| 7 | 45* | 9.2 | 3 | 1.1 | 0.14 |
| 8 | 51 | - | - | - | - |
| 9 | 53* | 11.8 | 3.9 | 0.9 | 0.13 |
| 10 | 55 | 13.4 | 4.8 | 1.7 | 1.04 |
| Average Deviation (m) | | | | | 0.27 |

| Estimated Progress | 90% |
|--------------------|-----|
|--------------------|-----|

* The refined RTLS locations by integrated method using DNN algorithm.

As illustrated in Table 4.7, the use of Vercator Cloud enhances the detection rate of the chairs due to the optimized algorithms and its larger dataset compared to the PointNet algorithm. These characteristics result in more accurate coordinates for the chairs identified through the integrated method. However, one of the chairs is still not identified through the integrated method (i.e., chair number 8 in Table 4.5).

4.5 Summary

The methods developed in this study are validated through experimental and fieldwork. A laboratory environment is selected for the experimental work, and 65 tie-points with known coordinates are mapped on the floor. Some objects, including the chairs that are the target objects in the experiment, are placed on the selected tie-points. The chairs are labelled with passive RFID tags (placed at the top of the chair-back at a height of 1 m) and positioned on the targeted tie-points on the floor. The laboratory is also scanned with a LiDAR device to calibrate the RTLS and collect the PCD required for the DNN algorithms.

The fieldwork involves tracking and reporting the progress of component installations in two mechanical rooms (the filtration room and the boiler room) as part of an actual pool construction project, the target objects (i.e., mechanical components) being furnished with passive RFID tags. The RTLS data for the integrated RFID–UWB method is collected using cloud-based GIS packages. A reporting hierarchy is also developed to track the components assigned to various activities in these rooms. The identification and localization information of the tagged objects, along with the status information collected, is mapped to the GIS packages with BIM capabilities for the purpose of generating reports via MSI and QSI indices.

The digital-twin platform is also tested through experimental work in the laboratory. The refined coordinates of tagged objects obtained via RTLS–PCD integration, detected and localized by the DNN algorithm, PointNet, and Vercator Cloud platform, are used for generation of the onsite inspection report.

CHAPTER 5: Conclusion

5.1 Summary and Concluding Remarks

This aim underlying this research is to improve construction operations by automating tracking and progress reporting using integrated technologies such as Real-time Location System (RTLS) and Point Cloud Data (PCD) for indoor object localization in 2D and 3D formats. The integrated use of these technologies, leveraging the capabilities of a cloud-based Building Information Modeling (BIM) platform and computer vision, improves indoor object localization and facilitates automated generation of onsite inspection reports. To achieve this, four main methods are developed: (1) an Indoor Positioning System (IPS) based on integrated RTLS technologies, Radio Frequency Identification Device (RFID), and Ultra-WideBand (UWB) for location identification of tagged objects in an indoor environment; (2) the joint use of the IPS and cloud-based BIM tools to enhance data collection and visualization, visualizing the information associated with tracking and automated progress reporting through two developed indices, Material Status Index (MSI) and Quality Status Index (QSI) (where identification of the quantity, status, and location of the components present on site aids in estimating project progress and facilitates retrieval of the tagged components for inspection purposes); (3) computer-vision and deep-learning algorithms are used for object recognition and refined 3D localization, implemented on integrated RTLS–PCD data; and (4) a digital-twin platform comprising RTLS, PCD, and cloud-based BIM tools is developed that enables the automated generation of onsite inspection reports containing information on installation progress and targeted locations. A construction twin dashboard is developed to ensure bi-directional communication between the physical and digital environments via BIM plug-ins. The developed methods are validated through laboratory experiments and a case study.

5.2 Research Contributions

The main contributions of this research are:

- I. Developing of an improved localization method for automated 2D and 3D localization of objects in an indoor space using integrated RFID and UWB technologies;
- II. Integration of material tracking with progress tracking via the developed indices for the purpose of monitoring the quantity and status of materials used in a project and generating progress reports;
- III. Enhanced 3D localization accuracy of objects in an indoor space using computer vision and leveraging the accurate 3D coordinates in PCD collected by the Light Detection

and Ranging (LiDAR) device in integration with the RTLS technologies (i.e., RFID data); and

- IV. Development of a digital-twin platform for the automated generation of onsite inspection reports (achieved by identifying the 3D coordinates of objects using RTLS and computer-vision capabilities).

The minor contributions of this research are:

- I. Enhancing current trilateration techniques for localization by considering the geospatial distribution of the roving receiver (reader) to improve localization accuracy. Additionally, the integrated RFID-UWB error has been calibrated by incorporating the error into the trilateration technique, which increases the chance of object identification through the integrated method.
- II. Considering the quality alongside the physical progress of construction operations. This is achieved by introducing the QSI, which accounts for the quality of installed materials such as pipes, tanks and HVAC ducts on the job site and extends its application to quality assurance and quality control of installations on the job site.
- III. Enabling the use of actual data collected on site for generating onsite inspection reports, rather than relying on data provided through updated BIM models with a high Level of Development (LoD), which are not timely available during the construction phase of a project.

5.3 Research Limitations

The main limitations of this research are as follows:

- I. The 3D localization of the developed IPS is not as precise as the 2D localization.
- II. In integrating the RTLS with the cloud-based BIM, the MSI needs to be compared with available indices such as SPI and CPI in the EVM technique for project control and tracking of construction operations. Additionally, the QSI is limited to showcasing damaged or broken components in each activity. The quality aspect could be more integrated with the onsite inspection reports in order to capture the quality of the work performed.
- III. The mapping of the RTLS data to the cloud-based BIM platform is not automated. The objects' coordinates need to be geo-referenced manually, and the BIM platform is updated manually with the information about the status and coordinates of the target

objects. Additionally, field data collection is conducted manually to ensure that the updated status of the tagged components is recorded on each reporting day.

- IV. Available dataset benchmarks are used to train and test computer-vision algorithm, PointNet, to refine the 3D coordinates of the target objects (i.e., chairs, in this study). This affects the evaluation accuracy of the algorithm's segmentation of the PCD collected.
- V. The bi-directional communication of the construction twin dashboard requires debugging. Additionally, the computer-vision and RTLS information were manually fed into the cloud-based BIM platform.

5.4 Opportunities for Future Work

Based on the research outcomes and limitations as outlined above, the following avenues for future work are identified.

- I. The 3D localization capability of the developed IPS could be improved by employing innovative techniques such as machine learning and optimization to better calibrate the RFID and UWB devices, and by using filters to improve the localization information obtained by the UWB system. Additionally, the thresholds used in the trilateration technique need to be further investigated and (potentially) adjusted.
- II. The application of the computer-vision algorithm used in this study could be extended to other construction components, such as MEP components, which are among the most challenging components to track and report on job sites.
- III. Available PCD benchmarks assist in detecting some objects (i.e., chairs, in this study) without the need to manually prepare annotated datasets. However, segmentation accuracy is not acceptable for classes of objects with small datasets due to the imbalance in the training dataset size for these objects compared to others. Future investigations are needed to improve the object detection and segmentation performance of computer-vision algorithms using PCD.
- IV. The integration of the RTLS and PCD can be further automated. In the future, the PCD detected and labelled by the computer-vision algorithms could be mapped to the RTLS data via clustering techniques as a way of boosting the efficiency of the integration. Additionally, the object detection capability of Deep Neural Network (DNN) algorithms could be leveraged to improve the object identification of the RTLS (bearing

in mind that DNN algorithms still lack the ability to distinguish between identical objects).

- V. Further integration with BIM platforms is required in order to refine the construction twin dashboard and to ensure bi-directional communication regarding objects in the physical and digital environments.

REFERENCES

- Akhavian, R., and Behzadan, A. H. (2015). "Construction equipment activity recognition for simulation input modeling using mobile sensors and machine learning classifiers." *Advanced Engineering Informatics*, 29(4), 867–877.
- Almeida, A., and Almeida, J. (2005). "Real-time tracking of moving objects using particle filters." *Proceedings of the IEEE International Symposium on Industrial Electronics*, Dubrovnik, Croatia, pp. 1327–1332.
- Amer, A. (2020). "Automated segmentation and reconstruction of structural elements for indoor multi-level room environment." Master's dissertation, Concordia University, Montréal, QC, Canada.
- Andoh, A. R., Su, X., and Cai, H. (2012). "A framework of RFID and GPS for tracking construction site dynamics." *Proceedings of the 2012 Construction Research Congress: Construction Challenges in a Flat World*, pp. 818–827.
- Armeni, I., Sener, O., Zamir, A. R., Jiang, H., Brilakis, I., Fischer, M., and Savarese, S. (2018). "3D semantic parsing of large-scale indoor spaces supplementary material." *Proceedings of the 2016 IEEE Conference on Computer Vision and Pattern Recognition*, pp. 1534–1543.
- Azarm, R. (2013). "Material status index for tracking and progress reporting of construction projects." Master's dissertation, Concordia University, Montréal, QC, Canada.
- Available online (2024): <https://paperswithcode.com/sota/3d-point-cloud-classification-on-modelnet40>
- Available online (2024): <https://vercator.com/>
- Balali, A., Valipour, A., Antucheviciene, J., and Šaparauskas, J. (2020). "Improving the results of the earned value management technique using artificial neural networks in construction projects." *Symmetry*, MDPI, 12(10), 1745.
- Bardareh, H., and Moselhi, O. (2020). "Automated data acquisition for indoor localization and tracking of materials onsite." *Proceedings of the International Symposium on Automation and Robotics in Construction (ISARC)*, 37, pp. 765–772.
- Bardareh, H., and Moselhi, O. (2022). "An integrated RFID-UWB method for indoor localization of materials in construction." *Journal of Information Technology in Construction*, 27, 642–661.
- Bardareh, H., and Moselhi, O. (2023). "Integrated real-time location system information and 3D point clouds for object localization onsite using deep neural networks." *AACE International Conference & Expo 2023*, Chicago, IL, USA, DSAA-4094.
- Bosché, F., and Ahmed, M. (2015). "The value of integrating Scan-to-BIM and Scan-vs-BIM techniques for construction monitoring using laser scanning and BIM: The case of cylindrical MEP components." *Automation in Construction*, 49(B), 201–213.
- Cai, H., and Andoh, A. (2014). "A boundary condition based algorithm for locating construction site components using RFID and GPS." *Advanced Engineering Informatics*, 28(4), 455–468.

- Chen, Q., Adey, B. T., Haas, C., and Hall, D. M. (2020). "Using look-ahead plans to improve material flow processes on construction projects when using BIM and RFID technologies." *Construction Innovation*, 20(3), 471–508.
- Cheng, T., and Venugopal, M. (2011). "Performance evaluation of ultra wideband technology for construction resource location tracking in harsh environments." *Automation in Construction*, 20(8), 1173–1184.
- Costin, A. M., Teizer, J., and Schoner, B. (2015). "RFID and BIM-enabled worker location tracking to support real-time building protocol and data visualization." *Journal of Information Technology in Construction*, 20(29), 495–517.
- DecaWave Ltd. (2016). "EVK1000 user manual, how to use, configure and interface to the dw1000 evaluation kit." Version 1.13.
- Deng, J., Zhou, W., Zhang, Y., and Li, H. (2021). From multi-view to hollow-3D: Hallucinated hollow-3D R-CNN for 3D object detection." *IEEE Transactions on Circuits and Systems for Video Technology*, 31(12), 4722–4734.
- El-Omari, S. (2008). "Automated data acquisition for tracking and control of construction projects." Doctoral dissertation, Concordia University, Montréal, QC, Canada.
- Feng, Y., and Golparvar-Fard, M. (2019). "Image-based localization for facilitating construction field reporting on mobile devices." *Advances in Informatics and Computing in Civil and Construction Engineering*, pp. 585–592.
- Gopalakrishna Adusumilli, (2020): <https://towardsdatascience.com/lidar-point-cloud-based-3d-object-detection-implementation-with-colab-part-1-of-2-e3999ea8fdd4>.
- Huang, Y., Hammad, A., Torabi, G., Ghelmani, A., and Guevremont, M. (2021). "Towards near real-time digital twins of construction sites: Developing high LOD 4D simulation based on computer vision and RTLS." *Proceedings of the International Symposium on Automation and Robotics in Construction (ISARC)*, pp. 248–255.
- Ibrahim, M. (2015). "Models for efficient automated site data acquisition." Doctoral dissertation, Concordia University, Montréal, QC, Canada.
- Ibrahim, M., and Moselhi, O. (2014). "Automated productivity assessment of earthmoving operations." *Journal of Information Technology in Construction*, 19(9), 169–184.
- Jimenez, A., and Seco, F. (2016). "Comparing DecaWave and BeSpooon UWB location systems: Indoor/outdoor performance analysis." *Proceedings of the 6th International Conference of Indoor Positioning Indoor Navigation (IPIN)*, Alcal'a de Henares, Spain, Oct. 4–7, 2016.
- Jo, K., Lee, M., and Sunwoo, M. (2015). "Road slope aided vehicle position estimation system based on sensor fusion of GPS and automotive onboard sensors." *IEEE Transactions on Intelligent Transportation Systems*, 17(1), 250–263.
- Kalikova, J., and Krcal, J. (2017). "People counting by means of wi-fi." *Proceedings of the Smart City Symposium (SCSP)*, Prague, Czech Republic, 25–26.
- Khamooshi, H., and Golafshani, H. (2014). "EDM: Earned Duration Management, a new approach to schedule performance management and measurement." *International Journal of Project Management*, 32(6), 1019–1041.

- Kropp, C., and Koch, C. (2018). "Interior construction state recognition with 4D BIM registered image sequences." *Automation in Construction*, 86, 11–32.
- Labant, S., Gergel'ová, M., Weiss, G., and Gašinec, J. (2017). "Analysis of the use of GNSS systems in road construction." *Proceedings of the IEEE Baltic Geodetic Congress (BGC Geomatics)*, pp. 72–76.
- Li C., Mo, L., and Zhang, D. (2019). "Review on UHF RFID localization methods." *IEEE Journal of Radio Frequency Identification*, 3(4), 205–215.
- Li, C. Z., Zhong, R. Y., Xue, F., Xu, G., Chen, K., Huang, G. G., and Shen, G. Q. (2017). "Integrating RFID and BIM technologies for mitigating risks and improving schedule performance of prefabricated house construction." *Journal of Cleaner Production*, 165, 1048–1062.
- Li, H., and Chan, G. (2013). "Integrating real time positioning systems to improve blind lifting and loading crane operations." *Journal of Construction Management and Economics*, 31, 596–605.
- Li, N., and Becerik-Gerber, B. (2011). "Performance-based evaluation of RFID-based indoor location sensing solutions for the built environment." *Advanced Engineering Informatics*, 25(3), 535–546.
- Ma, J. W., and Leite, F. (2022). "Performance boosting of conventional deep learning-based semantic segmentation leveraging unsupervised clustering." *Automation in Construction*, 136, 104167.
- Maneesilp, J., and Wang, C. (2012). "RFID support for accurate 3D localization." *IEEE Transactions on Computers*, 62(7), 1447–1459.
- Masiero, A., and Fissore, F. (2017). "A low cost UWB based solution for direct georeferencing UAV photogrammetry." *Remote Sensing*, 9(5), 414.
- Montaser, A., and Moselhi, O. (2014). "RFID indoor location identification for construction projects." *Automation in Construction*, 39, 167–179.
- Moselhi, O., and Azarm, R. (2013). "Material status index in support of EVM." *Proceedings of the International Symposium on Automation and Robotics in Construction (ISARC)*, pp. 488–496.
- Moselhi, O., Bardareh, H., and Zhu, Z. (2020). "Automated data acquisition in construction with remote sensing technologies." *Applied Sciences*, 10(8), 2846.
- Munaro, M., Radu, B., and Emanuele, M. (2016). "3D robot perception with Point Cloud Library." *Robotics and Autonomous Systems*, 78, 97–99.
- Nasrollahi, M., Bolourian, N., and Hammad, A. (2019). "Concrete surface defect detection using deep neural network based on LiDAR scanning." *Proceedings of the CSCE Annual Conference*, Montréal, QC, Canada, pp. 12–15.
- Nurminen, H., and Ardeshiri, T. (2015). "A NLoS-robust TOA positioning filter based on a skew-t measurement noise model." *Proceedings of the International Conference on Indoor Positioning and Indoor Navigation (IPIN)*, Banff, Alberta, Canada, 7 pages.
- Omar, T., and Moncef, L. N. (2016). "Data acquisition technologies for construction progress tracking." *Automation in Construction*, 70, 143–155.

- Pang, G., and Neumann, U. (2016). "3D point cloud object detection with multi-view convolutional neural network." *Proceedings of the 23rd International Conference on Pattern Recognition (ICPR)*, pp. 585–590.
- Park, J., and Cho, Y. K. (2016). "A BIM and UWB integrated mobile robot navigation system for indoor position tracking applications." *Journal of Construction Engineering and Project Management*, 6(2), 30–39.
- Qi, C. R., Su, H., Mo, K., and Guibas, L. J. (2017). "PointNet: Deep learning on point sets for 3d classification and segmentation." *Proceedings of the IEEE Conference on Computer Vision and Pattern Recognition*, pp. 652–660.
- Rahman, M. M., Yap, Y. H., Ramli, N. R., Dullah, M. A., and Shamsuddin, M. S. W. (2017). "Causes of shortage and delay in material supply: a preliminary study." *Conference Series: Materials Science and Engineering*, 271(1), 012037.
- Razavi, S. R., Montaser, A., and Moselhi, O. (2012). "RFID deployment protocols for indoor construction." *Construction Innovation*, 12(2), 239–258.
- Roghabadi, M. A., and Moselhi, O. (2020). "Forecasting project duration using risk-based earned duration management." *International Journal of Construction Management*, 22(16), 3077–3087.
- Ruppert, T., and Abonyi, J. (2016). "Integration of real-time locating systems into digital twins." *Journal of Industrial Information Integration*, 20, 100174.
- Ruiz, A. R. J., and Granja, F. S. (2017). "Comparing Ubisense, BeSpoon, and DecaWave UWB location systems: Indoor performance analysis." *IEEE Transactions on Instrumentation and Measurement*, 66(8), 2106–2117.
- Sacks, R., Brilakis, I., Pikas, E., Xie, H. S., and Girolami, M. (2020). "Construction with digital twin information systems." *Data-Centric Engineering*, 1, e14.
- Sander, P., Spiegl, M., Burns, T., and Reilly, J. (2022). "Digital project twin for quantitative cost, risk and schedule assessment of capital projects." *Australian Journal of Multi-Disciplinary Engineering*, 18(1), 34–46.
- Seo, W., Hwang, S., Park, J., and Lee, J. M. (2013). "Precise outdoor localization with a GPS–INS integration system." *Robotica*, 31(3), 371–379.
- Shahi, A., Safa, M., Haas, C. T., and West, J. S. (2014). "Data fusion process management for automated construction progress estimation." *Journal of Computing in Civil Engineering*, 29(6), 04014098.
- Siddiqui, H. (2014). "UWB RTLS for construction equipment localization: Experimental performance analysis and fusion with video data." Master's dissertation, Concordia University, Montréal, QC, Canada.
- Song, L., and Tanvir, M. (2015). "A cost effective material tracking and locating solution for material laydown yard." *Procedia Engineering*, 123, 538–545.
- Su, X., Li, S., Yuan, C., Cai, H., and Kamat, V. R. (2014). "Enhanced boundary condition-based approach for construction location sensing using RFID and RTK GPS." *Journal of Construction Engineering and Management*, 140(10), 04014048.

- Sun, M., and Wang, Y. (2020). "Indoor positioning integrating PDR/geomagnetic positioning based on the genetic-particle filter." *Applied Sciences*, 10(2), 668.
- Ta, V. C. (2017). "Smartphone-based indoor positioning using Wi-Fi, inertial sensors and Bluetooth in machine learning." Doctoral dissertation, Université Grenoble, Alpes, France, 2017.
- Tran, T. A., Ruppert, T., Eigner, G., and Abonyi, J. (2021). "Real-time locating system and digital twin in Lean 4.0." *Proceedings of the IEEE 15th International Symposium on Applied Computational Intelligence and Informatics (SACI)*, pp. 369–374.
- Valero, E., Adán, A., and Bosché, F. (2016). "Semantic 3D reconstruction of furnished interiors using laser scanning and RFID technology." *Journal of Computing in Civil Engineering*, 30(4), 04015053.
- Wang, Z., Hu, H., and Zhou, W. (2017). "RFID enabled knowledge-based precast construction supply chain." *Journal of Computer-Aided Civil and Infrastructure Engineering*, 32(6), 499–514.
- Wu, C., Wang, X., Chen, M., and Kim, M. J. (2019). "Differential received signal strength based RFID positioning for construction equipment tracking." *Advanced Engineering Informatics*, 42, 100960.
- Xiahou, X., Li, Q., Yuan, J., and Tang, Y. (2018). "Integrating RFID and BIM to design a real-time position tracking system for subway projects lifecycle safety management." *Proceedings of the Joint CIB W099 & TG59 International Safety, Health, and People in Construction Conference*.
- Xu, L. D., Xu, E. L., and Li, L. (2018). "Industry 4.0: state of the art and future trends." *Journal of Production Research*, 56(8), 2941–2962.
- Xu, Y., and Shmaliy, Y. S. (2018). "Robust and accurate UWB-based indoor robot localization using integrated EKF/EFIR filtering." *IET Radar Sonar Navigation*, 12, 750–756.
- Yin, S. Y., Tserng, H. P., Wang, J. C., and Tsai, S. C. (2009). "Developing a precast production management system using RFID technology." *Automation in Construction*, 18(5), 677–691.
- Yoo, J., and Park, J. (2019). "Indoor localization based on Wi-Fi received signal strength indicators: Feature extraction, mobile fingerprinting, and trajectory learning." *Applied Sciences*, 9(18), 3930.
- Zhou, Y., and Tuzel, O. (2018). "Voxelnet: End-to-end learning for point cloud based 3d object detection." *Proceedings of the IEEE Conference on Computer Vision and Pattern Recognition*, pp. 4490–4499.
- Zhu, Z., and Ren, X. (2016). "Visual tracking of construction jobsite workforce and equipment with particle filtering." *Journal of Computing in Civil Engineering*, 30(6), 04016023.

Appendix I:

Mapping of the RTLS Data into ArcGIS

In this study, Real-Time Location System (RTLS) data collected by the integrated RFID-UWB system are mapped into ArcGIS. This mapping offers several benefits, including the centralization of data collection, processing, and visualization through ArcGIS cloud packages. Additionally, the local coordinates of objects tagged with passive RFID tags are converted into geocoordinates within ArcGIS. The detailed steps for this mapping process are provided below:

- Step I. Data is collected using a hand-held RFID reader equipped with a UWB tag. This device scans the RFID tags attached to the target objects.
- Step II. Raw RFID and UWB .txt files are directly uploaded into server using ArcGIS Survey123 and Field Maps for further processing, as outlined in Figure I.1 and Figure I.2. A digital survey form within ArcGIS Survey123 mobile app. is used to collect the acquired data and upload the files into the server as depicted in Figure I. 2 (b).

```
Test01- axiab RFID calibration with o25 with UWB tag attached moving randomly - Notepad
File Edit Format View Help
DT: 2022-09-21T11:58:14
EV: Power up
DT: 2022-09-21T11:58:14
EV: Connected USB
CS: .iv LCMD 000005 -dton -o25 -ron
DT: 2022-09-21T12:00:33
ME: No Transponder found
ER:005

CS: .iv
DT: 2022-09-21T12:05:14
EP: FFFEEEEEDDDCCBBBBA101
RI: -52
OK:

CS: .iv
DT: 2022-09-21T12:05:30
ME: No Transponder found
ER:005

CS: .iv
DT: 2022-09-21T12:05:30
EP: FFFEEEEEDDDCCBBBBA003
RI: -77
OK:

CS: .iv
DT: 2022-09-21T12:05:30
ME: No Transponder found
ER:005

CS: .iv
DT: 2022-09-21T12:05:31
ME: No Transponder found
ER:005

CS: .iv
```

(a)

```
Test01- axiab UWB calibration with o25 dbm and UWB tag attached moving randomly - Notepad
File Edit Format View Help
T: 120455057:DecaRangeRTLS:LogFile:Ver: 2.10 TREK:Conf:Anchor0:0:Chan2
T: 120455198:AP:0:0:0:1.65
T: 120455198:AP:1:7.4279:0.0298:1.65
T: 120455198:AP:2:6.9373:7.612:1.65
T: 120455198:AP:3:-3.045:8.9009:2.45
T: 120455240:RR:0:0:1892:1892:19:25280
T: 120455240:RR:0:1:6477:6477:19:25280
T: 120455240:RR:0:3:10048:10048:19:25280
T: 120455240:RM:0:11:19:25280
T: 120455240:NL:0:137:19:[nan,nan,nan]:1892:6477:0:10048
T: 12045520:RR:0:0:1906:1906:20:25286
T: 12045520:RR:0:1:6519:6519:20:25286
T: 12045520:RR:0:3:10053:10053:20:25286
T: 12045520:RM:0:11:20:25286
T: 12045521:NL:0:137:20:[nan,nan,nan]:1906:6519:0:10053
T: 120455800:RR:0:0:1901:1901:21:25292
T: 120455800:RR:0:1:6576:6576:21:25292
T: 120455800:RR:0:3:10081:10081:21:25292
T: 120455800:RM:0:11:21:25292
T: 120455800:NL:0:137:21:[nan,nan,nan]:1901:6576:0:10081
T: 120456080:RR:0:0:1883:1883:22:25298
T: 120456080:RR:0:1:6487:6487:22:25298
T: 120456080:RR:0:3:10057:10057:22:25298
T: 120456080:RM:0:11:22:25298
T: 120456080:NL:0:137:22:[nan,nan,nan]:1883:6487:0:10057
T: 120456360:RR:0:0:1873:1873:23:25304
T: 120456360:RR:0:1:6463:6463:23:25304
T: 120456360:RR:0:3:10076:10076:23:25304
T: 120456360:RM:0:11:23:25304
T: 120456360:NL:0:137:23:[nan,nan,nan]:1873:6463:0:10076
T: 120456640:RR:0:0:1934:1934:24:25310
T: 120456640:RR:0:1:6566:6566:24:25310
T: 120456640:RR:0:3:10104:10104:24:25310
T: 120456640:RM:0:11:24:25310
T: 120456640:NL:0:137:24:[nan,nan,nan]:1934:6566:0:10104
T: 120456920:RR:0:0:1887:1887:25:25316
T: 120456920:RR:0:1:7288:7288:25:25316
T: 120456920:RR:0:3:10053:10053:25:25316
T: 120456920:RM:0:11:25:25316
T: 120456920:NL:0:137:25:[nan,nan,nan]:1887:7288:0:10053
T: 120457200:RR:0:0:1682:1682:26:25323
T: 120457200:RR:0:1:6533:6533:26:25323
```

(b)

Figure I.1: Sample raw files of the collected RFID and UWB data: (a) RFID .txt file, and (2) UWB .txt file.

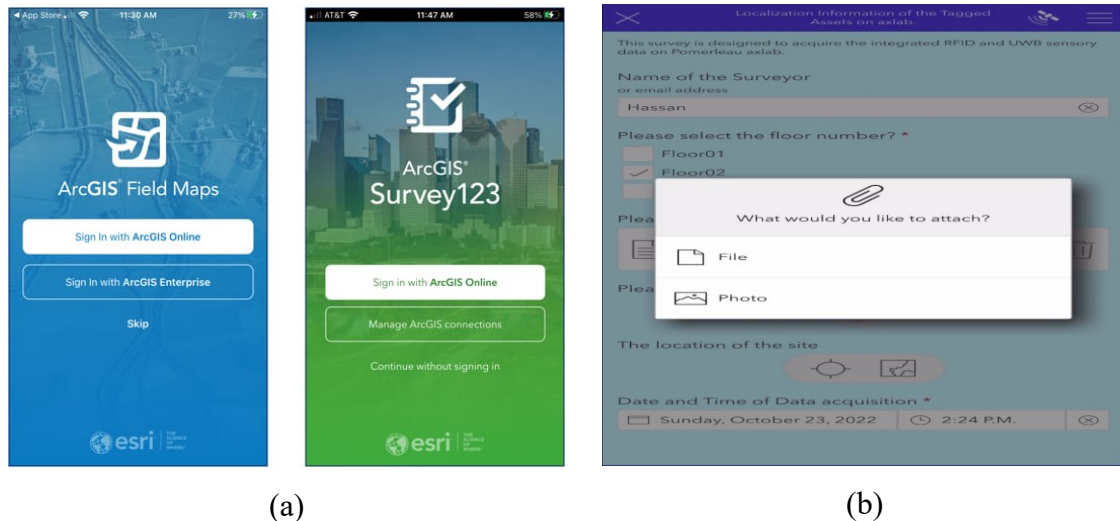


Figure I.2: The ArcGIS tools used for data collection and transfer into server: (a) Survey123 and Field Maps, and (2) sample survey for field data collection and transfer.

The raw .txt files are processed on the server to generate 2D and 3D coordinates (local coordinates) of the tagged objects using the improved trilateration method developed in this study. Appendix III provides details on the Python code developed for the integration of RFID and UWB files for the localization. The code highlights lines for reading the collected .txt files, their integration, and exporting the Excel file of the localization information.

Step III. To transition the collected coordinates from the local to the global system, five georeferenced points of the project site with visibility to both interior and exterior spaces are selected. These points, known as tie points, help establish a transformation matrix that accurately converts local coordinates to global coordinates. In this study, this process was performed manually. However, in the future, ArcGIS georeferencing tools (e.g., move, rotate, flip, scale, etc.) could be used to automate this step. Additionally, ArcGIS GeoEvent Server could be utilized to ensure real-time connection between tracking technologies and the ArcGIS server. The detailed procedure is outlined in Figure I.3 and Figure I.4.

| Tag No. | x | y | z | Average Error (m) |
|---------------------|------|------|------|-------------------|
| 1 | 3.49 | 2.15 | 3.89 | 1.30 |
| 2 | 3.25 | 1.11 | 0.08 | 0.66 |
| 3 | 5.12 | 1.24 | 0.72 | 0.59 |
| 4 | 4.86 | 2.60 | 1.19 | 0.94 |
| 5 | 2.49 | 1.28 | 0.24 | 2.22 |
| 6 | 4.53 | 3.36 | 0.69 | 2.16 |
| 7 | 0.00 | 0.00 | 0.00 | 0.00 |
| 8 | 3.12 | 1.40 | 0.08 | 2.00 |
| 9 | 3.81 | 1.57 | 1.44 | 2.16 |
| 10 | 4.78 | 2.87 | 2.65 | 1.39 |
| Total Average Error | | | | 1.49 |

Figure I.3: Exported local coordinates achieved for the tagged objects.

| Point Name | Northing (m) | Easting (m) | Elevation (m) | Latitude (WGS 84) | Longitude (WGS 84) | Height (WGS84) |
|------------|--------------|-------------|---------------|-------------------|--------------------|----------------|
| Point1 | 500000.00 | 400000.00 | 100.00 | 45.1234 | -75.1234 | 100.00 |
| Point2 | 500100.00 | 400100.00 | 101.00 | 45.5678 | -75.5678 | 101.00 |
| Point3 | 500200.00 | 400200.00 | 102.00 | 45.9101 | -75.9101 | 102.00 |
| Point4 | 500300.00 | 400300.00 | 103.00 | 46.1234 | -76.1234 | 103.00 |
| Point5 | 500400.00 | 400400.00 | 104.00 | 46.5678 | -76.5678 | 104.00 |

Figure I.4: Sample of the five tie-points used for coordinates' transition from local to global.

Step IV. The georeferenced coordinates are mapped to visualize the associated tagged objects in ArcGIS Pro, either through the BIM model or point cloud data. The developed framework in the study eliminates the need for an accurate BIM model with a high Level of Development (LoD), which is not available at the time of the method's application to track the objects in a timely manner. This is because the tagged objects are identified and localized through field data collection, rather than relying on a pre-existing model to derive the coordinates. Furthermore, ArcGIS provides an efficient computational platform, executed within the ArcGIS environment, and offers visualization tools for the localized objects. Figure I.5 illustrates the visualized information within the 3D environment.

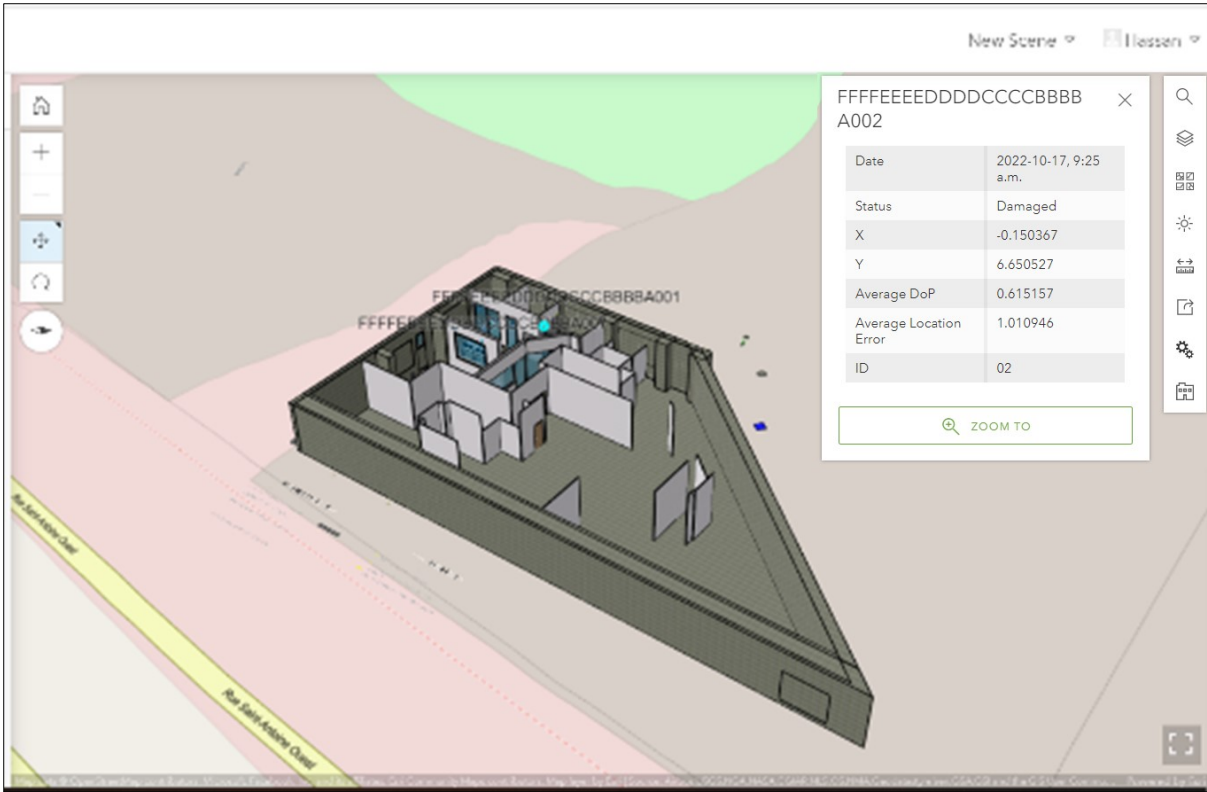


Figure I.5: Mapped information in ArcGIS Pro.

Appendix II:

Guideline on the Application of the Developed Framework on Job Site

To apply the developed method in the study for digitalizing progress reporting on a job site, the following steps are followed:

Step I. Review the project's planned document with a site manager or superintendent to identify tracking needs and select near-critical activities and important components. Figure II.1 illustrates a sample of the planned document used in the study to identify near-critical activities and sub-activities. The criticality can be determined either by defining a customized ratio value of the activities' float time divided by their duration, or through expert judgment for progress reporting.

| POMERLEAU | | CAL - Échéancier salles mécaniques - R01 - 2023/09/01 | | | | | |
|-----------|---------|---|----------|--------------|--------------|----------------|---|
| ID | % Comp. | Name | Duration | Start | Finish | Predecessors | Notes |
| 1 | 12% | PROJET | 102 d | Mon 23-08-21 | Fri 24-01-26 | | |
| 2 | 20% | SOUS-SOL | 94 d | Fri 23-08-25 | Mon 24-01-22 | | |
| 3 | 27% | SS-TEC-101 | 90 d | Thu 23-08-31 | Mon 24-01-22 | | *Incluant secteur bulleur corridor 105 |
| 4 | 0% | MÉCANIQUE DE PISCINE | 74 d | Mon 23-09-11 | Mon 24-01-08 | | |
| 5 | 0% | CONTRÔLES (panneaux et variateurs) | 10 d | Thu 23-08-31 | Fri 23-09-15 | 6SF | |
| 6 | 0% | ÉLECTRICITÉ | 70 d | Fri 23-09-15 | Mon 24-01-08 | 4FF | |
| 7 | 66% | TUYAUTERIE | 80 d | Thu 23-08-31 | Mon 24-01-08 | 4FF | Coordination avec Soucy sera faite pour libérer les travaux restants de SCV et permettre de réduire la durée ci-indiquée. |
| 8 | 70% | VENTILATION | 60 d | Thu 23-08-31 | Mon 23-11-27 | 7SS | Coordination avec Soucy sera faite pour libérer les travaux restants de SCV et permettre de réduire la durée ci-indiquée. |
| 9 | 0% | CALORIFUGE VENT. | 15 d | Tue 23-11-21 | Mon 23-12-11 | 8FS-5 d | |
| 10 | 0% | CALORIFUGE TUY. | 15 d | Tue 23-12-19 | Mon 24-01-22 | 7FS-5 d | |
| 11 | 0% | CONTRÔLES | 20 d | Tue 23-12-05 | Mon 24-01-15 | 6FS-15 d;7FS-1 | |
| 12 | 3% | SS-TEC-110 | 88 d | Fri 23-08-25 | Fri 24-01-12 | | |
| 13 | 29% | Bases de propreté (fin) | 14 d | Fri 23-08-25 | Thu 23-09-14 | | |
| 14 | 0% | CONTRÔLES (panneaux et variateurs) | 10 d | Thu 23-09-21 | Thu 23-10-05 | 15SF | |
| 15 | 0% | ÉLECTRICITÉ | 55 d | Thu 23-10-05 | Fri 23-12-22 | 16SS+15 d | |
| 16 | 0% | TUYAUTERIE | 60 d | Thu 23-09-14 | Fri 23-12-08 | 13SS+13 d | Demande SCV: prolonger jusqu'au 19 janvier 2024. POM: Délai prolongé de 3 semaines, 60 jours accordés. |
| 17 | 6% | VENTILATION | 25 d | Tue 23-09-05 | Tue 23-10-10 | 13SS+6 d | Demande SCV: prolonger de 3 semaines, locaux fermés. POM: Ok. |
| 18 | 0% | CALORIFUGE VENT. | 15 d | Tue 23-10-03 | Tue 23-10-24 | 17FS-5 d | |
| 19 | 0% | CALORIFUGE TUY. | 15 d | Mon 23-12-04 | Fri 23-12-22 | 16FS-5 d | |
| 20 | 0% | CONTRÔLES | 20 d | Mon 23-12-04 | Fri 24-01-12 | 15FS-15 d;16F | |

Figure II.1: The planned document of the selected project encompasses the activities in two mechanical rooms.

Step II. Design the reporting hierarchy to identify project zones, activities, sub-activities, and their associated components based on technology usage and the level of automation required. In the study investigated in the research, tracking began from the site inventory or stock rooms by labeling the received components (e.g., mechanical equipment). However, in the future, depending on project needs, tracking can start from the supplier side by monitoring the delivery of components from manufacturing to the site, or from the time the components are installed on the job site. This largely depends

on the end user of the digitalized progress reporting method and the level of visibility they require for tracking the project. It is also possible to design the hierarchy for a more automated or semi-automated data acquisition workflow. Tagging can be performed either at the factory before the arrival of important components to the site, or by the person in charge at the job site. Additionally, it is essential to define the required technologies to track whether the materials are delivered, shipped, received, etc. Figure II.2 illustrates how the developed framework can be utilized for semi-automated tracking of assemblies using the RTLS technologies in this study.

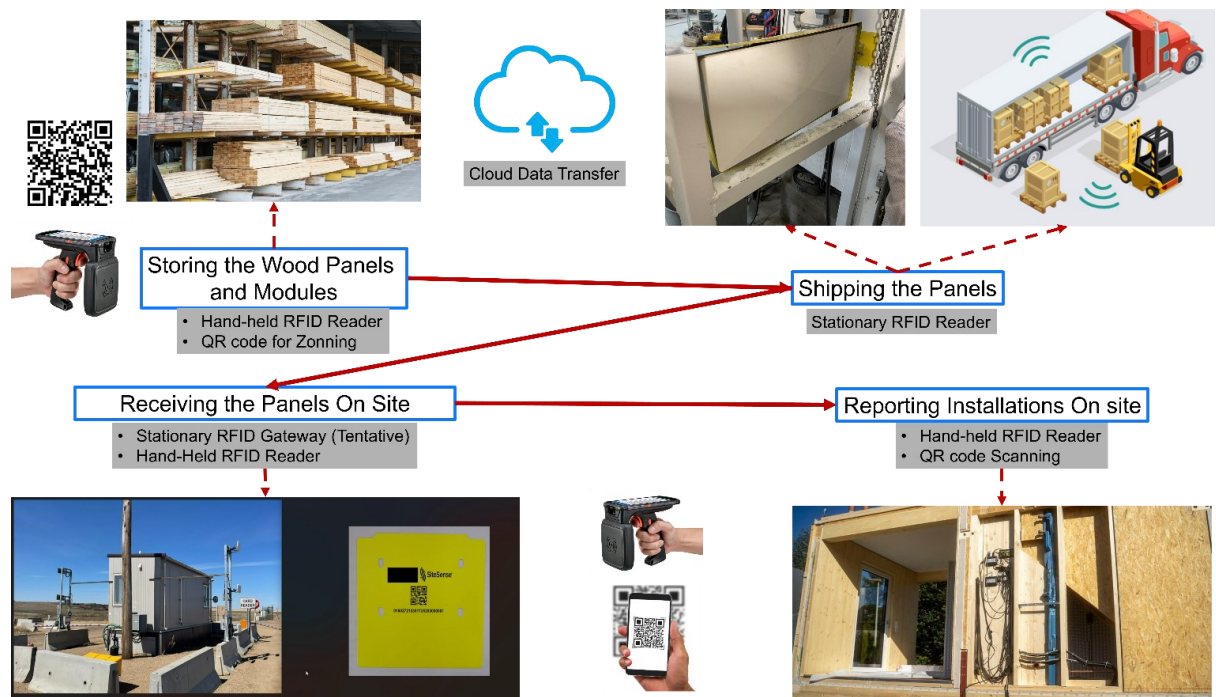


Figure II.2: Conceptual framework for a semi-automated tracking of assemblies from manufacturing to the site.

Step III. Tag the selected components on the job site with QR code-RFID tags. Since the progress of activities associated with these components will represent the overall project's progress, it is crucial to ensure the highest visibility of activities by tracking these tagged components. Additionally, tagging only the critical components, rather than all components, will significantly reduce the data acquisition effort and the cost of technology usage on the job site. However, this might result in losing some details on tracking activities but will not affect the overall project progress tracking.

Step IV. Install the UWB receivers at the end corners of the targeted zones on the job site. Additionally, scan the site area with a LiDar device to provide accurate coordinates of the UWB receivers, calibrating the RTLS for enhanced localization purposes.

Step V. On each reporting day, data about the tagged components and their associated activities are manually collected through a digital survey prepared in ArcGIS Survey123, by scanning the QR code-RFID tag. The component status data are manually collected by scanning the QR code with a mobile phone camera or the RFID tag (embedded in the QR code) using a hand-held RFID gun. This process is conducted during site inspections by the site coordinators or superintendents, who then transmit the collected data to the server via a mobile phone or a tablet. Manual inspection also offers the advantage of expert judgment for on-site quality control. Since the occurrence of damaged or broken components is infrequent, manual data collection is more practical than an automated approach for these close inspections using QR codes.

The advantage of using RFID over QR codes is the ability to scan tagged components that are not visible or are covered by obstacles as the project progresses. Additionally, RFID data are used to automatically localize the tagged components each reporting day through the integrated RFID-UWB method. In the future, point cloud data collected with a LiDAR device, leveraging computer vision, could be used to refine the 3D localization of the tagged components. The accurate 3D coordinates acquired from labeled point cloud data can be used to precisely measure the installed components' coordinates and automatically identify deviations from planned models. Figure II.3 illustrates a sample of the information collected in each reporting day.

| No. | Activity Name | ID | Duration (days) | Float (days) | Float/Duration | Class of Object | Status | Time | X | Y | Z | Progress (%) | Total Progress (%) | Total Quality (%) |
|-----|---|---------|-----------------|--------------|----------------|-----------------|-----------|------|---|---|-----|--------------|--------------------|-------------------|
| 1 | Activity I | ID 1.1 | 50 | 5 | 0.1 | 1 | Completed | | | | | 100 | 78 | 80 |
| 2 | | ID 1.2 | | | | 4 | Completed | | | | 100 | | | |
| 3 | | ID 1.3 | | | | 1 | Installed | | | | 40 | | | |
| 4 | | ID 1.4 | | | | 1 | Completed | | | | 100 | | | |
| 5 | | ID 1.5 | | | | 1 | Completed | | | | 100 | | | |
| 6 | | ID 1.6 | | | | 3 | Completed | | | | 100 | | | |
| 7 | | ID 1.7 | | | | 2 | Inspected | | | | 0 | | | |
| 8 | | ID 1.8 | | | | 2 | Installed | | | | 40 | | | |
| 9 | | ID 1.9 | | | | 1 | Completed | | | | 100 | | | |
| 10 | Activity II | ID 2.1 | 25 | 3 | 0.12 | 1 | Inspected | | | | | 80 | 44 | 50 |
| 11 | | ID 2.2 | | | | 2 | Completed | | | | 100 | | | |
| 12 | | ID 2.3 | | | | 2 | Completed | | | | 100 | | | |
| 13 | | ID 2.4 | | | | 2 | Inspected | | | | 0 | | | |
| 14 | | ID 2.5 | | | | 1 | Inspected | | | | 0 | | | |
| 15 | Activity III | ID 3.1 | 100 | 2 | 0.02 | 3 | Damaged | | | | | 20 | 50 | 60 |
| 16 | | ID 3.2 | | | | 1 | Completed | | | | 100 | | | |
| 17 | | ID 3.3 | | | | 3 | Inspected | | | | 80 | | | |
| 18 | | ID 3.4 | | | | 3 | Inspected | | | | 0 | | | |
| 19 | | ID 3.5 | | | | 3 | Inspected | | | | 80 | | | |
| 20 | | ID 3.6 | | | | 3 | Inspected | | | | 80 | | | |
| 21 | | ID 3.7 | | | | 3 | Inspected | | | | 80 | | | |
| 22 | | ID 3.8 | | | | 4 | Inspected | | | | 0 | | | |
| 23 | | ID 3.9 | | | | 4 | Inspected | | | | 80 | | | |
| 24 | | ID 3.10 | | | | 4 | Inspected | | | | 80 | | | |
| 25 | Total Progress and Quality of the Project | | | | | | | | | | | | 56.67 | 66.67 |

Figure II.3: The sample information of the selected activities and components in a reporting day.

Step VI. The data collected each reporting day, encompassing time, ID, status, and location of the identified tagged components, were aggregated and processed through the progress tracking method. This process generates reports on the Material Status

Index (MSI), Quality Status Index (QSI), and detailed progress of each activity and its status. These reports are visualized using dashboards designed in ArcGIS or other platforms like PowerBI, utilizing appropriate plug-ins.

Appendix III:

Python Code for 3D Localization using Integrated RFID-UWB

```
# RFID-UWB 3D Localization
"""
Created on Mon Nov 16 15:32:37 2020
@author: Hassan.B
This script is for RFID Tags localization with UWB data
"""

# Reading RFID and UWB .txt files in the server or in
Google Drive

file_1 = open('/content/Test01- RFID calibration with o20 with UWB tag
attached moving randomly.TXT', 'r')
f1= file_1.readlines()
file_2 = open('/content/- CAL Experiment Real Values with
A4=2.15m.txt', 'r')
f2= file_2.readlines()
file_3 = open('/content/- CAL RFID Reference Tags Experimental Real
values.txt', 'r')
f3= file_3.readlines()
file_4 = open('/content/Test01- UWB calibration with o20 dbm and UWB
tag attached moving randomly.txt', 'r')
f4= file_4.readlines()
n1= int (len(f1))
n2= int (len(f4))
TagNo = 10
n=0
n3=0
k=0
k1=0
q1=0.0001
q2=0.0001
q3=0.0001
q4=0.0001
q5=0.0001
q6=0.0001
q7=0.0001
q8=0.0001
q9=0.0001
q10=0.0001
Q=1
Qn=0
l=0
p=0
```

```

p1=0
D0=0
h1=0.0001
p2=0
p3=0
RSSIdistancecumulative=0
RSSIcumulative=0
Row=0
SumX = 0
SumY = 0
SumZ = 0
SumR1 = 0
SumR2 = 0
SumR3 = 0
SumR4 = 0
p4=0
quwb=0.0001
RSSIA001 = 0
RSSIA002 = 0
RSSIA003 = 0
RSSIA004 = 0
RSSIA005 = 0
RSSIA006 = 0
RSSIA007 = 0
RSSIA008 = 0
RSSIA009 = 0
RSSIA010 = 0
p1_1 = 0
p1_2 = 0
p1_3 = 0
p1_4 = 0
p1_5 = 0
p1_6 = 0
p1_7 = 0
p1_8 = 0
p1_9 = 0
p1_10 = 0

# Defining the reading range of the RFID reader based
on its output power of the hand-held RFID gun
# Defining the Ratio for the points in intersected
area of the circles (here we set it to 0.1) for
trilateration

IdentificationNo= 8
RR=300
Ratiolimit = 0.1
for e1 in range (0,n1):

```

```

newlist = f1[e1] # RSSI value
m1 =int (len(newlist))
for g1 in range (0,m1):
    if ( (newlist [g1] == 'R') and (newlist [g1+1] == 'I') ):
        n= n+1

# Data structuring of the raw RFID file, and put them in a dataframe

LEmatrix = [ [0 for x in range (3)] for y in range (n)]
LEmatrix_real = [ [0 for x in range (1)] for y in range (35)]
LEmatrix_real_Reftags = [ [0 for x in range (1)] for y in range
(TagNo)]
RSSIave =[ [0 for x in range (TagNo+1)] for y in range (n)]
distanceeq =[ [0 for x in range (TagNo+1)] for y in range (n)]

import re
for e in range (2,n1):
    newlist1 = f1[e] # RSSI value
    newlist2 = f1[e-1] # Tag ID
    newlist3 = f1[e-2] # Time & date
    m =int (len(newlist1))
    for g in range (0,m):
        if ( (newlist1 [g] == 'R') and (newlist1 [g+1] == 'I') and
(newlist3 [g] == 'D') and (newlist3 [g+1] == 'T') and newlist2
[4:25]=='FFFFFFFFDDDDCCCCBBBBA' ):
            RSSI = re.findall(r"[-+]?[d*]\.[d+|\d+", newlist1)
            TagID = newlist2 [4:28]
            Time = re.findall(r"[-+]?[d*]\.[d+|\d+", newlist3)
            LEmatrix [k] = [int(Time[3])*3600 + int(Time[4])*60+
int(Time[5]), TagID, - int (RSSI [0]) ]
            k = k +1
            #for Repetative RSSI values in each second
        elif ((newlist1 [g] == 'R') and (newlist1 [g+1] == 'I') and
(newlist3 [g] == 'R') and (newlist3 [g+1] == 'I') and newlist2
[4:25]=='FFFFFFFFDDDDCCCCBBBBA'):
            RSSI = re.findall(r"[-+]?[d*]\.[d+|\d+", newlist1)
            TagID = newlist2 [4:28]
            Time = LEmatrix [k-1][0]
            LEmatrix [k] = [Time, TagID, - int (RSSI [0]) ]
            k = k +1

#Finding range and location of Tag and put it in a
matrix

import re
for l1 in range (0,35):
    LEmatrix_real [l1] = re.findall(r"[-+]?[d*]\.[d+|\d+", f2[l1])

```

```

for l2 in range (0,TagNo):
    LEmatrix_real_Reftags [l2] = re.findall(r"[-+]?[d*]\.\d+|\d+",
f3[l2])

for z1 in range (0,n):
    if (LEmatrix [z1][1] == 'FFFFFFFFEDDDDDCCCCBBBBBA101' and (Qn==0) ):
        T0 = LEmatrix [z1][0]
        T1 = LEmatrix [z1+1][0]
        T0ref= T0
        Qn= 1
while (l < n):
    if ( LEmatrix [l][0] <= T0 ):
        RSSIA001 = 0
        RSSIA002 = 0
        RSSIA003 = 0
        RSSIA004 = 0
        RSSIA005 = 0
        RSSIA006 = 0
        RSSIA007 = 0
        RSSIA008 = 0
        RSSIA009 = 0
        RSSIA010 = 0

        if ( (LEmatrix[l][0] <= (T1)) and (LEmatrix[l][1]
=='FFFFFFFFEDDDDDCCCCBBBBBA001') ):
            RSSIA001= RSSIA001 + float(LEmatrix[l][2])
            q1=q1+1
            Q=1
            #print (l, 'Second line read', q1)
        if ( (LEmatrix[l][0] <= (T1)) and (LEmatrix[l][1]
=='FFFFFFFFEDDDDDCCCCBBBBBA002') ):
            RSSIA002= RSSIA002 + float(LEmatrix[l][2])
            q2=q2+1
            Q=1
            #print (l, 'third line read')
        if ( (LEmatrix[l][0] <= (T1)) and (LEmatrix[l][1]
=='FFFFFFFFEDDDDDCCCCBBBBBA003') ):
            RSSIA003= RSSIA003 + float(LEmatrix[l][2])
            q3=q3+1
            Q=1
        if ( (LEmatrix[l][0] <= (T1)) and (LEmatrix[l][1]
=='FFFFFFFFEDDDDDCCCCBBBBBA004') ):
            RSSIA004= RSSIA004 + float(LEmatrix[l][2])
            q4=q4+1
            Q=1
        if ( (LEmatrix[l][0] <= (T1)) and (LEmatrix[l][1]
=='FFFFFFFFEDDDDDCCCCBBBBBA005') ):
            RSSIA005= RSSIA005 + float(LEmatrix[l][2])
            q5=q5+1

```

```

    Q=1
    if ( (LEmatrix[l][0] <= (T1)) and (LEmatrix[l][1]
=='FFFFFFFFEDDDDDCCCCBBBBBA006') ):
        RSSIA006= RSSIA006 + float(LEmatrix[l][2])
        q6=q6+1
        Q=1
    if ( (LEmatrix[l][0] <= (T1)) and (LEmatrix[l][1]
=='FFFFFFFFEDDDDDCCCCBBBBBA007') ):
        RSSIA007= RSSIA007 + float(LEmatrix[l][2])
        q7=q7+1
        Q=1
    if ( (LEmatrix[l][0] <= (T1)) and (LEmatrix[l][1]
=='FFFFFFFFEDDDDDCCCCBBBBBA008') ):
        RSSIA008= RSSIA008 + float(LEmatrix[l][2])
        q8=q8+1
        Q=1
    if ( (LEmatrix[l][0] <= (T1)) and (LEmatrix[l][1]
=='FFFFFFFFEDDDDDCCCCBBBBBA009') ):
        RSSIA009= RSSIA009 + float(LEmatrix[l][2])
        q9=q9+1
        Q=1
    if ( (LEmatrix[l][0] <= (T1)) and (LEmatrix[l][1]
=='FFFFFFFFEDDDDDCCCCBBBBBA010') ):
        RSSIA010= RSSIA010 + float(LEmatrix[l][2])
        q10=q10+1
        Q=1
    if (Q!=0 or ((LEmatrix[l][1] !='FFFFFFFFEDDDDDCCCCBBBBBA001') and
(LEmatrix[l][1] !='FFFFFFFFEDDDDDCCCCBBBBBA002') and (LEmatrix[l][1]
!='FFFFFFFFEDDDDDCCCCBBBBBA003') and (LEmatrix[l][1]
!='FFFFFFFFEDDDDDCCCCBBBBBA004') and (LEmatrix[l][1]
!='FFFFFFFFEDDDDDCCCCBBBBBA005') and (LEmatrix[l][1]
!='FFFFFFFFEDDDDDCCCCBBBBBA006') and (LEmatrix[l][1]
!='FFFFFFFFEDDDDDCCCCBBBBBA007') and (LEmatrix[l][1]
!='FFFFFFFFEDDDDDCCCCBBBBBA008') and (LEmatrix[l][1]
!='FFFFFFFFEDDDDDCCCCBBBBBA009') and (LEmatrix[l][1]
!='FFFFFFFFEDDDDDCCCCBBBBBA010'))):
        l=l+1
        Q=0
    else:

        RSSIave[p][0:TagNo] = [LEmatrix[l-1][0], RSSIA001/q1,
RSSIA002/q2, RSSIA003/q3, RSSIA004/q4, RSSIA005/q5, RSSIA006/q6,
RSSIA007/q7, RSSIA008/q8, RSSIA009/q9, RSSIA010/q10]
        T1 = T1 + (LEmatrix[l][0] - LEmatrix[l-1][0])

        q1=q2=q3=q4=q5=q6=q7=q8=q9=q10=0.0001
        p = p+1
        RSSIA001 = 0

```

```

RSSIA002 = 0
RSSIA003 = 0
RSSIA004 = 0
RSSIA005 = 0
RSSIA006 = 0
RSSIA007 = 0
RSSIA008 = 0
RSSIA009 = 0
RSSIA010 = 0

# Equivalent distance for average RSSI value based on  
the Calibration Module for RFID tags

for x1 in range (0,p):
    for x2 in range (1,TagNo+1):
        if (RSSIave[x1][x2]==0):
            distanceeq [x1][x2] = 0.0
        else:
            #distanceeq [x1][x2] = 2.718281828459045 ** (-
(RSSIave[x1][x2]+72.483)/3.914)
            distanceeq [x1][x2] = -0.4616 * RSSIave[x1][x2]- 32.5333

# Data structuring of the raw UWB file, and put them  
in a dataframe

for e2 in range (0,n2):
    newlist = f4[e2]
    m2 =int (len(newlist))
    for g2 in range (0,m2):
        if ( newlist [g2] == '[' and newlist [g2+1] != 'n'):
            Row= Row+1

LEmatrix_uwb = [ [0 for x in range (1)] for y in range (Row)]
LEmatrix_real_uwb = [ [0 for x in range (1)] for y in range (35)]
T =[ [0 for x in range (1)] for y in range (Row)]
T_equal =[ [0 for x in range (8)] for y in range (Row)]
b =[ [0 for x in range (8+TagNo)] for y in range (p)]
c =[ [0 for x in range (1)] for y in range (10)]
Locationmatrix = [ [0 for x in range (1)] for y in range (40000)]
Locationmatrixfinal = [ [0 for x in range (1)] for y in range (TagNo)]
Locationmatrix_DoP = [ [0 for x in range (1)] for y in range (TagNo)]

for e in range (0,n2):
    newlist = f4[e]
    m =int (len(newlist))
    for g in range (0,m):
        if (newlist [g] == '[' and newlist [g+1] != 'n'):

```

```

LEmatrix_uwb [k1] = re.findall(r"[+]?[d*\.|d+|\d+",
newlist)
TimeinS =(int (newlist [2])*10+ int (newlist [3]) )*3600+
(int (newlist [4])*10+ int( newlist [5]))*60+ (int( newlist [6])*10+
int (newlist [7])) + (int (newlist [8])*100+ int (newlist [9])*10+ int
(newlist [10]) )/1000
T [k1][0:1] = [TimeinS]
#print (k1, 'Out of : ', Row-1, ' ', 'Toal: ', n2, ' time =
', float (T[k1][0]), ' ', LEmatrix_uwb [k1][0] )
k1 = k1 +1

```

Time synchronization of the RFID and UWB sensors

```

dt0 = T0ref - T[0][0]
T0uwb = T0ref
for w in range (0,Row):
    T_equal [w] = [T [w][0] + dt0, LEmatrix_uwb[w][4],
LEmatrix_uwb[w][5], LEmatrix_uwb[w][6], LEmatrix_uwb[w][7],
LEmatrix_uwb[w][8], LEmatrix_uwb[w][9], LEmatrix_uwb[w][10]]

```

Forming the Fusion matrix of integrated RFID and UWB data to shape Radius and Center of circles (sphers) to shape trilateration circles (sphers) # Matrix b = [Time (s), corresponding distance based on path-loss model, UWB (x,y,z, R1, R2, R3, R4)]

```

for r in range (0,p):
    for l in range (0,Row):
        if ( (T_equal[l][0]) >= (RSSIave[r][0]-0.5) and (T_equal[l][0])
<= (RSSIave[r][0] + 0.5) ):
            SumX= SumX + float (T_equal [l][1])
            SumY= SumY + float (T_equal [l][2])
            SumZ= SumZ + float (T_equal [l][3])
            SumR1= SumR1 + float (T_equal [l][4])
            SumR2= SumR2 + float (T_equal [l][5])
            SumR3= SumR3 + float (T_equal [l][6])
            SumR4= SumR4 + float (T_equal [l][7])
            quwb =quwb+1

    b[r][0:18] = [RSSIave[r][0], distanceeq [r][1], distanceeq [r][2],
distanceeq [r][3], distanceeq [r][4], distanceeq [r][5], distanceeq
[r][6], distanceeq [r][7], distanceeq [r][8], distanceeq [r][9],
distanceeq [r][10], (SumX/quwb), (SumY/quwb), (SumZ/quwb),
(SumR1/quwb)/1000, (SumR2/quwb)/1000, (SumR3/quwb)/1000,
(SumR4/quwb)/1000]
    quwb=0.0001
    SumX = 0

```

```

SumY = 0
SumZ = 0
SumR1 = 0
SumR2 = 0
SumR3 = 0
SumR4 = 0

for r1 in range (0,TagNo):
    c[r1].remove(0)
    for l1 in range (0,p):
        if (b[l1][r1+1] > 0 and len(c[r1]) < IdentificationNo):
            c[r1].append ([r1+1, b[l1][0], b[l1][r1+1], b[l1][TagNo+1],
b[l1][TagNo+2], b[l1][TagNo+3],      b[l1][TagNo+4], b[l1][TagNo+5],
b[l1][TagNo+6], b[l1][TagNo+7]])

Pmatrix = [len(c[0]),len(c[1]), len(c[2]), len(c[3]), len(c[4]),
len(c[5]), len(c[6]), len(c[7]), len(c[8]), len(c[9])]
print (Pmatrix)
import math

# Generating manipulated point cloud data with
distance increments of 10 cm
# Factorial seletion of the scenarios for RFID-UWB
integration, calculating Spatial of Distribution
(SoD) and varying the radius

for L in range (0,TagNo):
    count = 0
    nprim = 1
    mprim = 1
    xcm=0
    ycm=0
    zcm=0

    xmin = [min(i) for i in zip(*c[L])][3] *100
    xmax = [max(i) for i in zip(*c[L])][3] *100
    ymin = [min(i) for i in zip(*c[L])][4] *100
    ymax = [max(i) for i in zip(*c[L])][4] *100
    zmin = [min(i) for i in zip(*c[L])][5] *100
    zmax = [max(i) for i in zip(*c[L])][5] *100
    print ('X ',xmin,'--',xmax)
    print ('Z ',zmin,'--',zmax)
    for l1 in range (0,len(c[L])):
        for l2 in range (l1+1,len(c[L])):
            for l3 in range (l2+1,len(c[L])):
                for l4 in range (l3+1, len(c[L])):
                    Cmatriceq = c[L]

```

```

        if (Cmatriceq[l1][0] !=0 and Cmatriceq[l2][0] !=0
and Cmatriceq[l3][0] !=0 and Cmatriceq[l4][0] !=0 ):
            print ('Tag',L+1, 'l1:',l1,'l2:', l2, 'l3:',l3,
'l4:',l4)

            ncounter1=0
            ncounter2=0
            for x in range (int(xmin)-RR,int(xmax)+RR):
                for y in range (int(ymin)-RR,int(ymax)+RR):
                    for z in range
(int(zmin),int(zmax)+RR):

                        #print ('x:',x,'y:',y,'z:',z)
                        if ( ((x/100-Cmatriceq[l1][3])**2 +
(y/100-Cmatriceq[l1][4])**2 + (z/100-Cmatriceq[l1][5])**2 <=
(Cmatriceq[l1][2])**2) and ((x/100-Cmatriceq[l2][3])**2 + (y/100-
Cmatriceq[l2][4])**2 + (z/100-Cmatriceq[l2][5])**2 <=
(Cmatriceq[l2][2])**2) and ((x/100-Cmatriceq[l3][3])**2 + (y/100-
Cmatriceq[l3][4])**2 + (z/100-Cmatriceq[l3][5])**2 <=
(Cmatriceq[l3][2])**2) and ((x/100-Cmatriceq[l4][3])**2 + (y/100-
Cmatriceq[l4][4])**2 + (z/100-Cmatriceq[l4][5])**2 <=
(Cmatriceq[l4][2])**2)):

                            nprim = nprim + 1
                            xcm = xcm + x
                            ycm = ycm + y
                            zcm = zcm + z

                                if ( ((x/100-Cmatriceq[l1][3])**2 +
(y/100-Cmatriceq[l1][4])**2 + (z/100-Cmatriceq[l1][5])**2 <=
(Cmatriceq[l1][2])**2) or ((x/100-Cmatriceq[l2][3])**2 + (y/100-
Cmatriceq[l2][4])**2 + (z/100-Cmatriceq[l2][5])**2 <=
(Cmatriceq[l2][2])**2) or ((x/100-Cmatriceq[l3][3])**2 + (y/100-
Cmatriceq[l3][4])**2 + (z/100-Cmatriceq[l3][5])**2 <=
(Cmatriceq[l3][2])**2) or ((x/100-Cmatriceq[l4][3])**2 + (y/100-
Cmatriceq[l4][4])**2 + (z/100-Cmatriceq[l4][5])**2 <=
(Cmatriceq[l4][2])**2)):

                                    mprim = mprim + 1
                                    if ( (nprim/mprim)<=Ratiolimit and nprim!=1):
                                        count = count +1
                                        ratio = nprim/mprim
                                        XCM = xcm/((nprim-1)*100)
                                        YCM = ycm/((nprim-1)*100)
                                        ZCM = zcm/((nprim-1)*100)
                                        error = math.sqrt ((XCM-
float(LEmatrix_real_Reftags[L][2]) )**2 + (YCM-
float(LEmatrix_real_Reftags[L][3]) )**2 + (ZCM-
float(LEmatrix_real_Reftags[L][4]) )**2)
                                        #DoP calculation
                                        ux=
(Cmatriceq[l1][3]+Cmatriceq[l2][3]+Cmatriceq[l3][3]+Cmatriceq[l4][3])/4

```

```

        uy=
(Cmatrizeq[l1][4]+Cmatrizeq[l2][4]+Cmatrizeq[l3][4]+Cmatrizeq[l4][4])/4
        uz=
(Cmatrizeq[l1][5]+Cmatrizeq[l2][5]+Cmatrizeq[l3][5]+Cmatrizeq[l4][5])/4
        sx2= ((Cmatrizeq[l1][3]-
ux)**2+(Cmatrizeq[l2][3]-ux)**2+(Cmatrizeq[l3][3]-
ux)**2+(Cmatrizeq[l4][3]-ux)**2)/3
        sy2= ((Cmatrizeq[l1][4]-
uy)**2+(Cmatrizeq[l2][4]-uy)**2+(Cmatrizeq[l3][4]-
uy)**2+(Cmatrizeq[l4][4]-ux)**2)/3
        sz2= ((Cmatrizeq[l1][5]-
uz)**2+(Cmatrizeq[l2][5]-uz)**2+(Cmatrizeq[l3][5]-
uz)**2+(Cmatrizeq[l4][5]-ux)**2)/3
        s2= sx2+sy2+sz2

        Locationmatrix [n3] = [count, L+1, nprim,
mprim, ratio, XCM, YCM, ZCM, s2, error]
        n3 = n3+1
        print (count,'-', 'Tag ID:', L+1, 'n:',
nprim, 'divided by m:', mprim, '= ratio:', ratio, 'The CM is:
(',XCM,',',YCM,',',ZCM, ')', 'The SoD is:', s2,' The error is:', error)
        nprim=1
        mprim=1
        xcm=0
        ycm=0
        zcm=0
        elif (nprim==1):
            while (nprim==1 and ncounter1 <=5):
                Cmatrizeq[l1][2] = Cmatrizeq[l1][2] +
0.1
                Cmatrizeq[l2][2] = Cmatrizeq[l2][2] +
0.1
                Cmatrizeq[l3][2] = Cmatrizeq[l3][2] +
0.1
                Cmatrizeq[l4][2] = Cmatrizeq[l4][2] +
0.1
                ncounter1 = ncounter1 +1
                print ('ncounter 1=', ncounter1)
                for x in range (int(xmin)-
RR,int (xmax)+RR) :
                    for y in range (int(ymin)-
RR,int (ymax)+RR) :
                        for z in range (int(zmin)-
RR,int (zmax)+RR) :
                            if ( ((x/100-
Cmatrizeq[l1][3])**2 + (y/100-Cmatrizeq[l1][4])**2 + (z/100-
Cmatrizeq[l1][5])**2 <= (Cmatrizeq[l1][2])**2 and ((x/100-
Cmatrizeq[l2][3])**2 + (y/100-Cmatrizeq[l2][4])**2 + (z/100-

```

```

Cmatriceq[l2][5]**2 <= (Cmatriceq[l2][2])**2) and ((x/100-
Cmatriceq[l3][3])**2 + (y/100-Cmatriceq[l3][4])**2 + (z/100-
Cmatriceq[l3][5])**2 <= (Cmatriceq[l3][2])**2) and ((x/100-
Cmatriceq[l4][3])**2 + (y/100-Cmatriceq[l4][4])**2 + (z/100-
Cmatriceq[l4][5])**2 <= (Cmatriceq[l4][2])**2):
                                nprim = nprim + 1
                                xcm = xcm + x
                                ycm = ycm + y
                                zcm = zcm + z
                                if ( ((x/100-
Cmatriceq[l1][3])**2 + (y/100-Cmatriceq[l1][4])**2 + (z/100-
Cmatriceq[l1][5])**2 <= (Cmatriceq[l1][2])**2) or ((x/100-
Cmatriceq[l2][3])**2 + (y/100-Cmatriceq[l2][4])**2 + (z/100-
Cmatriceq[l2][5])**2 <= (Cmatriceq[l2][2])**2) or ((x/100-
Cmatriceq[l3][3])**2 + (y/100-Cmatriceq[l3][4])**2 + (z/100-
Cmatriceq[l3][5])**2 <= (Cmatriceq[l3][2])**2) or ((x/100-
Cmatriceq[l4][3])**2 + (y/100-Cmatriceq[l4][4])**2 + (z/100-
Cmatriceq[l4][5])**2 <= (Cmatriceq[l4][2])**2):
                                mprim = mprim + 1
                                if (nprim!=1):
                                    count = count + 1
                                    ratio = nprim/mprim
                                    XCM = xcm/((nprim-1)*100)
                                    YCM = ycm/((nprim-1)*100)
                                    ZCM = zcm/((nprim-1)*100)
                                    error = math.sqrt ((XCM-
float(LEmatrix_real_Reftags[L][2]) )**2 + (YCM-
float(LEmatrix_real_Reftags[L][3]) )**2 + (ZCM-
float(LEmatrix_real_Reftags[L][4]) )**2)
                                    #DoP calculation
                                    ux=
(Cmatriceq[l1][3]+Cmatriceq[l2][3]+Cmatriceq[l3][3]+Cmatriceq[l4][3])/4
                                    uy=
(Cmatriceq[l1][4]+Cmatriceq[l2][4]+Cmatriceq[l3][4]+Cmatriceq[l4][4])/4
                                    uz=
(Cmatriceq[l1][5]+Cmatriceq[l2][5]+Cmatriceq[l3][5]+Cmatriceq[l4][5])/4
                                    sx2= ((Cmatriceq[l1][3]-
ux)**2+(Cmatriceq[l2][3]-ux)**2+(Cmatriceq[l3][3]-
ux)**2+(Cmatriceq[l4][3]-ux)**2)/3
                                    sy2= ((Cmatriceq[l1][4]-
uy)**2+(Cmatriceq[l2][4]-uy)**2+(Cmatriceq[l3][4]-
uy)**2+(Cmatriceq[l4][4]-uy)**2)/3
                                    sz2= ((Cmatriceq[l1][5]-
uz)**2+(Cmatriceq[l2][5]-uz)**2+(Cmatriceq[l3][5]-
uz)**2+(Cmatriceq[l4][5]-uz)**2)/3
                                    s2= sx2+sy2+sz2

```

```

        Locationmatrix [n3] = [count, L+1,
nprim, mprim, ratio, XCM, YCM, ZCM, s2, error]
        n3 = n3+1
        print (count,'R1-', 'Tag ID:', L+1,
'n:', nprim, 'divided by m:', mprim, '= ratio:', ratio, 'The CM is:
(',XCM,',',YCM,') The SoD is:', s2,' The error is:', error)
        nprim=1
        mprim=1
        xcm=0
        ycm=0
    elif ((nprim/mprim)> Ratiolimit and nprim!=1):
        while ((nprim/mprim)> Ratiolimit and
ncounter2 <=5):
            Cmatrizeq[l1][2] = Cmatrizeq[l1][2] -
0.1
            Cmatrizeq[l2][2] = Cmatrizeq[l2][2] -
0.1
            Cmatrizeq[l3][2] = Cmatrizeq[l3][2] -
0.1
            Cmatrizeq[l4][2] = Cmatrizeq[l4][2] -
0.1
            ncounter2 = ncounter2 +1
            print ('ncounter 2=', ncounter2)
            for x in range (int(xmin)-
RR,int (xmax)+RR) :
                for y in range (int(ymin)-
RR,int (ymax)+RR) :
                    for z in range (int(zmin)-
RR,int (zmax)+RR) :
                        if ( ((x/100-
Cmatrizeq[l1][3])**2 + (y/100-Cmatrizeq[l1][4])**2 + (z/100-
Cmatrizeq[l1][5])**2 <= (Cmatrizeq[l1][2])**2) and ((x/100-
Cmatrizeq[l2][3])**2 + (y/100-Cmatrizeq[l2][4])**2 + (z/100-
Cmatrizeq[l2][5])**2 <= (Cmatrizeq[l2][2])**2) and ((x/100-
Cmatrizeq[l3][3])**2 + (y/100-Cmatrizeq[l3][4])**2 + (z/100-
Cmatrizeq[l3][5])**2 <= (Cmatrizeq[l3][2])**2) and ((x/100-
Cmatrizeq[l4][3])**2 + (y/100-Cmatrizeq[l4][4])**2 + (z/100-
Cmatrizeq[l4][5])**2 <= (Cmatrizeq[l4][2])**2)):
                            nprim = nprim + 1
                            xcm = xcm + x
                            ycm = ycm + y
                            zcm = zcm + z
                        if ( ((x/100-
Cmatrizeq[l1][3])**2 + (y/100-Cmatrizeq[l1][4])**2 + (z/100-
Cmatrizeq[l1][5])**2 <= (Cmatrizeq[l1][2])**2) or ((x/100-
Cmatrizeq[l2][3])**2 + (y/100-Cmatrizeq[l2][4])**2 + (z/100-
Cmatrizeq[l2][5])**2 <= (Cmatrizeq[l2][2])**2) or ((x/100-
Cmatrizeq[l3][3])**2 + (y/100-Cmatrizeq[l3][4])**2 + (z/100-

```

```

Cmatriceq[l3][5])**2 <= (Cmatriceq[l3][2])**2) or ((x/100-
Cmatriceq[l4][3])**2 + (y/100-Cmatriceq[l4][4])**2 + (z/100-
Cmatriceq[l4][5])**2 <= (Cmatriceq[l4][2])**2)):
        mprim = mprim + 1
        if ((nprim/mprim)<
Ratiolimit):
                count = count +1
                ratio = nprim/mprim
                XCM = xcm/((nprim-1)*100)
                YCM = ycm/((nprim-1)*100)
                ZCM = zcm/((nprim-1)*100)
                error = math.sqrt ((XCM-
float(LEmatrix_real_Reftags[L][2]) )**2 + (YCM-
float(LEmatrix_real_Reftags[L][3]) )**2 + (ZCM-
float(LEmatrix_real_Reftags[L][4]) )**2)
                #DoP calculation
                ux=
(Cmatriceq[l1][3]+Cmatriceq[l2][3]+Cmatriceq[l3][3]+Cmatriceq[l4][3])/4
                uy=
(Cmatriceq[l1][4]+Cmatriceq[l2][4]+Cmatriceq[l3][4]+Cmatriceq[l4][4])/4
                uz=
(Cmatriceq[l1][5]+Cmatriceq[l2][5]+Cmatriceq[l3][5]+Cmatriceq[l4][5])/4
                sx2= ((Cmatriceq[l1][3]-
ux)**2+(Cmatriceq[l2][3]-ux)**2+(Cmatriceq[l3][3]-
ux)**2+(Cmatriceq[l4][3]-ux)**2)/3
                sy2= ((Cmatriceq[l1][4]-
uy)**2+(Cmatriceq[l2][4]-uy)**2+(Cmatriceq[l3][4]-
uy)**2+(Cmatriceq[l4][4]-uy)**2)/3
                sz2= ((Cmatriceq[l1][5]-
uz)**2+(Cmatriceq[l2][5]-uz)**2+(Cmatriceq[l3][5]-
uz)**2+(Cmatriceq[l4][5]-uz)**2)/3
                s2= sx2+sy2+sz2
                Locationmatrix [n3] = [count, L+1,
nprim, mprim, ratio, XCM, YCM, ZCM, s2, error]
                n3 = n3+1
                print (count,'R2-', 'Tag ID:', L+1,
'n:', nprim, 'divided by m:', mprim, '= ratio:', ratio, 'The CM is:
(',XCM,',',YCM,',',ZCM,') The SoD is:', s2,' The error is:', error)
                nprim=1
                mprim=1
                xcm=0
                ycm=0
                zcm=0

for m in range (0, TagNo):
        Locationmatrixfinal[m].remove (0)
        kn=0
        for u in range (0,n3):

```

```

        if (Locationmatrix[u][1]== (m+1)):
            Locationmatrixfinal[m].append (Locationmatrix[u])
            kn=kn+1
    if (kn==0):
        Locationmatrixfinal[m].append([0,0,0,0,0,0,0,0,0,0])

import numpy as np
for i in range (0,TagNo):
    mat = np.array(Locationmatrixfinal [i])
    mat_sort = mat[mat[:,7].argsort()]
    if (len(mat_sort)==1):
        Locationmatrix_DoP [i] = [i+1,mat_sort[len(mat_sort)-
1][5],mat_sort[len(mat_sort)-1][6],mat_sort[len(mat_sort)-
1][7],mat_sort[len(mat_sort)-1][8] ,mat_sort[len(mat_sort)-1][9]]
    if (len(mat_sort)==2):
        Locationmatrix_DoP [i] = [i+1,(mat_sort[len(mat_sort)-
1][5]+mat_sort[len(mat_sort)-2][5])/2,(mat_sort[len(mat_sort)-
1][6]+mat_sort[len(mat_sort)-2][6])/2,(mat_sort[len(mat_sort)-
1][7]+mat_sort[len(mat_sort)-2][7])/2,(mat_sort[len(mat_sort)-
1][8]+mat_sort[len(mat_sort)-2][8])/2,(mat_sort[len(mat_sort)-
1][9]+mat_sort[len(mat_sort)-2][9])/2]
    if (len(mat_sort)==3):
        Locationmatrix_DoP [i] = [i+1,(mat_sort[len(mat_sort)-
1][5]+mat_sort[len(mat_sort)-2][5]+mat_sort[len(mat_sort)-
3][5])/3,(mat_sort[len(mat_sort)-1][6]+mat_sort[len(mat_sort)-
2][6]+mat_sort[len(mat_sort)-3][6])/3,(mat_sort[len(mat_sort)-
1][7]+mat_sort[len(mat_sort)-2][7]+mat_sort[len(mat_sort)-
3][7])/3,(mat_sort[len(mat_sort)-1][8]+mat_sort[len(mat_sort)-
2][8]+mat_sort[len(mat_sort)-3][8])/3,(mat_sort[len(mat_sort)-
1][9]+mat_sort[len(mat_sort)-2][9]+mat_sort[len(mat_sort)-3][9])/3]
    if (len(mat_sort)==4):
        Locationmatrix_DoP [i] = [i+1,(mat_sort[len(mat_sort)-
1][5]+mat_sort[len(mat_sort)-2][5]+mat_sort[len(mat_sort)-
3][5]+mat_sort[len(mat_sort)-4][5])/4,(mat_sort[len(mat_sort)-
1][6]+mat_sort[len(mat_sort)-2][6]+mat_sort[len(mat_sort)-
3][6]+mat_sort[len(mat_sort)-4][6])/4,(mat_sort[len(mat_sort)-
1][7]+mat_sort[len(mat_sort)-2][7]+mat_sort[len(mat_sort)-
3][7]+mat_sort[len(mat_sort)-4][7])/4,(mat_sort[len(mat_sort)-
1][8]+mat_sort[len(mat_sort)-2][8]+mat_sort[len(mat_sort)-
3][8]+mat_sort[len(mat_sort)-4][8])/4 ,(mat_sort[len(mat_sort)-
1][9]+mat_sort[len(mat_sort)-2][9]+mat_sort[len(mat_sort)-
3][9]+mat_sort[len(mat_sort)-4][9])/4]
    if (len(mat_sort)>=5):
        Locationmatrix_DoP [i] = [i+1,(mat_sort[len(mat_sort)-
1][5]+mat_sort[len(mat_sort)-2][5]+mat_sort[len(mat_sort)-
3][5]+mat_sort[len(mat_sort)-4][5]+mat_sort[len(mat_sort)-
5][5])/5,(mat_sort[len(mat_sort)-1][6]+mat_sort[len(mat_sort)-
2][6]+mat_sort[len(mat_sort)-3][6]+mat_sort[len(mat_sort)-

```

```
4][6]+mat_sort[len(mat_sort)-5][6])/5, (mat_sort[len(mat_sort)-1][7]+mat_sort[len(mat_sort)-2][7]+mat_sort[len(mat_sort)-3][7]+mat_sort[len(mat_sort)-4][7]+mat_sort[len(mat_sort)-5][7])/5, (mat_sort[len(mat_sort)-1][8]+mat_sort[len(mat_sort)-2][8]+mat_sort[len(mat_sort)-3][8]+mat_sort[len(mat_sort)-4][8]+mat_sort[len(mat_sort)-5][8])/5 , (mat_sort[len(mat_sort)-1][9]+mat_sort[len(mat_sort)-2][9]+mat_sort[len(mat_sort)-3][9]+mat_sort[len(mat_sort)-4][9]+mat_sort[len(mat_sort)-5][9])/5]
```

Export the localization information in Excel format

```
import pandas as pd
df1 = pd.DataFrame(Locationmatrix)
df1.to_excel('Tags 3D location o20 before DoP analysis_5 highest no initial SoD IdentificationNo=8.xlsx')

df2 = pd.DataFrame(Locationmatrix_DoP)
df2.to_excel('Tags 3D location o20 after DoP analysis_5 highest no initial SoD IdentificationNo=8.xlsx')
```